BEST AVAILABLE IMAGES

Defective images within this document are accurate representations of the original documents submitted by the applicant.

Defects in the images may include (but are not limited to):

- BLACK BORDERS
- TEXT CUT OFF AT TOP, BOTTOM OR SIDES
- FADED TEXT
- ILLEGIBLE TEXT
- SKEWED/SLANTED IMAGES
- COLORED PHOTOS
- BLACK OR VERY BLACK AND WHITE DARK PHOTOS
- GRAY SCALE DOCUMENTS

IMAGES ARE BEST AVAILABLE COPY.

As rescanning documents *will not* correct images, please do not report the images to the Image Problem Mailbox.

Appl. Phys. A 70, 489–534 (2000) / Digital Object Identifier (DOI) 10.1007/s003390000458

Applied Physics A
Materials Science & Processing

Invited paper

Iron contamination in silicon technology

A.A. Istratov[1], H. Hieslmair[1], E.R. Weber[2]

[1] University of California, Lawrence Berkeley National Laboratory, 1 Cyclotron Road, Mail Stop 62-203, Berkeley, CA 94720, USA
(Fax: +1-510/486-4995, E-mail: istratov@socrates.berkeley.edu)
[2] Department of Materials Science and Engineering, University of California, 475 Evans Hall, Berkeley, CA 94720-1760, USA
(Fax: +1-510/642-2069, E-mail: weber@socrates.berkeley.edu)

Received: 16 November 1999/Accepted: 7 January 2000/Published online: 5 April 2000 –

Abstract. This article continues the review of fundamental physical properties of iron and its complexes in silicon (Appl. Phys. A **69**, 13 (1999)), and is focused on ongoing applied research of iron in silicon technology. The first section of this article presents an analysis of the effect of iron on devices, including integrated circuits, power devices, and solar cells. Then, sources of unintentional iron contamination and reaction paths of iron during device manufacturing are discussed. Experimental techniques to measure trace contamination levels of iron in silicon, such as minority carrier lifetime techniques (SPV, μ-PCD, and ELYMAT), deep-level transient spectroscopy (DLTS), total X-ray fluorescence (TXRF) and vapor-phase decomposition TXRF (VPD-TXRF), atomic absorption spectroscopy (AAS), mass spectrometry and its modifications (SIMS, SNMS, ICP-MS), and neutron activation analysis (NAA) are reviewed in the second section of the article. Prospective analytical tools, such as heavy-ion backscattering spectroscopy (HIBS) and synchrotron-based X-ray microprobe techniques (XPS, XANES, XRF) are briefly discussed. The third section includes a discussion of the present achievements and challenges of the electrochemistry and physics of cleaning of silicon wafers, with an emphasis on removal of iron contamination from the wafers. Finally, the techniques for gettering of iron are presented.

PACS: 61.72.-y; 66.30.-h; 71.55.Cn; 78.70.Gq; 81.05.Cy; 81.65.-b; 81.70.-q; 82.80.-d; 85.30.-z; 85.40.-e

Progress in silicon technology has been phenomenal since the invention of the transistor some fifty years ago. Device performance has improved by at least a factor of a million in every respect. As the number of transistors per chip increases past 200 million for 256 MB DRAM and 20 million for microprocessors, device yield is becoming ever more sensitive to defects and impurities. The Semiconductor Industry Association (SIA) International Technology Roadmap specifies $1.4 \times 10^{10}\,cm^{-2}$ as the maximum allowable surface iron contamination in the year 2000, decreasing to $5 \times 10^{9}\,cm^{-2}$ of iron in 2005 [1]. These low levels of acceptable contamination require ultrapure environment on all steps of the technological process and are close to the limit of the present capabilities of most diagnostic tools.

Iron is certainly one of the most troubling contaminants in the IC industry. Iron is a very common element in nature, and is difficult to completely eliminate on a production line. Therefore, the unintentional iron contamination level in wafers is usually higher than that of other metal impurities [2]. The major reasons why transition metals in general, and iron in particular, are detrimental for silicon devices are (i) transition metals as well as their complexes and precipitates introduce deep levels in the band gap, reducing the minority carrier lifetime, or generating minority carriers in depleted regions; (ii) the incorporation of metals into the gate oxides, or their precipitation at Si/SiO_2 interfaces degrades MOS device yield; (iii) very high diffusion coefficients at high processing temperatures can result in fast contamination of large wafer areas even from point sources and from the wafer backside; (iv) the steep temperature dependence of the solubility means that metals become supersaturated during cooling even at relatively low concentrations, and may form precipitates or complexes, deleteriously affecting the device yield; and (v) the relatively high diffusivity of most transition metals even at low temperatures facilitates the defect reactions involving supersaturated metals [3].

In this article, we will discuss the iron-related issues that the silicon industry has to deal with on a daily basis, and will show that all these problems can be traced back to the fundamental physical properties of iron in silicon. The outline of this review is as follows: first, we will discuss the impact of iron on device yield, possible sources of iron contamination on the production line, and the reaction paths of iron in silicon wafers during device manufacturing. Then, we will give an overview of measurement techniques for trace concentrations of iron on the surface and in the bulk of silicon. This is followed by a discussion of the physics and chemistry of the cleaning of silicon wafers and the gettering techniques of iron in silicon.

1 Effect of iron on the device performance

1.1 Effect of iron on metal-oxide-semiconductor (MOS) devices

Iron contamination was found to significantly decrease the breakdown voltage of gate oxides. The commonly reported mechanism for electrical field breakdown failure from iron contamination is the formation of iron precipitates at the Si/SiO_2 interface, which frequently penetrate into the silicon dioxide. The nucleation and growth of iron-silicide precipitates at the Si/SiO_2 interface is stimulated by excess silicon self-interstitials injected into the wafer from the growing oxide. The excess self-interstitials relieve the tensile strain around the growing $FeSi_2$ precipitates caused by a difference in lattice volumes of iron-silicide and silicon [4, 5]. Iron-silicide precipitates were observed in the form of pyramidal β-$FeSi_2$ [6], rod-like α-$FeSi_2$ [7–11], or FeSi [12]. Some authors reported precipitates of α-$FeSi_2$ [11], γ-Fe_2O_3, or γ-Fe_2SiO_4 [12] in the oxide layer itself. The breakdown strength of the oxide is decreased by either local thinning of the oxide near a precipitate, or by the increased concentration of the electric field at the tip of the precipitate [8, 13, 14]. Additionally, formation of iron-related traps in the oxide may increase the probability of tunneling of charge carriers through the oxide [15–17]. Other mechanisms of metal-enhanced oxide breakdown include the increase of surface roughness in the presence of metal contamination (see Sect. 5.3), the decomposition of the oxide in the presence of metals [18], and the formation of metal-silicates in the oxide [19].

While the possible degradation mechanisms are generally agreed upon, establishing a quantitative correlation between the breakdown electric field strength, E_{BD}, and surface or bulk iron concentration is difficult since E_{BD} depends not only on the iron concentration, but also on the oxide thickness and the presence of gettering mechanisms. The comprehensive study of Henley et al. [14, 20–22] revealed that the breakdown voltage of thin oxides is much more sensitive to iron contamination than that of thick oxides.

The dependence of critical iron bulk contamination level for different oxide thickness, based on the data of Henley [14] as well as on the other literature data [7, 8, 23–32] is plotted in Fig. 1. It must be noted that the authors did not always supply all the information needed to generate this plot and some reasonable assumptions had to be made. The reader should refer to the individual papers for the details of those studies. The scatter in the data points in Fig. 1 for thicker oxides is partly explained by the difference in bulk properties of the wafers. For instance, Mertens et al. [25] demonstrated that Fe-contaminated FZ wafers showed much lower gate oxide integrity than identically contaminated and treated CZ wafers. This was explained as gettering effects, i.e., inability of FZ wafers to trap the Fe in the bulk, leaving all the metal free to reach the wafer surface. In fact, the observed difference in surface Fe concentration between FZ and CZ wafers after identical heat treatment was about a factor of 5 [25]. Analysis of data points in Fig. 1 shows that there is an obvious trend that oxide breakdown becomes more sensitive to iron contamination as oxides become thinner, at least down to 8 nm. The question whether the linear fit can be extrapolated to the oxides thinner than 5 nm (the cross-hatched area in Fig. 1) remains uncertain. Recent study by D'Amico et al. [15], who

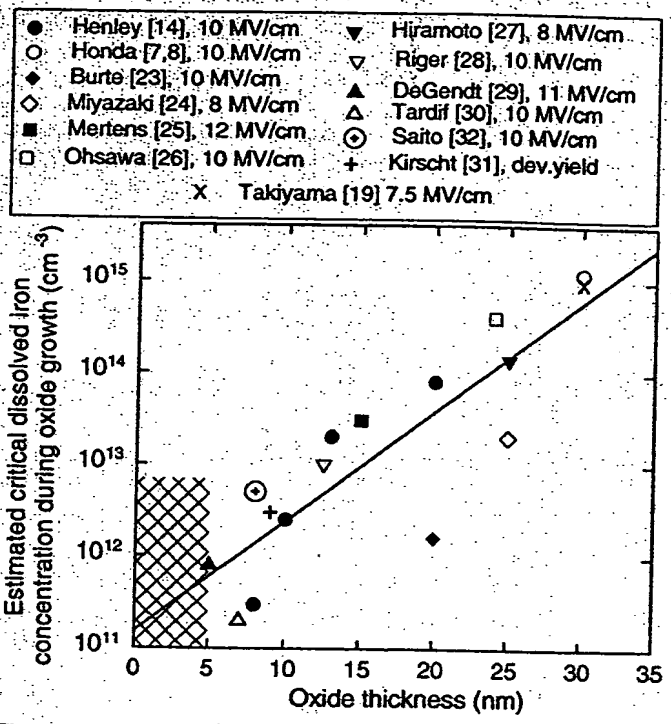

Fig. 1. The dependence of the critical bulk iron contamination level for gate oxide breakdown versus oxide thickness. The breakdown electrical field is indicated in the legend. The *solid line* was obtained by a least-squares fit to the data points and is given by the equation $N(\mathrm{Fe}) = 1.53 \times 10^{11} \times 10^{0.12d}$, where N(Fe) is the bulk iron concentration in cm^{-3}, and d is the oxide thickness in nm. The cross-hatched pattern highlights the area of thin oxides, which is not yet sufficiently studied

compared the effect of iron on 7-nm and 3.5-nm oxides, indicated that thin (3.5 nm) oxides are actually less sensitive to trace iron contamination than thicker (7 nm) oxides. This was explained by a different mechanism of electrical breakdown of thick and thin oxides: whereas leakage currents of oxides thicker than 5–10 nm are determined primarily by metal precipitates at the Si/SiO_2 interface, trap-assisted tunneling, and recently suggested mechanism of local increase of dielectric permittivity of the oxide by electrical charge trapped inside of SiO_2 [17], leakage and breakdown of very thin oxides is determined by direct tunneling of charge carriers through the oxide [15, 16]. In other words, ultrathin oxides are inherently leaky, but their leakage currents appear to be weakly affected by iron concentration, at least as long as the contamination level is low. Further investigations are required to verify this finding and to quantify the effect of iron on ultrathin oxides. In any case, the value of approximately 2×10^{11} cm^{-3} of dissolved iron, obtained by extrapolation of the straight line in Fig. 1 to the zero oxide thickness, can be used as a lower estimate of the maximum dissolved iron concentration, which would not affect the gate oxide integrity. This bulk concentration would correspond to approximately 1.5×10^{10} cm^{-2} of surface iron contamination, assuming that all iron diffuses into the bulk during oxidation. However, it should be emphasized that several literature reports indicated (see discussion in Sect. 3) that under certain oxidation conditions, the surface iron contamination may remain bound in the oxide, supposedly due to the formation of iron oxides or silicates, rather than diffuse into the bulk. In this case, one may expect unproportionally strong effect of the surface contamination as

compared to the bulk contamination. Takiyama et al. [19] provided a convincing example how the breakdown yield of MOS devices may depend on the distribution of iron in the oxide.

Another important detrimental effect of iron on MOS devices is that interstitial iron, and to a lesser extent FeB pairs, act as minority carrier generation sites when minority carriers are depleted. In a dynamic random access memory (DRAM) cell, the stored charge becomes corrupted at a faster rate if minority carrier generation sites such as iron are present. This requires the DRAM cell to be more frequently refreshed and can lead to refresh failures [28]. In charge-coupled device (CCD) imagers, thermally generated minority carriers cannot be distinguished from photon-generated minority carriers, and thus give false photon counts [33].

Assuming that the main generation centers are interstitial iron and FeB pairs, the iron concentration can be deduced from the difference in generation rate before and after a thermal or light dissociation of FeB pairs. Obermeier et al. [34] give an expression relating the generation lifetime, τ, to iron concentration, N(Fe), as,

$$N(\mathrm{Fe}) \approx 8 \times 10^8 \left[\frac{1}{\tau_{\mathrm{Fe}_i}} - \frac{1}{\tau_{\mathrm{FeB}}} \right] \quad (1)$$

where the lifetimes, τ_{Fe_i}, and τ_{FeB}, are measured in seconds, and N(Fe) is measured in cm^{-3}. Walz et al. [35] observed a linear dependence between $(\tau_{\mathrm{Fe}_i}^{-1} - \tau_{\mathrm{FeB}}^{-1})$ and Fe_i concentration a few years before [34]. Although they did not suggest an expression of the type (1), their data enable one to extract a proportionality coefficient in (1) of 5.7×10^8. Note that (1) does not take into account the possibility of generation of minority carriers by complexes of iron other than FeB, although recent studies of McColgin et al. [33] indicated that clusters of iron atoms, whose microscopic structure is not understood yet, may have generation rates orders of magnitude higher than Fe_i, and thus are extremely deleterious for devices sensitive to minority carrier generation.

1.2 Effect of iron on junction devices

When dissolved in silicon, iron forms deep levels [36] which act to degrade junction device performance by the generation of carriers in any reverse-biased depletion region [37, 38]. In bipolar junction transistors, generation-recombination centers formed by dissolved iron generally increase the base currents, degrading the emitter efficiency and base transport factors. The net result is an increase in leakage currents [39–41], the lowering of the reverse-bias breakdown voltage in thyristors [42], and the increase of the device noise [43], power consumption and heat production [44]. Even more debilitating are the effects of iron rod-like precipitates, which have been observed to cause emitter–collector shorts [45–47].

In crystalline and polycrystalline photovoltaics, iron contamination provides recombination centers which reduce the minority carrier diffusion length and consequently the solar cell efficiency. In general, minority carrier diffusion lengths in solar cells should be equal to or exceed the wafer thickness. For a 300-μm-thick solar cell, the concentration of iron–boron pairs which would limit the diffusion length at $L_D = 300\,\mu\mathrm{m}$ is approximately $5 \times 10^{11}\,\mathrm{cm}^{-3}$ [48]. This estimate agrees with recent studies of Reiss et al. [49], who found that $5 \times 10^{11}\,\mathrm{cm}^{-3}$ of iron in the form of FeB pairs may decrease the efficiency of CZ solar cells by 3%–4%. In multicrystalline solar cells, iron was found to decorate extended defects, making them extremely recombination active [50–54]. Furthermore, precipitation of Fe in areas of high defect densities leads to regions of low minority carrier diffusion lengths, which result in locally low generated open-circuit voltages, V_{OC}. In terms of the wafer efficiency, these local regions act as shunts for power generated in neighboring regions with higher V_{OC}, which results in unproportionally lower cell performance [55]. The effect of enhanced precipitation of iron in areas of high density of intragranular microdefects has been demonstrated by Bailey et al. [56]. Additionally, Miremadi et al. [57] suggested that iron contamination of grain boundaries may enhance the electrical conductivity along these boundaries, which also can potentially shunt the solar cells.

2 Sources of unintentional iron contamination

Wafer manufacturing includes a number of technological processes, starting with the growth of silicon crystals, followed by slicing, polishing, cleaning, and packaging of wafers, and then IC fabrication which entails a number of thermal treatments, chemical cleanings, and ion implantation. Each of these steps can either add iron contamination to the wafers, or remove it (for example, cleaning steps). The exact amount of contaminants introduced in each step, and the nature of accidental increases of contamination levels are usually kept confidential by semiconductor companies. Those data that are disclosed often become obsolete by the time they are published. Hence, it makes little sense to discuss specific contamination levels that occurred in a specific piece of equipment years ago. However, the sensitivity of different process steps to unintentional contamination and the physics of contamination and its prevention seem to be weakly dependent on details of technological processes and deserve to be addressed in this study.

Contaminations can be classified as grown-in (impurities in polysilicon feedstock and contamination during crystal growth), and as introduced from chemicals (for example, gases, wet chemistry, photoresist, water), from processing equipment (furnaces, ion implanters, reactive ion etching and rapid thermal annealing systems, polishing machines, electrical measurement tools, wafer handlers, or tools for numbering or marking), and from handling between these steps (by wafer carriers of even from the ambient air) [58–61]. Stainless steel, widely used in fabrication facilities, is thought to be one of the major sources of iron [20, 62]. Gas delivery systems are one of possible sources of contaminants, moisture, and particles [63, 64]. Humidity in gas delivery systems may result in the corrosion of gas pipes, which leads to an enhanced metal contamination of the wafers [64]. Avoiding contamination from the gases is particularly crucial in epitaxial chemical vapor deposition reactors.

The starting concentration of iron in polysilicon feedstock steadily decreases with the development of silicon purification technology. The 1957 studies of James et al. [65] revealed iron concentration in silicon at about $10^{16}\,\mathrm{cm}^{-3}$, which is close to the maximum solubility of interstitial iron in Si. In 1975, Fe concentration in polysilicon was about

3×10^{14} cm^{-3} [66, 67]. Relatively recent studies of Huber et al. [68] revealed that the iron concentration in polysilicon is below 2.5×10^{11} cm^{-3}. Although these iron concentrations may appear high as compared to the SIA roadmap requirements [1], they are not transferred to the wafers since Czochralski (CZ) or float-zone (FZ) crystal growth is the most powerful purifying step in the whole process of production of silicon devices. This is because iron, as well as many other transition metals, has a low, $S \ll 1$, segregation coefficient (also known as distribution coefficient for the case of segregation between the crystal and the melt), which means that silicon is purified during crystal growth by segregation of impurities in the melt. One of the experimental confirmations for this was obtained in the neutron activation analysis (NAA) studies of Schmidt and Pearce [69]. They found that the silicon crystal, grown from severely contaminated melt, contained iron in concentrations below the sensitivity limit (5×10^{13} cm^{-3}), whereas the polysilicon residue, which remained in the quartz crucible after the growth (about 10% of the original charge) contained 6×10^{17} cm^{-3} of iron.

Literature data on the distribution coefficient of iron between silicon solid crystal and the melt are in reasonably good agreement: 10^{-4}, as reported by James et al. [65], 8×10^{-6} as reported by Trumbore [70], 3×10^{-5} as reported by Bugay et al. [71], 4.6×10^{-6} as reported by Mishra et al. [72], 5×10^{-6} to 1×10^{-5} as follows from the experiments of Collins [73], and 7×10^{-6} as derived by Weber [74, 75]. Thus, the average value of distribution coefficient is about 10^{-5}. This segregation effect enables the silicon suppliers to grow crystals with an iron content below the sensitivity limit of the available analytical tools, and below the requirements of the SIA roadmap, i.e., 10^{8}–10^{9} cm^{-3} [76, 77]. Despite purification during crystal growth, precautions should still be taken to avoid severe additional contamination from the dopants, quartz crucible [76], or puller assembly. The graphite parts of the puller assembly are of particular importance, since the graphite can emit iron as a vapor which is then transported to the melt [78, 79]. Photovoltaics manufacturing uses simplified low-cost technologies for the growth of multicrystalline silicon (mc-Si), and cannot benefit from the segregation effects of transition metals in the melt to the same extent as monocrystalline technology does. For instance, relatively recent studies of the silicon wafers for solar cells, reported by Huber et al. [68] revealed iron concentrations of about 1 ppb (2.5×10^{13} cm^{-3}).

Slicing and mechanical lapping are, according to [69], very dirty operations, which may badly contaminate wafers with a variety of impurities. Fortunately, the wafers are sliced and lapped at room temperature, where the diffusivity of most transition metals (with the only exception of copper, [80]) is so low that the metals do not penetrate into the bulk of silicon. Thus, almost all of this contamination can be easily removed in the subsequent chemical cleaning step.

The possibility to contaminate the wafers during handling is now well known, and metal tweezers are never used if the wafer will be inserted in the furnace on the next step. Schmidt et al. [69] showed that one can introduce about 2×10^{13} cm^{-3} of Fe in a 3-inch silicon wafer just by lifting it repeatedly with metal tweezers. Correspondingly, surface haze was observed at the wafer surface where contact with stainless steel or kovar tweezers was made [81]. Despite the use of plastics instead of metals, contamination of wafers from handling (although on much lower levels) remains one of the important sources of transition metals, and usually occurs as backside contamination [82].

Cleaning processes can paradoxically be not only a remedy against unintentional contamination, but also one of the major sources of impurities in silicon wafers [2, 83, 84]. The quality of chemicals used in the semiconductor industry has improved drastically: the concentration of anions, cations, and particles in the chemicals has decreased by 5 orders of magnitude over the last 12 years [85]. Unfortunately, even if the incoming chemicals are strictly controlled, chemicals can be contaminated during their distribution in the recirculation/filtering loop of the wet benches by defects, such as a corroded valve or a loss of pump integrity [3, 83]. It was reported that ion-exchange resins, used in water regeneration systems, may under certain conditions become crucial iron contamination sources [86].

Contamination of wafers during high-temperature anneals, particularly during steam oxidation, was a major source of metal contamination in the silicon industry in the beginning of the 1980s (most of the "quenched-in" defects [87–90] and "thermally induced donors" [91–93], discussed at that time, were associated with unintentional iron contamination). Contamination is most easily possible at temperatures larger than 1100 °C since (i) metal species become volatile at these temperatures and can be transported inside of the furnace via the gas phase, and (ii) because SiC, used instead of fused silica in high-temperature furnaces, contains more impurities than the silica [3, 82, 94]. Although the temperatures of anneals and oxidations have decreased in the last years, thus decreasing the probability of contamination, contamination from the furnaces remains an important source of iron as the maximum tolerable contamination levels also continue to decrease [2, 82, 95–97]. Weber and Riotte [98] suggested two contamination processes, a fast diffusion of the surface iron contamination into the bulk and a slower contamination from the furnace ambient. DeBusk et al. [99] pointed out that rust on various stainless steel, fused silica, and O-ring components can be transported as vapor by the oxidation ambient of a furnace system and contaminate the wafers.

The authors of this review expect that heating coils are a major source of iron contamination in furnaces. Analysis of Schmidt et al. [69] revealed that metals diffuse from the furnace metal parts and impure SiC liners through the walls of the quartz tube. This diffusion was found to have a very steep temperature dependence, resulting in an enormous increase in the contamination level of the wafers if the temperature exceeded approximately 1150 °C. Schmidt et al. [69, 100] suggested that at high temperatures transition metals diffuse preferentially along incipient grain boundaries in vitreous quartz. They showed that an effective way to eliminate contamination from the metal parts of the furnace is to use a double-walled quartz tube with an HCl-containing gas flowing between the inner and outer walls of the tubes [69, 100, 101].

Quartz itself may contain significant amounts of transition metals, and may thus be a source of unintentional contamination [102–104]. Iron in the form of $NaFeSi_2O_6$ or $Na_5FeSi_4O_{12}$ is a common impurity in natural and synthetic quartz [105]. Natural quartz has higher concentration of impurities than the fused quartz, but it also has a higher mechanical stability at elevated temperatures. The follow-

ing values for iron concentration were reported in the literature: 4 ppm and less in natural quartz [69, 106]; 70 to 200 ppb in electric-fused and flame-fused quartz [68, 102, 106], and below 10 ppb in highly purified quartz glass [102]. Feichtinger [107] and Borchardt et al. [108] showed that the level of unintentional iron contamination can be drastically reduced by using silicon sample holders instead of the quartz holders.

Hattori [109] and Sigiura [110] pointed out that generally, all equipment that utilizes plasma and ions (ion implantation, dry etching, resist ashing, sputtering, plasma CVD equipment, etc.) may introduce significant (in some instances, up to 10^{12}–10^{13} cm^{-2}) metal contamination. The unanticipated sputtering of metallic parts in the plasma equipment by ions and by abnormal discharges (or what is called micro-arcing) can lead to metal deposition. Zoth and Bergholz [111, 112], Jastrzebski et al. [2, 21], Polignano et al. [113] and Joubert et al. [114] reported that ion implantation could cause iron contamination up to 10^{13} cm^{-2}, whereas a plasma etch and resist ashing could introduce iron in concentrations up to 10^{12} cm^{-2}. One should keep in mind that much effort has been done to reduce the contamination from these processing steps, and the actual contamination levels are steadily decreasing and are presently below 10^{11} cm^{-2} [59, 82]. Since contamination during ion implantation mainly comes from ions sputtered from sample holders or metal parts of the chamber, impacted by the ion beam [113, 115], the energy of these ions is much lower than that of the beam ions, and they do not penetrate deep into the wafer. It was shown that a sacrificial oxide of about 20 nm, which is removed after the implantation, is sufficient to completely protect the silicon from contamination during ion implantation [82, 113]. An improved design of the implanter, which includes installation of silicon sputtering protection boards, was also shown to decrease the metal contamination levels [115].

3 Physics of iron contamination: reaction paths of iron in silicon

Only a thin layer at the top of the silicon wafers, usually on the order of 1 μm, is used to manufacture integrated circuits. The rest of the wafer, i.e., over 99.8% of its volume, is used only as a substrate to mechanically support the device layer. Transition metal contaminants, introduced at the front or back surface of the wafer, will diffuse through the wafer and may form complexes/agglomerates/precipitates either at the devices, or somewhere in the substrate. Clearly, iron will affect devices only if it is located in their close vicinity. The final location of iron depends to a significant extent on the physical properties of the wafer (such as concentrations of oxygen, carbon, type of surface defects and type of devices fabricated on the wafer) and the sequence of heat treatments, implantations, and oxidations done to the wafer. Understanding of the sources of iron contamination on the production line can help to decrease the iron contamination levels, but cannot eliminate iron completely. To fully understand and predict the detrimental effect of iron on devices, and to engineer its behavior in silicon wafers by gettering, it is important to know the defect reactions of iron during the process of fabrication of integrated circuits.

The analysis of the physics of iron, given in the first part of our review [116], demonstrated that iron dissolves and diffuses in silicon in the interstitial state. If an iron-contaminated wafer is cooled down rapidly, all iron will be quenched at interstitial sites and will form a deep level at $E_V + (0.38 \pm 0.01)$ eV. However, since Fe_i is mobile and can diffuse short distances in the wafer at room temperature (its diffusion coefficient at 20 °C is approximately 3×10^{-15} cm^2/s), it quickly forms pairs with shallow acceptors, for example, boron. The driving force for this reaction is electrostatic attraction between positively charged (in p-Si at room temperature) interstitial iron and negatively charged boron. FeB pairs form a donor level at $E_V + 0.1$ eV, and an acceptor level at $E_C - (0.26 \pm 0.03)$ eV. Although FeB pairs are stable at room temperature, they can be easily dissociated by annealing the sample at 200 °C, or by shining bright white light on the wafer. The reactions of association and dissociation of FeB pairs, which reversibly change the electrical levels associated with iron and its recombination activity, is the major fingerprint of interstitial iron in silicon. Besides complexes with shallow acceptors (B, Al, Ga, In, Tl), interstitial iron is known to form electrically active complexes with gold, silver, zinc, platinum, palladium, sulfur, and oxygen. These complexes altogether form about 20 energy levels in the silicon band gap. Furthermore, several types of agglomerates of interstitial iron atoms and vacancies were observed (see [116] for a detailed discussion and bibliography). The versatility of defect reactions involving iron makes understanding and modeling the behavior of iron in real-life processing conditions very difficult, and requires precise knowledge of all reaction constants. Although a great number of issues remains unresolved, significant progress has been made in the past years. In the following, we will discuss the physics of some of the defect reactions, which were out of the scope of our first review [116], such as precipitation of iron in the bulk at extended defects, and at the silicon–silicon dioxide interface. Additionally, in Sect. 6, we will discuss engineering of iron in silicon by gettering.

Bulk precipitation of transition metals in the form of the metal-silicide is thoroughly investigated for fast diffusing metals such as copper and nickel (see [117–119] and references therein). Similarly to other transition metals, iron forms a number of silicide phases, including cubic ε-FeSi, tetragonal α-$FeSi_2$, orthorhombic β-$FeSi_2$, hexagonal Fe_5Si_3, and cubic Fe_3Si [12, 120]. A phase diagram of iron-silicides can be found in [121]. Note that it is usually much more difficult to find iron-silicide precipitates in the bulk of a silicon wafer after thermal diffusion and cool down, than to find precipitates of copper or nickel. This is because the solubility of iron (around 10^{16} cm^{-3} at 1200 °C, or around 3×10^{12} cm^{-3} at 800 °C) is much lower than that of Cu or Ni, and the resulting density of precipitates, if they are formed in the bulk, is low. Additionally, low strain fields around the precipitates make their TEM observation difficult. Furthermore, the pairing of iron with boron is an efficient trapping mechanism, which significantly reduces the driving force for the precipitation of iron in the bulk. Several groups [47, 122–124] succeeded in finding rod-like $FeSi_2$ precipitates, up to 0.5 μm long and a few tenths of a nanometer thick, in TEM samples prepared from devices or wafers after thermal indiffusion of iron. As discussed in Sect. 1.1 above, these iron-silicide precipitates were frequently found at Si/SiO_2 interfaces. However, most

observations of iron-silicide precipitates were done after implantation of high doses of iron (which results in extremely high local concentrations of iron) with subsequent annealing [6, 125–134]. These studies were stimulated by the possibility of using iron-silicide as a prospective material for silicon-based optoelectronics (see, for example, [135–137]) since its direct band gap of about 0.87 eV makes it suitable for the fabrication of infrared detectors or emitters integrated to silicon circuits.

In contrast to bulk precipitates of iron, agglomeration of iron at extended defects, such as dislocations or low-angle boundaries, can easily be observed after thermal diffusion of iron. A significant increase in the recombination activity of iron-contaminated dislocations, silicon-oxide precipitates, and misfit dislocations in Si/SiGe epitaxial structures has been reported in [50–54, 138, 139]. Kittler et al. [50] studied gettering of iron by grain boundaries in mc-Si and demonstrated an increase in the recombination activity of a grain boundary along with a distinctive reduction in the iron concentration around the boundary. Portier et al. [140] showed that the precipitation of iron at grain boundaries in a silicon bicrystal resulted in the formation of iron silicide precipitates of the ε-FeSi or α-$FeSi_2$ type. However, the formation of distinctive iron-silicide precipitates at extended defects is very uncommon. With a few exceptions (such as [140]), it was found that iron precipitates along dislocation lines very uniformly, and does not form any contrast spots in EBIC images, common for Cu-contaminated samples [124, 141].

Decoration of dislocations and oxidation-induced stacking faults (OSF) with iron is a well-known cause for pn-junction leakage, breakdown of oxides, and retention time (refresh) failures of DRAMs [28, 142–144]. Interestingly, iron not only decorates the existing stacking faults, but also affects their growth. As discussed in the first part of our review [116], the data on the effect of iron on nucleation of silicon-oxide precipitates are contradictory. However, everyone agrees that iron enhances the final stage of growth of silicon-oxide precipitates, i.e., the formation of OSFs [12, 24, 28, 94, 145–147]. Fujino et al. [94] showed that the density of OSFs increased by nearly 5 orders of magnitude as the iron surface contamination level increased from $3 \times 10^{11}\,cm^{-2}$ to $10^{13}\,cm^{-3}$. Likewise, Miyazaki et al. [24] observed higher OSF densities for iron concentrations above $5 \times 10^{12}\,Fe/cm^3$.

The increase of the precipitation rate of iron in polycrystalline silicon, proportional to the density of dislocations, grain boundaries, and intragranular defects, was observed by Bailey et al. [56], and clearly indicated that iron precipitates at these defects. A similar correlation of precipitation rate of iron with the density of silicon-oxide precipitates has been done by Gilles et al. [148, 149]. Experimental studies of Aoki et al. [150–152] showed that the presence of silicon-oxide precipitates does not affect the solubility of iron in the bulk, but changes the kinetics of its precipitation [152]. Aoki et al. [152] performed TEM-EDX (transmission electron microscopy combined with energy-dispersive X-ray analysis) measurements and were able to directly detect iron at silicon-oxide precipitates. Hieslmair et al. [153] developed a quantitative technique for analysis of iron precipitation kinetics. Application of this technique to CZ silicon with different density of silicon-oxide precipitates confirmed that the effective density of precipitation sites for iron correlates well with the density of silicon-oxide precipitates. Hieslmair et al. [154] concluded from their studies that iron is gettered by the surface of silicon-oxide precipitates rather than by associated dislocations. In contrast, Sadamitsu et al. [155], and Ogushi et al. [156] argued that iron is most probably gettered by the bulk of the precipitates.

Besides precipitation of iron at extended defects in the bulk, accumulation of iron at the Si/SiO_2 interfaces or at the bare silicon surface has also been observed [8, 12, 133, 157–162]. We will not discuss in this section the case of a mechanically damaged surface, which provides an efficient gettering sink. Our discussion will be confined to ideal or nearly ideal wafer surfaces or Si/SiO_2 interface. The precipitation of iron near the growing Si/SiO_2 interface may be stimulated by silicon self-interstitials, injected by the growing oxide and consumed by the iron-silicide precipitates, or by local strain fields at the Si/SiO_2 interface [159, 160]. In most cases, outdiffusion of iron to the wafer surface has been observed only as a decrease of iron concentration in thin (a few μm) near-surface regions, and could be suppressed in the presence of internal gettering sites in the wafer bulk [161]. Heiser and Mesli [163, 164] observed the outdiffusion of neutral iron in n-Si to the surface during low-temperature anneals (around 130 °C). They measured the iron distribution profiles within 10 μm from the surface and obtained a good agreement by modeling the surface as an infinite sink. They argued that the outdiffusion has never been observed in p-Si at these temperatures because of the strong interaction of Fe with shallow acceptors, which trap iron in the bulk of silicon before it can diffuse to the surface, and because the electric field in the Schottky–diodes repels the ionized interstitial iron from the surface. However, at higher annealing temperatures, outdiffusion of iron has also been observed in p-Si. Gao et al. [165] measured depth profiles of interstitial iron in the near-surface region and reported a decrease in the near-surface iron concentration after anneals at 400 °C for 2 to 30 min, which can be interpreted as diffusion of Fe from a near-surface layer to the surface. Zoth and Bergholz [48] found that the outdiffusion of iron during cooldown of samples can lead to inverted U-shaped Fe-concentration profiles. Finally, recent studies of Hieslmair et al. [166], who observed outdiffusion profiles of iron after anneals at 525 °C, confirmed that bare silicon surface is an efficient sink for iron in p-Si.

The thermal stability of precipitated iron was studied by Ramappa et al. [167], Colas et al. [168], and Aoki et al. [169] in FZ silicon, and by Aoki et al. [169, 170] in CZ wafers with silicon-oxide precipitates. All of these studies showed that iron is weakly bound at iron-silicide precipitates, and can be dissolved back into the silicon by annealing the samples. Detailed studies of McHugo et al. [171] indicated that the stability of iron at oxygen precipitates somewhat depends on carbon content of the sample. It was found that iron is more stable at oxygen precipitates formed in silicon with low carbon content. It was suggested that carbon reduces the strain, which stabilizes the iron at oxygen precipitates [171].

It is important to note that the relatively low thermal stability refers only to iron, precipitated at already existing extended defects. As we will show below, the presence of iron on the wafer surface *during* silicon dioxide growth may lead to the formation of strong chemical bonds between iron, oxy-

gen, and silicon, with the formation of iron oxides or iron silicides. A number of authors have discussed the possibility of forming other phases of iron which are thermodynamically more favorable than either α- or β-$FeSi_2$ [172–174]. Hackl et al. [174] presented a table of formation energies for possible iron-oxygen-silicon compounds to show that the highest formation energy is for a silicate of Fe_2SiO_4 followed by Fe_3O_4, while $FeSi_2$ has a lower energy of formation by a factor of 18.

Probably the first experimental observation of the effect of strong binding of iron in the surface silicon-dioxide was made in the studies of the solubility of iron in silicon [89, 98, 161, 175]. It was found that if there is no oxide on the surface, and the annealing ambient does not contain traces of oxygen to form such an oxide during the anneal, then all iron deposited on the surface easily diffuses into the bulk. If the wafer surface is covered by silicon dioxide, and particularly if trace concentrations of oxygen or residual water vapors [176] are present in the annealing ambient, iron becomes bound to the surface oxide instead of diffusing into the bulk [94]. Rotondaro et al. [177] reported that in dry O_2, only about 50% of the surface Fe contamination is found in the bulk after diffusion, while the use of N_2 results in a diffusion of 70% to 100% of the contamination into the bulk. Recent Auger electron spectroscopy (AES) and X-ray photoelectron spectroscopy (XPS) studies by Swart et al. [178] confirmed that iron in the oxide indeed forms chemical bonds to silicon and oxygen.

Note that the equilibrium bulk iron concentration after a diffusion in oxidizing ambient may be affected not only by the fraction of iron bound at the surface, but also by the fact that a new boundary phase is formed other than iron silicide $FeSi_2$. A phase with a larger formation energy results in a lower equilibrium solubility of iron in silicon. Colas et al. [168] studied the solution of iron in the presence of oxygen clusters of different morphology and speculated that they might have observed in some experiments formation of an oxygen-iron compound which is more stable that the $FeSi_2$ silicide. However, the possibility of formation of iron oxides or silicates in the silicon lattice was not fully explored until highly-sensitive synchrotron-radiation-based X-ray techniques, which can unambiguously distinguish different types of bonding, became available. Kitano [179] diffused iron into boron-doped CZ silicon wafers through a 20-nm SiO_2 film at 750 °C and 900 °C, removed oxide by HF chemical etching, and studied the state of iron at the silicon surface (former Si/SiO_2 interface) by using the angular-dependent total X-ray fluorescence and X-ray absorption fine structure techniques. It was found [179] that a significant amount of iron was concentrated at the SiO_2/Si interface and that chemical bonds of the type Fe–O, Fe–Si, and Fe–Fe were formed. The valence of iron was a mixture of Fe^{3+} and Fe^{2+}, but mostly Fe^{3+}. From these observations, Kitano [179] inferred that the layer formed by iron at the SiO_2/Si interface is iron silicate, in which a portion of Fe^{3+} ions are reduced to Fe^{2+}, similarly to the natural iron silicate $Fe^{3+}Fe^{2+}_{0.5}[SiO_4]$, known as laihunite. Clearly, similar behavior of iron may also be expected if iron and oxygen co-precipitate in the bulk of the wafer. This was confirmed by recent studies of McHugo [180, 181], who studied iron precipitates, located by X-ray fluorescence (XRF) microprobe in the bulk of mc-Si, with X-ray absorption spectroscopy. Although unambiguous identification of the phase of iron was not achieved, it was concluded that the agglomerated iron was certainly not iron-silicide, but rather an iron silicate, primarily with the valence Fe^{3+}. This is in agreement with the finding of Kitano [179].

Several other workers also discussed the possibility of the formation of iron oxides or silicides. Sadamitsu et al. [12] reported that they found inclusions in silicon oxide when they intentionally contaminated silicon with iron and oxidized it. They suggested from their TEM analysis that the inclusions might be either Fe_3O_4 or Fe_2SiO_4 [12]. The formation of the iron oxide imbedded into the chemical oxide on the wafer surface was suggested by Takizawa et al. [182]. Shimizu [183–186] argued that thermal oxidation of Fe- and Al-contaminated wafers leads to the incorporation of these metals into a growing oxide in the form of $(FeOSi)^-$ negative ions, which are oxidized, during the oxide growth, into neutral metal oxides. In agreement with the observations of [59, 94, 187–189], they found that metals were located primarily at the oxide surface, furthest from the Si/SiO_2 interface. A similar observation was made by Tardif et al. [190, 191], Hocket et al. [192], and Zhong et al. [193]. Takiyama et al. [19] investigated a possibility of chemical reactions of iron with SiO_2 by mixing powders of iron-oxide with silicon-dioxide, sintering them in a nitrogen ambient, and analyzing them by X-ray diffraction. They observed formation of iron-silicates, tentatively Fe_2SiO_4, after sintering at temperatures of 900 °C and above.

Some other models were discussed to explain the accumulation of iron in silicon dioxide. Shimizu et al. [183, 184] suggested that accumulation of iron in the growing silicon dioxide can be explained by slower diffusion of interstitial iron in SiO_2 than oxygen (which would mean that the oxide grows faster than iron can diffuse through it). However, the difference in diffusion coefficients is not so great to explain the aggregation of iron in the silicon dioxide, and also does not explain why iron does not diffuse into the bulk of silicon during post-oxidation anneals. The diffusion coefficient of oxygen in SiO_2 glasses at 1000 °C is from 3×10^{-14} to 3×10^{-15} cm^2/s and about 10^{-18} cm^2/s in quartz [194], whereas the diffusivity of iron in silicon dioxide is about 10^{-14} to 10^{-15} cm^2/s at 1000 °C [157, 195, 196]. The diffusion coefficient in the range of 10^{-14} cm^{-3} implies that iron would diffuse through a 10-nm oxide within several minutes at 1000 °C, i.e., a thin silicon dioxide layer will not keep iron from diffusion into the bulk unless the anneals are very short or the oxide layer is very thick. Hence, iron has to form a stable chemical bond to silicon be effectively bound in SiO_2 even at high temperatures.

One could argue that another possible explanation of agglomeration of iron in SiO_2 would be that amorphous silicon dioxide has a higher equilibrium solubility of interstitial iron than silicon and would serve as a segregation gettering layer (see Sect. 6 for details of segregation gettering mechanism) for iron dissolved in the bulk of the wafer. In this case, iron would segregate from the bulk into the oxide layer. However, experimental data do not support this hypothesis. Yoshimi et al. [161] conducted a series of oxidations of iron-contaminated wafers with intermediate removal of the grown oxide layer. They did not observe any increase in the minority carrier lifetime after this procedure, and concluded that there is no significant gettering of iron by silicon dioxide. Similarly, Smith et al. [197] observed by using NAA that the

concentration of iron in silicon dioxide exceeds the concentration in the bulk by a factor of only 1.3. The same trend, with the concentration ratio varying from 1.3 to 2.6, was observed for 14 other impurities, whereas the concentration of gold was found to be lower in the oxide than in silicon. This implies that the chemical binding of iron to silicon dioxide, reported in the references cited above and in the recent article by Ramappa et al. [196] can be formed only under very specific annealing/oxidation conditions, which are not quite understood yet.

Clearly, interaction of iron with silicon and oxygen with formation of iron oxides and iron silicates appears to be new promising area of research. We believe that the understanding of the interaction of iron with oxygen will give an important insight into the physics of the effect of iron on MOS devices and internal gettering and eventually may even explain the nature of gettering-resistant intragranular recombination centers in solar cells [198–200]. The difficulty with the analysis of these defect reactions is that they apparently occur primarily during growth of silicon dioxide, when both oxygen and iron are mobile and can form chemical bonds. Precipitation of iron at pre-existing extended defects does not seem to result in formation of thermally stable compounds.

4 Iron detection techniques: present state and future trends

Any analysis of iron contamination of silicon seeks answers to three questions: (i) how much iron is present in the sample?, (ii) where is it located?, and (iii) what is its chemical state? The first question can be translated to the integral sensitivity of the method, the second one to its spatial resolution, and the last one to its "chemical resolution". It is clear that the total iron concentration in the sample, although a valuable piece of information, is of limited use for prediction of its detrimental effect. Indeed, if iron is located at gettering sites away from the devices, it will be of no harm to the device performance, whereas the same concentration of iron at the devices may kill the chip. Furthermore, the chemical state of iron determines its electrical activity and the feasibility of gettering it, or its stability if the iron is already at a gettering site. Hence, it is important to know exactly where the iron is, and what complexes or compounds it forms.

Fabrication of today's advanced integrated circuits involves some very complex technology. With shrinking device dimensions and thickness of insulating layers, it has become imperative to reduce metal contamination to the level of $10^{10}\,cm^{-2}$ or less. The detection limit of analytical tools should be at least an order of magnitude below the required threshold contamination levels and at least 100 times less if these measurements are used for statistical process control [2]. Although iron can be accessed by nearly all measurement techniques suitable for studies of defects in silicon, only a few of these techniques can reach the detection limit required for the purposes of contamination control on a production line. Since this review is focused on iron-related problems encountered in today's silicon technology, we intentionally confined our discussion to the experimental techniques that are capable of detection of iron in the *ppt* range and below. These techniques are: minority carrier lifetime techniques, deep-level transient spectroscopy, total reflection X-ray fluorescence, atomic absorption spectroscopy, mass spectrometry, and neutron activation analysis. At the end of the section, we will discuss prospective analytical tools, which may find application in contamination control in the future.

4.1 Minority carrier lifetime techniques

4.1.1 Principles of lifetime measurement techniques. The dominant recombination mechanism in the bulk of nondegenerate extrinsic silicon at room temperature is multiphonon recombination through defect levels in the energy gap (see, for example, [201–206]), described by the model, developed independently by Hall [207] and Shockley and Read [37]. According to the Schokley–Read–Hall model, if excess electron–hole pairs are introduced into a semiconductor, they will recombine with a characteristic lifetime τ. During the time τ, they will diffuse a characteristic distance, $L_{diff} = \sqrt{D\tau}$, known as the minority carrier diffusion length. The diffusion length measurement is more commonly specified for photovoltaics, whereas lifetime is primarily used in integrated circuit engineering. The proportionality coefficient, D, is the minority carrier diffusion coefficient ($33.5\,cm^2/s$ for electrons and $12.4\,cm^2/s$ for holes at room temperature, according to the ASTM standard ASTM F1535-94). The recombination activity of each defect depends on a number of factors, such as the position of its level in the band gap, its capture cross-sections for electrons and holes, the conductivity type and the doping level of the wafer, the density of injected excess carriers, and the temperature. Since most impurities provide recombination channels for minority carriers, lifetime is an important characteristic of the purity of silicon. The sensitivity of lifetime measurements is limited only by the intrinsic band-to-band recombination lifetime, about 0.5 s for $10\,\Omega\,cm$ p-type silicon, which would correspond to the concentration of interstitial iron on the order of $10^7\,cm^{-3}$ [208]. Although more than ten different lifetime measurement techniques are known (see, for example, [206, 209]), we will discuss only the three most commonly used tools: surface photovoltage (SPV), microwave photoconductance decay (μ-PCD), and the electrolytic metal analysis tool (ELYMAT). SPV and ELYMAT measure the minority carrier diffusion length, whereas μ-PCD determines the minority carrier lifetime.

The SPV technique is based on the spectral dependence of surface photovoltage, and is presently used in the constant-flux modification of Lagowski [210]. A band diagram which illustrates the principle of the surface photovoltage effect is presented in Fig. 2. The surface of the wafer is illuminated with chopped monochromatic infrared light with energy slightly greater than the silicon band gap. A change of the near-surface band bending under the influence of illumination is the surface photovoltage, ΔV, which is capacitively captured from the Si surface by a transparent electrode that is brought close to the wafer surface [21, 210]. Assuming that the light intensity is so low that the surface charge density is not changed by the incident light, the relationship between optical absorption coefficient, α, minority carrier diffusion length, L, and surface photovoltage, ΔV, is [21, 210]:

$$\Phi/\Delta V = A(s + D/L)\left(1 + \frac{1}{\alpha L}\right), \qquad (2)$$

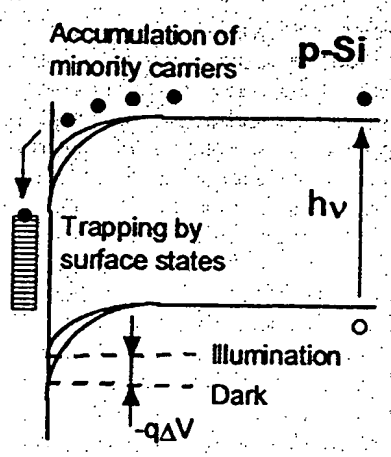

Fig. 2. The energy band diagram near a p-type semiconductor surface in the dark and under illumination. Illumination causes accumulation of minority charge carriers in the depletion layer and changes the surface potential by ΔV, the surface photovoltage. This change is measured by SPV systems.

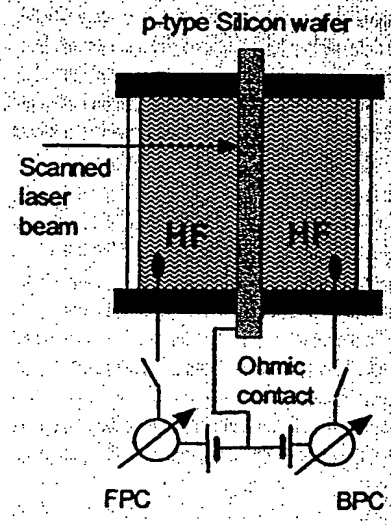

Fig. 3. Schematic diagram of the ELYMAT electrolytic double cell (after [83, 221, 222])

where Φ is the photon flux absorbed at the silicon surface, which is kept constant at all wavelengths, s is the surface recombination velocity of the sample, and A is an equipment constant. According to (2), the diffusion length can be determined from the linear plot of $\Phi/\Delta V$ versus $1/\alpha$ by extrapolating the linear fit to $\Phi/\Delta V = 0$, which corresponds to $L = -\alpha^{-1}$.

SPV is a rapidly evolving analytical tool. Recent advances reported in the literature include an increase in sensitivity by using a higher incident light intensity [211]; the use of a rigorous theoretical treatment of the small signal steady-state surface photovoltage [212], which overcomes the requirement that the diffusion length be shorter than a third of the wafer thickness [213, 214]; the use of a redesigned pick-up electrode to minimize the errors caused by three-dimensional diffusion of excess carriers [215]; an increase in the measurement speed up to about 1000 points per minute [211]; and the development of a procedure to measure oxidized wafers without removal of the oxide film [216, 217]. Additionally, optical dissociation of FeB pairs [218] and corona charging to enhance the SPV signal [215, 219] have been implemented in commercial SPV equipment.

The microwave photoconductance decay technique (μ-PCD) [220] is based on the fact that the absorption constant for microwave radiation propagating through a semiconductor and the reflectivity of the radiation from the wafer surface are determined by the density of charge carriers in the wafer. Modern μ-PCD systems determine the minority carrier lifetime by measuring the time dependence of the microwave reflection from the wafer surface after a short laser pulse. The time constant of the decay of the reflected microwave power to steady-state conditions is determined by bulk recombination lifetime and surface recombination velocity, and enables one to extract the minority carrier lifetime.

ELYMAT [221] determines minority carrier diffusion length from photocurrent generated in a collecting junction formed by a silicon-electrolyte (1% HF) contact illuminated with a laser beam. Figure 3 shows a simplified cross-section of the electrolytical double cell, used in ELYMAT measurements [83, 208, 221, 222]. The Si wafer is in contact with electrolyte on both sides. Since the HF-electrolyte–silicon junction behaves similarly to Schottky contacts [223], then a biased illuminated junction can be used essentially as a solar cell. One surface of the wafer is illuminated with a strongly absorbed scanning laser beam, focused to a spot of about 1 mm^2. Changing the position of the incident laser beam on the surface of the wafer, one can generate a high-resolution map of minority carrier diffusion lengths. Depending on the applied bias, the collecting junction may be on the unilluminated (back) or illuminated (front) surface. The ratio of the backside photocurrent (BPC) and the frontside photocurrent (FPC) gives the diffusion length as [224, 225],

$$I_{\mathrm{BPC}}/I_{\mathrm{FPC}} = 1/\cosh((d-w)/L)\,, \tag{3}$$

where d is the wafer thickness, and w is the thickness of the space-charge region at the biased HF–Si contact. ELYMAT attracted attention in the early 1990s due to its capability of fast high-resolution mapping [223, 226, 227], but has later lost its appeal due to the development of the SPV and μ-PCD techniques, which do not involve toxic HF and are better suited for in-line process control [83].

4.1.2 Identification of the recombination centers. Lifetime techniques, with their non-destructive nature, high sensitivity, and mapping capability would be ideal techniques for contamination control if in addition to an overall evaluation of the contamination level of a wafer, they also could establish the nature of the impurity that affects the lifetime. Unfortunately, as we will show below, only interstitial iron and, in some cases, interstitial chromium, can be reliably identified using lifetime techniques. This is because of the complexity of interpretation of the lifetime and diffusion length measurements. The first problem is that the measured minority carrier lifetime, τ_{m}, is determined by contributions from all defect centers plus a contribution from recombination of minority carriers at the surface:

$$\tau_{\mathrm{m}}^{-1} = \tau_{\mathrm{s}}^{-1} + \sum_{i=1}^{N} \tau_i^{-1}\,, \tag{4}$$

where τ_i is the contribution of each impurity to the bulk lifetime, and τ_s is the surface recombination lifetime. Since it is the bulk recombination lifetime that characterizes the contamination level of a wafer, one has to either make a correction to the measured lifetime for surface recombination in order to determine the bulk lifetime (see, for example, [228–232]), or (which is commonly done) achieve a negligibly low surface recombination rate by an appropriate surface treatment. In fact, lifetime measurements had been very ambiguous, difficult to interpret, and very unreproducible until reliable procedures for surface passivation were developed. Surface recombination is frequently characterized by a surface recombination velocity, s (see, for example, [206] for details). Although the relationship between s and τ_s for a general case is given implicitly by a transcendental equation, the following approximate expression is frequently used [233]:

$$\tau_s \approx \frac{d^2}{\pi^2 D} + \frac{d}{2s}, \tag{5}$$

where d is the wafer thickness, and D is the minority carrier diffusion coefficient.

Typical values of surface recombination velocity are up to 10^7 cm/s for abraded (lapped) surfaces [234], 10^3 to 10^5 cm/s for mechanically polished [203, 233, 235, 236] or chemically etched [228, 237] surfaces covered by native oxide, 1 to 100 cm/s for thermally oxidized Si surfaces [229, 230, 236–242], about 20 cm/s and 4 cm/s after immersion of the sample in bromine in methanol and iodine in methanol, respectively [236, 239, 242], and 1 to 0.25 cm/s after immersion in HF [239, 240]. The surface recombination velocity was shown to be also affected by the removal of hydrocarbon contamination (for example, by etching in a mixture of sulfuric acid and hydrogen peroxide) before HF etching [243], the duration of the HF etch [244], the oxidation temperature and the type of post-oxidation heat treatment [243], the annealing of the oxidized wafers [242], the application of corona charge to oxidized wafers [245], and the illumination of the wafers with ultraviolet light [246–249].

After the surface recombination is accounted for, and the bulk minority carrier lifetime is measured, one needs to identify the recombination centers and to determine their concentration. Essentially, there are five experimental approaches used to determine the nature of recombination centers in lifetime measurements: (i) the analysis of the dependence of lifetime on injection level [113, 208, 250–261], (ii) the analysis of the dependence of lifetime on temperature [234, 262–264], (iii) the comparison of the lifetime in samples, which have the same type of contamination, but different types of conductivity [265, 266] or different doping levels [267], (iv) the comparison of the bulk lifetime with surface recombination lifetime or ELYMAT dark current after application of a standard procedure of surface passivation (this procedure is expected to be effective for detection of haze-forming metals such as Ni or Cu since they tend to diffuse to the surface, which affects primarily the surface recombination velocity [21, 111, 112, 193, 210, 268–272]), and finally (v) the analysis of a change in lifetime (or diffusion length) as the result of a defect reaction, stimulated by heat or light (such as FeB dissociation) [48].

A dependence of lifetime on injection level can be measured only with ELYMAT or μ-PCD techniques since their injection level can easily be varied from $\eta = \Delta n/p_0 = 10^{-3}$ to 10 in 10 Ω cm p-type silicon (n is the density of injected electrons, and p_0 is the equilibrium hole density) by varying the laser power, or by using neutral density filters [208, 273, 274]. SPV is poorly suited for analysis of injection level dependence since it requires linear dependence between the surface photovoltage and the incident flux, which can be achieved only for very low injection levels of $\eta < 10^{-5}$ to 10^{-7}.

A dependence of lifetime on injection level for Fe_i and FeB pairs is shown in Fig. 4. The recombination activity of FeB pairs depends very weakly on the injection level. On the contrary, the recombination activity of interstitial iron changes by more than a factor of 40 over a change of the injection level by 4 orders of magnitude. For injection levels higher and lower than those shown in Fig. 4, the Fe_i-limited lifetime tends to saturate and becomes almost independent of the injection level.

The fact that the lifetime limited by FeB pairs is almost independent of injection level is frequently used in ELYMAT and μ-PCDS techniques to identify FeB pairs. It was shown that the lifetime limited by FeB pairs is inversely proportional to the concentration of FeB pairs [253, 275, 276]:

$$\tau\,(\mu s) = k/N_{FeB}\,(cm^{-3}), \tag{6}$$

where k is the proportionality coefficient, which lies, according to different literature sources, between 1×10^{13} [253], 1.04×10^{13} [252], 2×10^{13} [275], 2.5×10^{13} [187], and 2.9×10^{13} [276]. Our own fit, based on the data points

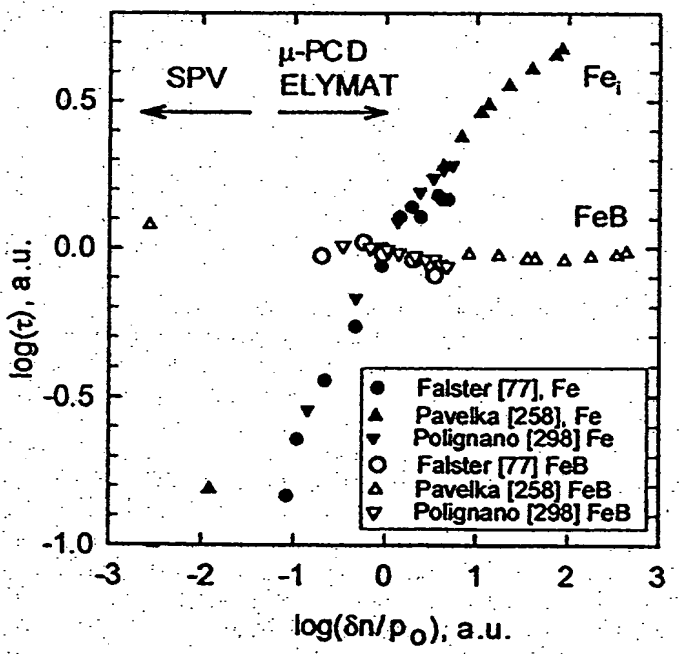

Fig. 4. The injection-level dependence of the lifetime in iron-contaminated samples before and after dissociation of FeB pairs. To plot data from [77, 258, 298] with different Fe contamination levels in a single graph, data points were normalized in such a way that all plots go through the origin. A strong dependence of the iron-limited lifetime on injection level is clearly seen. Resistivity of the samples was 50 Ω cm [77], 20 Ω cm [298], and 8–15 Ω cm [258]. The actual injection level at this cross-section point was equal to $\delta n/p_0 \approx 1$ in [77], $\delta n/p_0 \approx 0.5$ in [298], and $\delta n/p_0 \approx 0.1$ in [258]

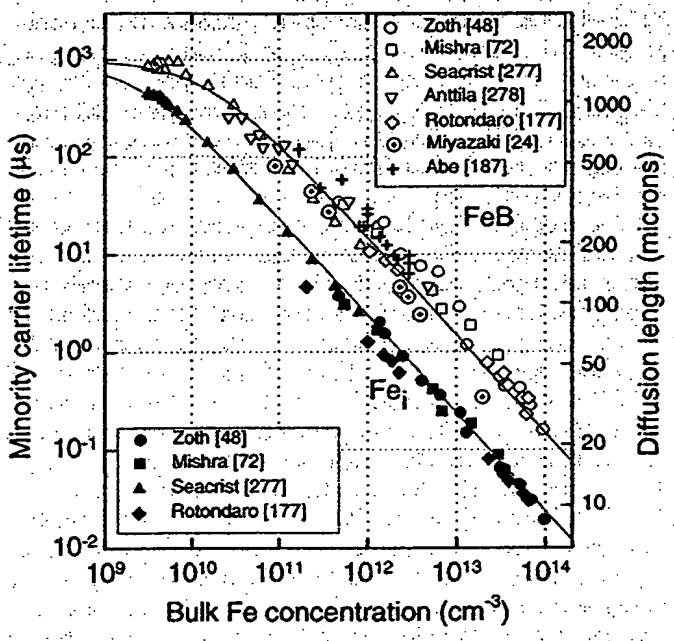

Fig. 5. The dependence of the lifetime limited by iron in the form of interstitial iron or FeB pairs on the iron contamination level. *Solid lines* are simulations according to (6) and (8), assuming $\tau_s = 1$ ms

from [24, 48, 72, 177, 277, 278] and presented in Fig. 5, resulted in the value of $k = 1.5 \times 10^{13}$ μs/cm^3. This value corresponds to the effective electron capture cross-section of FeB pairs of $\sigma_n^{eff} \approx 4 \times 10^{-15}$ cm^2, in agreement with the value reported in [225, 276, 279–281] and tentatively identified as the electron capture cross-section of the acceptor state of FeB pairs.

The main technique to determine the iron concentration by SPV is the analysis of the change of lifetime as the result of the dissociation of FeB pairs. It is now well established that for low injection levels, Fe_i is about 10 times more efficient a recombination center than FeB [48, 218] (see also Figs. 4, 5). Hence, the difference between the lifetimes determined by recombination via Fe_i and FeB pairs can be used to determine the interstitial iron concentration [48]. The minority carrier diffusion length measured by SPV before (L_0) and after (L_1) dissociation of the FeB pairs is quantitatively related to the concentration of interstitial iron, N_{Fe}, as follows [48]:

$$N_{Fe} = 1.06 \times 10^{16} \times (L_1^{-2} - L_0^{-2}) \ (cm^{-3}), \qquad (7)$$

where L_0 and L_1 are measured in μm. It is important to remember that (7) is valid only for low injection levels as used in the SPV technique. Furthermore, the coefficient 1.06×10^{16} in (7) is valid for silicon wafers with resistivity of 5 to 10 Ω cm silicon and may vary within the range of about ±30% depending on the Fermi energy level, i.e., on the resistivity of the wafers [282]. Using for the diffusion coefficient $D_n = 33.5$ cm^2/s for electrons in high-purity 10 Ω cm p-type silicon, the same equation in terms of lifetimes is

$$N_{Fe} = \frac{1.06 \times 10^{16}}{D_n} \left(\tau_1^{-1} - \tau_0^{-1}\right) = 3.16 \times 10^{12} \left(\tau_1^{-1} - \tau_0^{-1}\right), \qquad (8)$$

where τ_1 and τ_0 are measured in μs, and N_{Fe} is obtained in the units of cm^{-3}. Equations (7) and (8) were confirmed by studies of numerous groups [24, 48, 72, 177, 277, 278] and are valid in a wide range of iron contamination levels, as is demonstrated in Fig. 5. This procedure for measuring iron concentration can also be used with some limitations (low injection level) in ELYMAT and μ-PCD studies. Mishra et al. [72] reported that an equation similar to (7) holds also in aluminum-doped silicon, although with a different coefficient since the difference in recombination activity of FeAl pairs and Fe_i is about two times less than in the case of FeB and Fe_i.

FeB pairs can be reversibly dissociated either by a thermal anneal of the samples at 200 °C for 10 min followed by a quench, or by 15 to 90 s illumination with a halogen lamp. The important assumption which (7) and (8) are based on is that Fe_i is the only defect to undergo a point defect reaction at 200 °C, or under illumination. Unfortunately, it is now firmly established that several other defect reactions may also take place during heating or illuminating of wafers. The examples of other defect reactions that can be triggered by a treatment similar to that used for dissociation of FeB pairs, are dissociation of CrB pairs [283], dissociation of copper-related complexes [284], and formation/dissociation of boron–oxygen complexes [285–288]. Consequently, one has to take precautions to unambiguously distinguish the effect of iron contamination from that of other impurity complexes. The simplest test is to compare the absolute values of diffusion lengths before and after thermal/optical activation with the expected diffusion length for the calculated concentration of iron. If this test indicates that the diffusion length is much lower than expected for the iron contamination level, calculated from the difference in the diffusion lengths before and after dissociation of FeB pairs, one should be cautious with interpretation of the results. A useful (although time-consuming) method to distinguish iron from other impurities from diffusion length measurements is to follow the kinetics of formation of FeB pairs after dissociation [2, 111]. Since the time constant of association of metal-acceptor pairs is described by Hams law, $\tau_{pairing} \propto 1/N_A D$ (see [289, 290]), is inversely proportional to the interstitial diffusivity of the metals, D, this time constant is a good means for identification of the diffusing metal. For example, the recovery reaction of CrB pairs [283] is about an order of magnitude slower than that of FeB pairs [2], and the change of diffusion length measured at low injection level has different sign (increases for Fe and decreases for Cr, as the pairs are formed). Finally, the recently reported decrease in minority carrier lifetime in copper-contaminated wafers under the influence of light or heat, which was explained as dissociation of copper-related defects was found to be an irreversible reaction [284]. The formation of B–O complexes, stimulated by light, can be reversed only by annealing the samples at elevated temperature [285, 287, 288]. FeB and CrB pairs can be distinguished by comparing photo- and thermal dissociation of pairs: FeB pairs can be decomposed by light at room temperature, whereas an anneal at 200 °C would dissociate both FeB and CrB pairs. This is because CrB pairs [283] can be decomposed by light only if the temperature exceeds 60 °C [2, 258].

4.1.3 Comparison of lifetime measurement techniques. As discussed above, the sensitivity of lifetime measurement techniques to iron is limited by the sensitivity of the experimental equipment and by other recombination channels available in the wafer, including the surface recombination. Due to the improvements in the SPV apparatus and development of surface passivation methods, the detection limit of iron in silicon has been steadily improving during the last decade from about 10^{11} cm^{-3} [111] in 1992 to the present value of about 2×10^9 cm^{-3}, in the IC processing line environment [2, 277], and down to 8×10^7 cm^{-3} under laboratory conditions [218, 219].

Surface contamination levels can be measured only after diffusion of surface contaminants into the bulk [64]. Zoth and Bergholz [48] used RTA anneals at 1200 °C and found that about 80% of the Fe on the surface ends up in the bulk; the rest presumably evaporates or remains in the near-surface silicides. Assuming that 2×10^9 cm^{-3} is the sensitivity routinely achievable by SPV, then, using a clean RTA heat treatment to drive-in iron, one can expect the surface sensitivity of SPV to be of 8×10^7 cm^{-2} [2].

The sensitivity of μ-PCD and ELYMAT to iron is somewhat difficult to evaluate accurately since the dissociation of FeB pairs, which is the best technique to distinguish iron from other recombination centers, can only be used with these techniques if the injection level is kept much lower than is used in normal operating conditions. This results in poor signal-to-noise ratios and poor sensitivity. To improve the sensitivity of μ-PCD at low injection levels, Romanowski et al. [291, 292] suggested frequency-resolved μ-PCD, in which short pulses of light are substituted by sinusoidally-modulated light. Gaubas et al. [293] claimed that the use of μ-PCD technique in the transmission mode enables one to improve the sensitivity of the instrument.

The measurement of FeB concentrations at 5 or 9 points on a wafer using optical excitation can be done in about 1 min. A high-resolution map (about 6000 points) of the iron distribution throughout the wafer takes, using the modern SPV equipment, about 13–14 min [211, 219]. Recently developed non-steady-state algorithms (see [282]) should lead to even higher data acquisition rates and an increased accuracy of the long diffusion length measurements. The mapping capabilities of μ-PCD and ELYMAT are comparable to those of SPV. Mapping of silicon wafers can be extremely helpful in tracking down the sources of contamination by revealing the geometry of the contamination patterns [99, 294]. Such images can often result in a clear and instantaneous picture of the mechanism of how the contamination was introduced. For instance, the "butterfly" pattern with two high-lifetime zones surrounded by lower lifetime values is diagnostic for contamination from spray cleaning tools [275], whereas dot-like patterns usually point to supporting pins as the source of contamination. Furthermore, crystal defects other than metal contamination, such as oxygen precipitates or slip lines, can be readily identified and distinguished by their characteristic lateral configuration.

SPV is applicable only to wafers with resistivity greater than 0.1 Ω cm since recombination in heavily doped semiconductors is determined primarily by the Auger recombination, not related to the defects [21]. Although SPV can be applied to both n-Si and p-Si, quantitative determination of Fe concentration via the dissociation of FeB pairs is clearly possible only in p-Si. Furthermore, since neutral interstitial iron is a poor recombination center since $\sigma_n(Fe_i^+) \gg \sigma_p(Fe_i^0)$ (see [116]), detection of trace concentrations of iron in n-Si by lifetime methods is feasible only with poor sensitivity [295].

The fact that FeB dominates recombination in most silicon wafers and is weakly dependent on the injection level is the underlying reason why, in general, such surprisingly good correlation is found between such disparate (from an injection level perspective) measurement techniques as SPV (very low injection), ELYMAT (medium injection level), and μ-PCD (usually high injection level) [77]. A good correlation was reported by numerous groups who compared different lifetime measurement techniques, such as SPV and ELYMAT [225, 256, 261, 268, 275, 296], SPV and μ-PCD [177, 275, 277, 296, 297], or ELYMAT and μ-PCD [77, 256, 277, 298]. Although some discrepancies (usually within ±30%) were observed, they were not reproducible from group to group and could be explained [297] as the influence of different surface preparation, affecting each of the techniques to a different degree. Although these techniques are comparable in their capability of measuring and mapping the lifetime of minority carrier in silicon wafers, SPV is the most suitable technique for determination of iron contamination levels since it inherently uses low excitation levels, which enables one to use the algorithm given by (7). However, the concentration of iron can be determined reliably only as long as iron is homogeneously distributed throughout the wafer thickness, and as long as it does not form any complexes other than FeB pairs. If iron has precipitated, lifetime techniques will not be able to identify it or to determine its concentration.

A very important potential application of lifetime measurement methods is the characterization of epi-wafers. Several groups attempted to develop experimental procedures to measure lifetimes in p/p$^+$ epi-wafers [299–304]. The problems to be solved are how to confine injection and recombination of the minority charge carriers to the epitaxial layer only, and how to avoid effects from recombination at the surface or in the substrate. Lowell et al. [302] suggested to conduct SPV analysis of epi-wafers by using a set of filters with very shallow (several μm) light penetration depth. A similar idea was utilized by Pavelka et al. [303], who used short wavelength laser excitation to generate minority carriers primarily in the epi-layer. Using efficient surface passivation techniques (such as corona charge or the oxide or iodine passivation), Pavelka et al. [303] were able to characterize epi-layers by μ-PCD technique. A combination of low-penetration depth light, corona charge surface passivation, and frequency-resolved SPV technique has been recently introduced in a commercial instrument called "Epi-τ" by Semiconductor Diagnostics, Inc. This technique was recently evaluated by Buczkowski et al. [304], who reported that the minority carrier lifetime measured by the Epi-τ technique is not necessarily equal to the lifetime in the epi-layer since it can be affected to a certain extent by the substrate properties, surface barrier height, and surface recombination velocity. They pointed out that these effects are not properly taken into account in the presently available theoretical model. Nevertheless, they found that the instrument can de-

liver valuable data on lifetime useful in epi or denuded zone process monitoring [304].

4.2 *Deep-level transient spectroscopy (DLTS)*

DLTS was introduced in 1974 by Lang [305, 306] and quickly became a major laboratory technique for the detection of impurities in silicon and the investigation of defect reactions. DLTS proved to be a sensitive, relatively inexpensive, and very versatile research tool, which can identify and measure the concentrations of a wide range of impurities. DLTS detects deep level traps in a thin (about 0.5 to 3 μm) near-surface depletion layer formed by a reverse biased Schottky-diode or a p-n junction. The principles of the DLTS technique are illustrated in Fig. 6. The width of the depletion region is a function of the applied reverse bias and of the total concentration of ionized impurities (including shallow acceptors/donors and deep level defects). As the applied bias voltage is rapidly increased, the majority charge carriers will swiftly (typically within less than 10^{-10} s) drift out of the depletion region, leaving the ionized shallow donors/acceptors behind. The charge carriers trapped by the impurities will also eventually leave the depletion region after they are thermally emitted to the conduction (in n-Si) or valence (in p-Si) band. This process, however, is much slower than the drift of free charge carriers, and can be observed by monitoring changes in the capacitance of the diode. As shown in [307–309], the capacitance changes are exponential with the time constant $\tau \propto 1/(\sigma T^2 \exp(-\Delta E/k_B T))$, where σ is the capture cross-section of the trap, ΔE is the enthalpy of emission of a charge carrier from the trap, T is the temperature, and k_B is the Boltzmann constant. The amplitude of the capacitance transient, ΔC, is proportional to the density of traps, N_t, and inversely proportional to the doping level, N_d, as $2\Delta C/C = N_t/N_d$. The sensitivity of DLTS is usually in the range of $N_t/N_d \approx (10^{-5}$ to $10^{-6})$. Hence, the absolute sensitivity of DLTS measurements is determined as a fraction of the doping level, and is higher in the samples with higher resistivity. The essential feature of DLTS, which significantly improves its accuracy and sensitivity, is that the bias voltage is changed periodically up to 1000 times per second, and the observed capacitance decays can be accumulated and averaged over the time. Exponential analysis of the transients taken as a function of temperature gives activation energy for emission of charge carriers from the trap, majority carrier capture cross-section of the trap, and the trap concentration. By varying bias voltage, filling pulse duration, and amplitude of the pulses, one can study depth distribution of the traps in the depletion region, distinguish donor and acceptor traps, and make distinction between point and extended defects [308, 309].

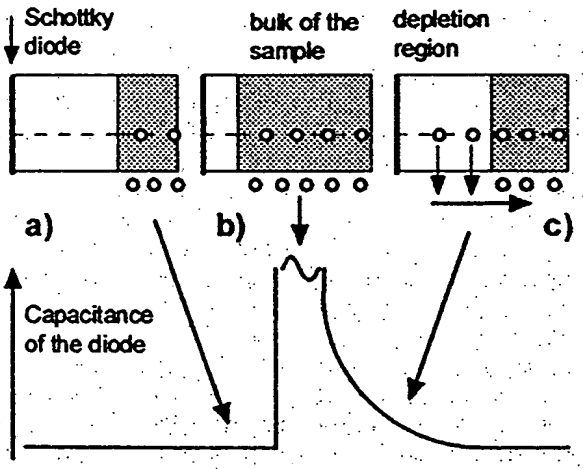

Fig. 6. A diagram illustrating the principle of DLTS. A reverse bias, applied to a Schottky diode (a) is decreased to a low value for the duration of a filling pulse (typically for less than 1 ms) (b), and then restored to its original value (c) Deep traps filled during the filling pulse emit the captured majority charge carriers with a time constant, determined by the temperature and parameters of the traps. The process of emission is observed by monitoring changes in capacitance of the diode. Parameters of the trap can be extracted from the temperature variation of the time constant of capacitance decay

As discussed in our first review [116], interstitial iron forms an energy level at $E_V + 0.38$ eV ($\sigma_p = 3.9 \times 10^{-16} \times \exp(-0.045\,\text{eV}/k_B T)$ cm^2, $\sigma_n \approx 4 \times 10^{-14}$ cm^2). Since interstitial iron is not stable in the silicon lattice due to its very low equilibrium solubility at room temperature, it forms pairs with shallow acceptors such as boron. FeB pairs form a level at $E_V + 0.1$ eV, $\sigma_p = 4 \times 10^{-15}$ cm^2 to 1.5×10^{-13} cm^2, $\sigma_n \approx 4 \times 10^{-13}$ cm^2. Both, the levels of Fe_i and FeB pairs, are easily accessible by DLTS. The detection limit of Fe_i or FeB pairs in silicon wafers with resistivity of 10 Ω cm ($N_d \approx 10^{15}$ cm^{-3}) is about 10^9 to 10^{10} cm^{-3}. One DLTS measurement (including chemical cleaning of sample surface, evaporation of Schottky diodes, and making a DLTS temperature scan) can be accomplished within 3 to 4 h.

Despite all the advantages mentioned above, DLTS has several limitations. It detects only those defects that have deep levels in the band gap. If an impurity has partly precipitated, only the concentration of its electrically active fraction can be determined. DLTS is a destructive technique and requires fabrication of a Schottky diode on the sample. Since DLTS probes defects only a few μm under a Schottky diode of 0.5 to 5 mm in diameter, one measurement represents deep levels in only 0.00005% of the volume of a 4″ wafer. A mapping capability of the DLTS technique is severely limited since each measurement takes several hours. Thus, a single DLTS measurement may not be representative of the total contamination level of the wafer, if the impurity is nonuniformly distributed. In the latter case, there is a substantial possibility of overlooking even a high contamination level by using DLTS measurements alone. Therefore, if possible, wafers should be first scanned by SPV, ELYMAT, or μ-PCD to check for possible inhomogenities in bulk contamination. DLTS cannot be applied to analysis of heavily doped substrates because one cannot prepare good Schottky diodes on p^+ or n^+ silicon.

Although the energy level and the capture cross-section of a deep level are, in principle, sufficient for identification of the impurity, uncertainties up to 5% in energy determination and up to 2 orders of magnitude in capture cross-section are not uncommon for DLTS (see [310]) and frequently make identification of traps ambiguous. For instance, it is usually hard to separate the level of FeB pairs from the overlapping levels of Cu-pairs in p-Si [311]. Although these uncertainties are not inherent in DLTS and can be overcome by using sophisticated techniques for evaluation of capacitance transients or DLTS spectra (see, for example, [312–314]), these accurate techniques are seldom used. Finally, DLTS scans only the upper (in n-Si) or lower (in p-Si) halves of the band gap, un-

less p–n junctions are used, and is poorly suited for detection of minority carrier traps. The latter drawback is overcome by using light pulses instead of a change in the reverse-bias voltage to disturb equilibrium occupancy of the traps. Several modifications of DLTS with optical excitation are known, such as deep level optical spectroscopy (DLOS) [309,315], optical DLTS (ODLTS) [309,316], and minority carrier transient spectroscopy (MCTS) [309,317].

DLTS can be used for surface analyses only if the surface contaminants are driven into the silicon bulk by a high-temperature heat treatment of the wafer [318]. For instance, a good correlation between the bulk and the surfaces concentrations in the contamination range from 10^{11} to 10^{13} cm^{-2} was reported by Anttila et al. [278], and Hackl et al. [174].

4.3 Total reflection X-ray fluorescence

X-ray fluorescence analysis is based on the interaction of X-ray photons with matter which results in the ejection of a core electron from the atoms in the sample. The ionized atom in nonequilibrium state returns to its normal state within an extremely short time via the transition of electrons from the outer shells to the inner shells and emission of an X-ray photon whose energy is the difference between the binding energies of the two shells. The energies of the emitted photons are characteristic for each individual element, and can be used to determine the composition of the sample. XRF analysis is a spectroscopic method, which can determine concentrations of a wide spectrum of elements from a single measurement, independently of the chemical state of these elements in the sample. Solids can be analyzed directly with no or little sample preparation, and no vacuum or control of the temperature of the sample is usually required. All elements with atomic number greater than $Z = 11$ (sodium) can be detected [58,319]. The light elements with $Z < 11$ are difficult to detect since their principal XRF emission lines are in the range of long wavelengths $\lambda \geq 10$ Å, where most X-ray detectors lose sensitivity. If a windowless detector is used and the measurements are done in vacuum, one can obtain acceptable sensitivity also for the lighter elements down to $Z = 6$ (carbon) [320–324].

Since the escape depth of emitted X-rays in the matter is usually limited to less than about 100 μm, XRF is well suited for analysis of impurities on the surface and in the near-surface layers of the samples. Unfortunately, the sensitivity of classical XRF does not exceed the ppm range, which is too low for trace analysis of impurities in silicon. This is because of the background radiation added to the XRF emission spectrum of the sample by elastic and Compton scattering of the exciting radiation in the substrate (silicon wafer), and by bremsstrahlung from photoelectrons induced by the incident X-rays. An important advance in the XRF technique, which improved the sensitivity to surface contaminants by about five orders of magnitude, was achieved by using the total reflection X-ray fluorescence technique [319,324–326]. A typical TXRF system is sketched in Fig. 7. An X-ray beam from a conventional X-ray tube illuminates the wafer surface at glancing incidence so that the condition for total external reflection of the X-rays is met, thereby limiting the X-ray penetration depth to the top 3 nm of the wafer. This greatly reduces the undesirable background X-ray radiation

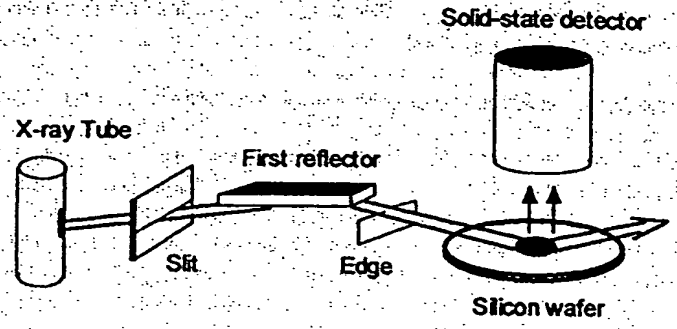

Fig. 7. The basic design of a TXRF instrument

from the substrate because the incident radiation practically does not penetrate into the material. Additionally, the fluorescence radiation from the surface contaminants is doubled in intensity because the impurity atoms are excited by both the incident and the reflected radiation [323]. The critical angle of total reflection of X-rays from silicon depends on the energy of the incident beam. The value of φ_{crit} is about 0.21° for the X-ray energy of 8.4 keV, 0.10° for X-ray energy of 17.44 keV, and 0.051° for X-ray energy of 35 keV [58]. To avoid technical difficulties with excessively low incidence angles, relatively low-energy X-rays are used (typically from 8 keV to approximately 30 keV). Since the emission spectrum of an X-ray tube is not monochromatic, it is first filtered by deflecting the X-rays by what is called the first reflector (Fig. 7). A simple quartz block acts as a totally reflecting mirror or low-pass filter and is generally sufficient, although more sophisticated systems may use multilayer filters. The fluorescence radiation from the surface atoms is detected using a Si(Li) X-ray energy-dispersive detector, located perpendicular and close to the sample surface. The details of the TXRF measurement systems and description of procedures used for analysis of obtained spectra can be found in [58,327,328].

TRXF requires calibration by measuring a standard with a known contamination level. A discussion of the issues or preparation of standards suitable for analysis of silicon wafers, and of accurate determination of absolute values of surface contamination can be found in [329–333]. The principle peaks of X-ray fluorescence spectra associated with iron are at 6.403 keV (K_{α_1}) and 7.057 keV (K_{β_1}). Usually, iron is considered to be unambiguously detected if both of these peaks are observed. Since the detection limit of TXRF is inversely proportional to the square root of the counting time, one has to find a compromise between the sensitivity and the throughput of the system. For trace analysis, the counting time is usually in the range of 100 s to 1000 s [83]. Mapping of a wafer is also possible, although it is time-consuming (a single map may take up to 12 h, [334]). TXRF usually focuses X-rays in an approximately 0.5 cm^2 spot on the wafer surface, so the resolution of the mapping is low.

TXRF can in principle be used to measure the bulk contamination of silicon [335,336]. For bulk analysis, the sample is dissolved in a mixture of HNO_3 and HF. Dissolution of silicon or silicon oxide results in formation of hexafluorosilic acid H_2SiF_6 : $3Si + 4HNO_3 + 18HF \rightarrow 3H_2SiF_6 + 4NO + 8H_2O$, or $SiO_2 + 6HF \rightarrow H_2SiF_6 + 2H_2O$. The compound H_2SiF_6 is unstable and is decomposed according to $H_2SiF_6 \rightarrow SiF_4 + 2HF$. The silicon fluoride SiF_4 is volatile

and is evaporated by heating the vessel with the solution. After evaporation and cooling, the residue is taken up with a small quantity of diluted HNO_3. About 10–50 µl of the solution is transferred to a cleaned quartz glass carrier, dried, and analyzed by TXRF. This procedure makes it feasible to determine bulk contaminants in the ppb range and eventually even in the ppt range. The same dissolution procedure is routinely used for atomic absorption spectroscopy, discussed in Sect. 4.4.

The composition, thickness, and even the density of the top layers in a range up to about 500 nm from the surface can be accessed by varying the penetration depth of X-rays into the substrate. This is achieved by a continuous variation of the angle of incidence [330, 337–342].

There is a noticeable trend of gradual improvement in the detection limit of TXRF for iron, and most other critical elements, from 10^{11}–3×10^{11} cm^{-2} in the late 1980s (see, for example, [343, 344]) to 10^{9}–10^{10} cm^{-2} in the 1990s (see, for example, [82, 83, 174, 322, 337, 339, 345–349]). The sensitivity of TXRF can be further improved by irradiating the sample surface by two X-ray beams incident from perpendicular directions in order to increase the intensity of the X-ray fluorescence [350, 351]. Another way to achieve higher detection limits is to use synchrotron radiation as a source of X-rays [352, 353]. A sensitivity of $(2-5) \times 10^{8}$ cm^{-2} was reported for synchrotron TXRF in [354–358]. This improvement is due to (i) a much higher photon flux illuminating the sample; (ii) synchrotron radiation that is over 95% linearly polarized in the horizontal plane, which reduces the Compton-scattered phonons by about an order of magnitude; (iii) a high degree of collimation of the synchrotron radiation, ensuring that the photons are incident on the sample at a well-defined angle [355, 359]. A clear disadvantage of synchrotron-radiation TXRF is that it requires a large-scale piece of equipment, the synchrotron, which is not widely available for research work and even less so for routine analysis.

A more common way to increase the sensitivity of TXRF analysis to surface contaminants is to use the vapor phase decomposition technique (VPD). The VPD technique was originally developed for use with atomic absorption spectroscopy (see Sect. 4.4) [360, 361], and was later adopted for TXRF [83, 348, 353, 361–363]. In a reaction chamber, the wafer is exposed to the vapor of hydrofluoric acid, which dissolves the SiO_2 surface layer (native or thermal oxide) according to the reaction: $SiO_2 + 6HF \rightarrow H_2SiF_6 + H_2O$. The impurities on the surface are contained in the resulting water droplet or moisture film. Then, a droplet of ultrapure water or an aqueous solution of H_2O_2 and/or HCl and/or HF and/or HNO_3 is swept across the surface to collect the contaminants. An automated system is required to ensure reliable reproducible collection of the dissolved impurities [353, 364]. After the water is evaporated, the residue is analyzed by TXRF. The VPD step prior to TXRF improves the sensitivity of the analysis up to two orders of magnitude (which is essentially the ratio of the total area of the wafer surface, from which the impurities were collected, to the analysis area of TXRF (0.5 cm^2)) and reaches 10^{9} cm^{-2} for 100-mm wafers and 5×10^{8} cm^{-2} for 150 mm wafers [209, 278, 348, 362, 365]; even the sensitivities of 1×10^{8} cm^{-2} [329] and 8×10^{7} cm^{-2} [82] were reported. The total time required for the VPD step is in the range of several hours. VPD-TXRF was demonstrated to have an excellent reproducibility [363]. One of the key points in VPD-TXRF analysis is the drying procedure. A good reproducibility was observed only if vacuum drying of the droplet was used [83].

Typical applications of TXRF in the semiconductor industry are: the analysis of starting wafers, the monitoring of cleaning processes, and the analysis of implanted wafers as equipment control step [174, 278, 321, 343, 347, 366, 367]. A disadvantage of TXRF is that it is limited to investigations of the polished front side, and generally cannot be applied to processed wafers. Lavoie et al. [368] tested how TXRF can be applied to actual product wafers at various points in the manufacturing process where the surface planarization technique has been used. They reported that although non-idealities of the processed and planarized wafers resulted in a decrease of sensitivity by a factor of 100, they could reach a detection limit of 10^{11} cm^{-2} by using a state-of-the-art TXRF spectrometer. Hockett [345] reported the application of TXRF to the unpolished backside of a wafer, also with a significant loss of sensitivity.

4.4 Atomic absorption spectroscopy

Atomic absorption spectroscopy (AAS) was introduced in 1955 by Walsh [369]. The technique is based on Beer's law, which states that if an atomized element is irradiated with the light of its own characteristic resonance wavelength, then the absorption of the light is exponentially proportional to the concentration of absorbing atoms of this element in the light path. An atomic absorption spectrometer, schematically presented in Fig. 8, consists of the following major components: a stable light source, emitting the sharp resonance line of the element to be determined (usually, so-called hollow-cathode lamps are used; special lamps for each element are available); an atomizer which has a sufficient temperature to produce an atomic vapor of the sample; a monochromator to isolate the resonance line; and a photomultiplier that detects the intensity of transmitted light and measures the absorption. The atomizer can be either a flame system (as shown in Fig. 8) or an electrothermal atomizer such as a graphite tube furnace (introduced by L'vov [370]; see also [371–373] for later modifications). A comprehensive description of the physics of AAS and of the experimental equipment can be found in numerous textbooks (see, for example, [374–377]).

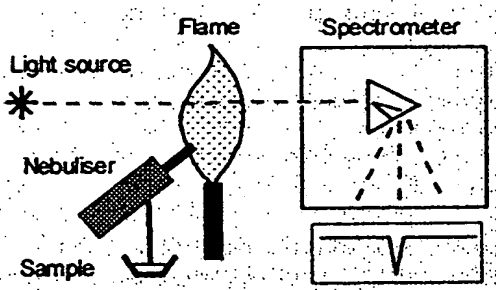

Fig. 8. A schematic diagram of an AAS instrument. The dissolved sample is injected into a flame, where it causes adsorption of the transmitted light. GF-AAS instruments use a graphite tube heated by electrical current instead of the flame torch to achieve better sensitivity

AAS can be readily applied for detection of iron in silicon by monitoring the absorption of light by iron atoms at 238.204 nm [378]. The modification of AAS utilizing a graphite furnace as an atomizer (known as GF-AAS) is more suitable for the detection of trace concentrations of iron in silicon than flame AAS. This is because the sensitivity of GF-AAS to iron is about 300 times higher than that of the conventional AAS [376]. This sensitivity improvement is mainly due to the conversion of nearly all of the analyte in the sample into atoms and to a longer lifetime of the individual atoms in the vapors in the light path than can be achieved by flame. GF-AAS found applications in the silicon industry only in 1996, when Okuuchi et al. [379] and Shabani et al. [158,380] developed an experimental procedure for quantitative studies of redistribution of transition metals in silicon wafers during outdiffusion and gettering. AAS analyzes mainly liquids, and thus requires that the sample containing the impurity is dissolved. The corresponding impurity concentration in the bulk of the sample must be then recalculated. A standard procedure used for dissolution of Si wafers is described in Sect. 4.3 above, and takes much longer than the measurement itself. It was pointed out in the literature [381] that the detection limit required by the silicon technology can be achieved only if AAS is operated in a class-10 cleanroom, and if all chemicals used in the analysis are pre-analyzed to verify their purity before use.

The etching of thin layers of silicon (0.01 to 10 μm) with subsequent AAS analysis of the etchant was suggested in 1994 by Takenaka et al. [382]. To achieve a better etching reproducibility, Shabani et al. [380] suggested the one-drop sandwich etching technique. In this method, one droplet (typically 1 ml) of a mixture of HF and HNO_3 solution is placed on the surface of a clean Teflon plate. The droplet is then sandwiched between the wafer and the plate. After 2 min, the wafer is removed and the droplet of etchant, remaining on the plate, is analyzed with GF-AAS. This technique enables one to achieve sensitivity for Fe of 10^{13} cm^{-3} [379], if only thin layers (1 μm) are etched from the surface of a silicon wafer and analyzed, and 5×10^{11} cm^{-3}, if the whole wafer is dissolved.

AAS is also suitable for the analysis of impurities in the oxide layer or on the wafer surface. This is possible using the vapor phase decomposition (VPD) technique or a one-drop sandwich etching technique. The VPD technique was discussed in Sect. 4.3 above. The combination of VPD technique with AAS, introduced by Shimazaki et al. [360], enabled them to achieve the sensitivity to metal contamination on the surface of silicon oxide up to 10^9 cm^{-2}. The detection limits in the subsequent reports were scattered from 3×10^{10} cm^{-2} down to 1×10^8 cm^{-2}, probably due to variations in the sample preparation procedure [82, 83, 209, 361, 383].

4.5 Mass spectrometry

A mass spectrometer is an apparatus that produces a beam of gaseous ions from a sample, sorts out the resulting mixture of ions according to their mass-to-charge ratios by utilizing electric and/or magnetic fields, and provides output signals that are a measure of the relative abundance of each ionic species present [384]. Every mass spectrometer consists of: (i) a source, where a beam of ionized atoms of the sample under investigation is generated; (ii) an analyzer, in which the separation of ions according to their mass-to-charge ratio is achieved; (iii) a detector, where the resolved ions are detected and their intensity is measured.

The most widespread mass-spectroscopy technique is the secondary-ion mass spectrometry (SIMS). A schematics of a SIMS instrument is presented in Fig. 9. The sample under investigation is bombarded, in a vacuum chamber, with a beam of primary ions (usually oxygen) having energies of typically 1 to 20 keV. Due to this ion impact, target atoms are sputtered away, with only a small fraction of them being ionized. These ions are extracted from the target region and sent into a mass analyzer, where the flux of the ions with a given mass-to-charge ratio is measured. Since the ion beam continuously removes the surface of the sample 'layer by layer', it is also possible to perform a depth analysis [385]. A detailed discussion of the SIMS technique and instrumentation can be found in textbooks such as [386–388], and in numerous review articles (for example, [385, 389–392]). For our further discussion it is important only to point out that there are two distinct modes of the SIMS analysis, determined by the sputtering rate: dynamic and static.

In dynamic SIMS, high ion current densities are used to erode successive atomic layers at a relatively fast rate. This increases the sensitivity of the method, and enables one to obtain depth distributions of impurities. Dynamic SIMS is one of the most widely used techniques to determine dopant distributions after diffusion or implantation [393–397], and has the following *mutually exclusive* ultimate limitations: detection limits between 10^{13} and 10^{16} cm^{-3}, a lateral resolution of 20 nm, and a depth resolution approaching 1–2 nm [387, 393, 395, 398].

Static SIMS is confined to analysis of the top monolayer of the sample. This is achieved by a very low primary ion beam intensity and by a correspondingly low sputtering rate (10^{-3} to 10^{-6} of a monolayer per second). To obtain a sufficient secondary-ion yield for such a slow sputtering rate, the secondary ions are sputtered from a larger area (about 0.1 cm^2) [395]. The major advantage of the static SIMS is its

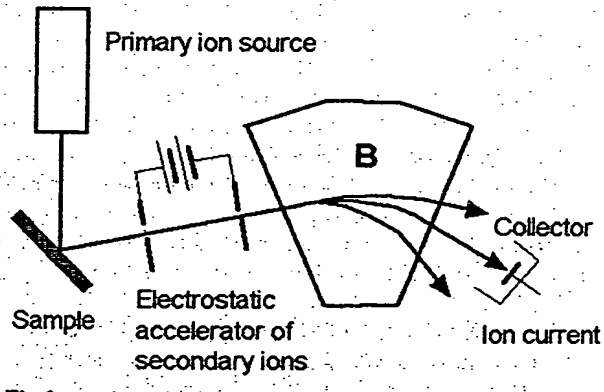

Fig. 9. A schematic diagram of a SIMS instrument. Primary ion beam hits the sample and sputters secondary ions, which are then accelerated by electrostatic accelerator to obtain an ion beam homogeneous in energy. The magnetic field in the mass-analyzer, B, (normal to the plane of the figure) has prism action on ions with different mass-to-charge ratios. Only the ions with a certain mass-to-charge ratio are detected by the collector. Scanning may be achieved by either varying the accelerating voltage, or the magnetic field

extremely high sensitivity to the surface contamination level, typically about 5×10^9 cm^{-2}.

The problems of a relatively low secondary-ion yield and its strong dependence on the matrix effects, which complicate the quantification of SIMS and limit its sensitivity, have stimulated the development of other techniques of mass spectroscopy. One of these techniques is sputtered neutral mass spectrometry (SNMS), where the processes of sputtering and ionization are decoupled. In SNMS, the sputtered neutrals are post-ionized (the probability of ionization of a sputtered neutral atoms usually exceeds 1%, which is up to four orders of magnitude higher than secondary ion yield in SIMS [399, 400]) by either a low-pressure rf discharge plasma (plasma SNMS) [401–403], by electron impact ionization (e-beam or e-gas SNMS) [404], or by laser photoionization [405–408]. Another way to ensure high sensitivity of a mass spectrometer is to increase the fraction of ions that are transmitted through the mass analyzer to the detector [409]. The transmission of ions through the mass analyzer depends on the construction of the analyzer and varies from approximately 10^{-5} to 0.5. Only time-of-flight (TOF) analyzers, which measure the time required for an ion of a known energy to traverse a certain distance, have transmission better than 0.1 [410]. This enables one to achieve the sensitivity of a SIMS machine by a factor of 100–1000 greater than that of a machine with the standard quadrupole analyzer. However, the TOF analyzer requires the ion beam to be pulsed, which implies a complex and expensive primary ion beam system.

The sensitivity of SIMS to the surface iron contamination of silicon wafers was reported to be between 6×10^8 cm^{-2}, determined by TOF-SIMS [411], and 5×10^9 cm^{-2}, reported from laser-SNMS measurements [409, 412, 413]. A number of other groups reported the detection limit of surface TOF-SIMS between 8×10^8 cm^{-2} and 5×10^9 cm^{-2} [209, 337, 414, 415] (Schnieders, 1996 #1022 [82, 416]). One of the important factors which determines the actual detection limit of iron by mass-spectroscopic techniques is interference of the iron peak with the other closely adjacent peaks in the mass spectrum. For example, the detection limit for iron $^{56}Fe^+$ is frequently affected by the interference with $^{28}Si_2^+$ [385] or with ArO^+ [383, 417], if argon plasma is used to produce secondary ions. Analysis of heavily boron-doped substrates can be hindered by interference of ^{10}B-Si-O trimers with the $^{54}Fe^+$ signal [418].

Pellin et al. [405] achieved the sensitivity to bulk contamination with iron of 2 ppb (5×10^{13} cm^{-3}) by using dynamic laser resonant ionization SNMS. McDaniel et al. [419] reported a detection limit for Fe of about 15 ppb (4×10^{14} cm^{-3}) using accelerator SIMS (see [420, 421] and references therein for details of the technique). The sensitivity of standard SIMS is usually limited to approximately 10^{16} cm^{-3} of iron [405].

Probably the most sensitive modification of mass spectrometry is the inductively coupled plasma mass spectrometry (ICP-MS) [417]. The advantage of the plasma ion source is its very high temperature (5000 to 8000 K), resulting in the almost complete atomization and ionization of the sample. The major problem with application of ICP ionization techniques to mass spectrometry was the development of the ion sampling interface, which would separate the area of ICP with atmospheric pressure and the high-vacuum area of the mass analyzer, and yet would allow most of the ionized atoms to get from the plasma into the mass spectrometer. The problem was solved by designing a system of two conical apertures with carefully adjusted diameters and distances between them. These apertures separate argon plasma torch, differentially pumped region between the apertures, and the high-vacuum mass spectrometer [422, 423]. According to Houk [424], the formation of singly charged ions is very efficient in the ICP. Some 54 elements, including iron, are expected to be ionized with an efficiency of 90% or more. The other advantages of ICP-MS are [390] the simple sample introduction in the ICP source at atmospheric pressure and the straightforward quantification of the results. ICP-MS is also very well suited for the rapid analysis of chemicals. It can be used for both the surface analysis of silicon wafers (by collecting surface contaminants using VPD technique) and for bulk analysis (dissolving complete wafers). Unfortunately, ICP-MS cannot be used for the analysis of volatile components such as boron or arsenic, which are lost during the sample evaporation step.

The reported sensitivity limits of the ICP-MS analysis for iron are scattered from 2.6×10^8 cm^{-2} after a VPD-type collection of iron from the surface of 200-mm wafers [425], to poorer detection limits of 2×10^{10} cm^{-2} for 6-inch wafers [84], and 2.5×10^9 cm^{-2}, as reported by Joly [82]. Gupta et al. [383] used ICP-MS to detect trace metals in ultrapure deionized water and 2% HF and reported detection limits of 16 ppt for water and 55 ppt for HF.

4.6 Neutron activation analysis (NAA)

Neutron activation analysis (NAA) is based on the quantitative detection of radioactive species produced in samples via nuclear reactions resulting from neutron irradiation of the samples. The samples are first irradiated with neutrons from a nuclear reactor, and then are moved to a counting facility to determine the amount of radioactivity induced by the interaction of impurities with neutrons. Counting is most efficient if radioactive isotopes have a half-life time, $t_{1/2}$, in the range of several days to several weeks. If $t_{1/2}$ is shorter than a day (which is the case for radioactive isotopes of such elements as B, Al, O, N, Cu, or Li), much of the radioactivity will decay before the sample is moved from reactor to a counting facility. Counting of radiation from isotopes with excessively long half-life times (greater than several weeks, such as Be) is complicated by background radiation (for example, by cosmic rays) since the intensity of gamma radiation from the samples is low.

The only radioactive isotope of iron with a suitable for NAA half-lifetime is ^{59}Fe ($t_{1/2} = 45$ days). This isotope is formed by neutron activation of ^{58}Fe. The radioactive decay of ^{59}Fe to the stable isotope ^{58}Co results in emission of γ radiation at several energies, the most probable being 1.2915 MeV and 1.0986 MeV [426]. Unfortunately, the isotopic abundance of ^{58}Fe is only 0.31% [426]. Thus, only 0.31% of the total iron impurity can be activated and detected by NAA. Consequently, the sensitivity of detection of iron in silicon is one of the poorest among about 43 to 53 elements detectable by NAA, and is about 3 orders of magnitude lower than that for Co or Au [68, 197].

NAA is used in two different forms: radiochemical and instrumental. Radiochemical NAA requires the chemical sep-

aration of radioactive isotopes under study before counting. The radiochemical method is slow, and can only be used for analysis of one impurity at a time. However, it is the only usable method if interferences (such as induced radioactivity of the matrix) are serious and cannot be removed by decay, spectrum subtraction, or computer simulation [427]. Radiochemical NAA also is useful for pure beta emitters (such as P, S, Tl, Pb, Bi), and enables one to improve sensitivity by using beta–gamma coincidence counting technique [66, 67, 428, 429]. Radiochemical NAA is the only technique applicable to III-V semiconductor compounds, which require removal of the matrix by means of inorganic retention media or ion exchangers.

Instrumental NAA is fast, nondestructive, and enables one to detect up to about 50 impurities after a single neutron irradiation [68, 197, 430]. This technique is based upon the quantitative detection of gamma-ray emitters formed by irradiation by means of multichannel gamma-ray spectrometry. The elements are identified by the energy of emitted gamma quanta. Fortunately, silicon is very well suited for instrumental NAA. The only silicon isotope which becomes radioactive after neutron irradiation is ^{30}Si (natural abundance 3.05%), which is activated by thermal neutrons to ^{31}Si and then decays to the stable isotope ^{31}P. The latter reaction, used for neutron transmutation n-type doping of silicon, is a beta-decay (γ ray abundance only 0.07%) with a short half-life time of 2.62 h. This makes matrix effects from the silicon itself negligibly small. Furthermore, since silicon is a light element, and since the purity of semiconductor-grade silicon is very high, there is very little attenuation of the incident neutron flux by the samples themselves or self-absorption of the emitted gamma rays [69]. NAA can be applied to intrinsic and, with some limitations, to doped silicon. Boron is an ideal dopant for NAA purposes. The fission reaction of ^{10}B with thermal neutrons generates no radioactivity, and the beta activity resulting from the ^{11}B(n, γ)^{12}B reaction has a half-life time of much less than 1 s [69]. In contrast, phosphorus becomes a 14-day half-life emitter of high-energy betas, which in turn give rise to the copious generation of bremsstrahlung X-rays, raising instrumental deadtime and background at lower energies to unacceptable levels. Likewise, arsenic is readily activated to the ^{76}As isotope with the lifetime of 26 h. Although the decay time of 26 h is much faster than that of iron, very high starting concentration of arsenic may make trace concentrations of iron undetectable on the background of the radioactive decay of the arsenic. Thus, highly phosphorus- and arsenic-doped silicon samples are poorly suited for instrumental NAA analysis.

Conventional instrumental NAA uses relative measurements. The amount of the impurity present in the sample is determined by comparing the intensity of gamma radiation with the energy specific for this particular element with that of a standard, which is co-irradiated with the sample. The impurity concentration can be calculated accurately only if the gamma activity of the sample and the standard are close. In lieu of standards containing iron in quantities relevant to the silicon industry (about 10^{10} to 10^{12} atoms), the impurity concentration is calculated by absolute counting, i.e., from the absolute number of γ-counts [431, 432]. This is the fastest approach since it does not require any chemical treatment of the samples (with the exception of cleaning), and avoids most of the work on standards. This method relies on explicit knowledge of parameters of the reactor, detector, and nuclear data, including an accurate knowledge of the fraction of impurities, activated in the sample for the given duration of the irradiation.

The NAA detection limit of iron in silicon has been steadily improving in the last years due to the development of underground laboratories which can decrease the intensity of background cosmic radiation by a factor of 40 [433] and even up to a factor of 1000 [197]. Additionally, sensitivity is improved by using larger samples since NAA detects the total number of radioactive isotopes in the samples rather than their concentration. The reported sensitivity of NAA to iron has increased over the years from 2 ppm (5×10^{16} cm^{-3}) in 1951 [434], 20 ppb to 120 ppb (5×10^{14} cm^{-3} to 3×10^{15} cm^{-3}) in the beginning of 1970s [435–437], 430 ppt (1.1×10^{13} cm^{-3}) in 1989 [438], to 8.3 ppt (about 2×10^{11} cm^{-3}) in 1993–1996 [68, 197].

Unlike DLTS or SPV, NAA measures total iron concentration in the bulk, no matter if it is in the form of electrically active or inactive point defects, complexes, or precipitates. Although NAA in its simplest form lacks any geometrical resolution (lateral or perpendicular distribution), profiles of the distribution of the impurities can be measured by repeatedly etching off thin layers from the surface of the specimen and measuring either γ-counts from the etchant, or from the sample after etching [439, 440]. A similar technique can be used for analysis of the surface contamination of the samples [441, 442]. Note that sample handling after irradiation is not critical since any contamination added after the sample is removed from the reactor will not be radioactive. Rath et al. [443] applied NAA for the analysis of surface contamination of 4-inch silicon wafers, obtaining a sensitivity to iron of 7×10^{10} cm^{-2}.

NAA studies have significantly contributed to the quantification of fundamental physical properties of iron in silicon. NAA was the chief method used for determination of the solubility of iron in silicon [98, 444–446]. The technique was also used in gettering studies [146, 447] and for studies of contamination by transition metals on different stages of IC manufacturing (see, for example, [60, 68, 69, 438]). However, NAA is hardly suitable for the routine control of the impurity contents in processed wafers. The method is expensive since measurements of low iron concentrations in high-purity silicon require the use of nuclear reactors and underground counting facilities, equipped with state-of-the-art radiation detectors. A typical turnaround time, needed for analysis of a silicon sample for iron, is as long as 4 to 8 weeks [68]. This makes NAA a tool for silicon research and development rather than for production control.

4.7 New prospective analytical tools

Only a few tools can achieve the sensitivity required by today's silicon technology. One of these techniques is a modification of Rutherford backscattering spectrometry (RBS), known as heavy-ion backscattering specrometry (HIBS). This technique was developed in the 1990s at Sandia National laboratory [448–453] and is suitable for high-sensitivity analysis of surface contamination (up to the depth of 0.5 μm, [454]). It is an ion-beam technique which uses the backscattering of moderate-energy heavy ions. Typically, C^+ or N^+ ions at

a few hundred keV are used in HIBS instead of 1–2 MeV $^4He^+$ ions used in RBS. The use of heavy ions makes it possible to achieve a sensitivity that is at least a factor of 10^3 greater than that of the conventional RBS. This is because the backscattering yield is proportional to the square of the atomic number of the analyzing beam and inversely proportional to the square of its energy. This potential yield enhancement has been well known for a long time (for example, [455]), but was not utilized until effective filters for backscattered ions, which would otherwise overload the detector, were developed. These filters are thin carbon or plastic foils. The thickness of the foil (typically 25 nm) is chosen such that particles scattered from the substrate are filtered out in the foil, while particles scattered from impurities heavier than the substrate (which have higher energy) pass through and are detected [450, 454]. The disadvantage of the foil filter is that ions lose energy when they pass through the foil. This results in a widening of the peaks and a loss in resolution [456], which limits the capability of HIBS to distinguish the elements with similar masses such as Fe and Ni. According to the literature reports, HIBS in combination with TOF detectors (see Sect. 4.5) has reached the sensitivity to gold of $3 \times 10^8\,cm^{-2}$ and that to Fe of $6 \times 10^9\,cm^{-2}$ [450]. Since HIBS as an ion-scattering technique does not require standards for calibration and has no matrix effects, it was suggested not only as a tool for contamination control, but also for the calibration of standard samples for other tools, such as TXRF [453, 457].

Other emerging methods include synchrotron-generated X-ray characterization techniques. One of these techniques, synchrotron TXRF, has already been mentioned in Sect. 4.3 above. The advantage of X-ray techniques is that they detect the total concentration of contaminants independently of their chemical state, and some of them are even sensitive to the chemical binding of the impurities, whereby the valence of the impurities and the type of chemical bonds can be accessed directly. However, sufficient sensitivity can be achieved only if extremely bright sources of X-rays, such as synchrotron accelerators, are used. Synchrotron-generated X-rays can be focused such that they can also be used for microscopy. Spot sizes as low as 300 nm have been obtained using zone plates, although typical spot sizes can be 1 to 3 μm. Within such a spot, synchrotron sources can deliver up to 10^{10} and 10^{12} monochromatic photons per second [458, 459]. X-ray fluorescence (XRF), X-ray absorption (such as XANES, X-ray absorption near-edge spectromicroscopy, and its modifications), and X-ray photo-emission spectroscopy (XPS) methods are the most relevant techniques for studying iron in silicon. In XRF, a core electron is ejected by the incoming X-ray. A higher valence electron then drops into the empty core shell and emits another X-ray which is characteristic of that particular atom. In X-ray absorption methods, electron transitions from lower filled to empty upper states are detected. The energy levels of these states, and the observed energy spectra, depend upon the element itself and the chemical state that the element is in. Typically, calibration standards are required to match the spectra of an element in various chemical states. In XPS, the kinetic energies of electrons ejected from the sample by monochromatic X-rays are examined. The ejected electron energy depends on the binding energy of the electron, which depends on the type of element and its chemical state. Since the escape depth of electrons (before they lose energy from collisions) is small, this technique is very surface sensitive, probing only several monolayers.

5 Reduction of iron contamination by chemical cleaning

Over 50% of the yield losses in integrated circuit fabrication are associated with the contamination of wafers with organics, particles, and metals [460]. Wafer cleaning is an important and ubiquitous process step in silicon technology, which not only removes contaminants from the wafer surfaces, but also prepares wafers for subsequent processing [461]. This includes stripping surface layers (for example, photoresist), etching surface layers (for example, oxides), removing sacrificial layers (for example, surface SiO_2), and drying wafers (for example, using isopropanol). Optimization of silicon cleaning technology has developed into an area of intensive research spanning materials science, chemistry, and electrochemistry. In this section, we will discuss the efficiency of available recipes for cleaning the silicon wafers, with a special emphasis on prevention of iron contamination.

5.1 RCA cleaning

The RCA cleaning procedure, developed at the Radio Corporation of America by Kern and Puotinen [462] in the 1960s, remains the basis of wet cleaning chemistry [463]. RCA cleaning consists of the sequential use of two solutions with intermediate rinse in running deionized (DI) water. The first solution, known as SC1 ("standard clean 1"), typically consists of 5–1–1 to 7–2–1 parts by volume of H_2O–H_2O_2–NH_4OH. It removes primarily organic contaminants and particles from the wafers. The second solution, known as SC2 ("standard clean 2"), consists of H_2O–H_2O_2–HCl in the proportion of 6–1–1 to 8–2–1 by volume and is used for desorption of heavy metals (such as iron) from the silicon surface. Cleaning in either mixture is typically carried out at 50 to 80 °C to sufficiently activate the mixtures without causing excessively fast decomposition of H_2O_2 [460, 462].

Frequently, SC1 and SC2 are used in combination with other cleaning steps. A preliminary clean-up treatment with a hot (100 °C and above) 4:1 H_2SO_4/H_2O_2 mixture (known as "piranha bath", or "Caro" cleaning) is used to remove organic contamination originating from the transportation in wafer carriers, residual photoresist, or organic adsorption from the atmosphere. The very strong oxidizing power of Caro etch results in a quick growth of a chemical oxide (up to 1.3 nm thick) on the top of the silicon wafer, which imbeds all surface contaminants (metallics and particles) [25, 463]. This silicon dioxide layer can be stripped together with the imbedded contaminants by an HF solution, which proved to be an efficient means to remove metals from wafers [25, 464]. However, the Caro–HF cleaning sequence is less efficient in the removal of particles than SC1 alone [25]. Another disadvantage of the Caro mixture is its high viscosity. This results in a residual boundary layer at the wafer surface which is difficult to remove by normal DI water rinsing [463, 465].

Etching in diluted HF is used to remove the thin layer of contaminated native oxide. The reason why HF-containing

chemistries have been demonstrated to be effective for metal removal is that HF simultaneously provides a low-pH environment, leading to high metal ion solubility, and a mechanism to dissolve the native oxide with imbedded contaminants [466]. It was noted [462] that SC1 and SC2 alone are effective for surface contaminants only. If a contaminant is already distributed within an oxide layer or is located at the Si/SiO_2 interface under the oxide, it can be removed only by etching with dilute HF between SC1 and SC2 steps. Unfortunately, the silicon surface becomes highly reactive after it is exposed to HF and immediately attracts particles and organic contaminants from the solutions, DI water, and the ambient air [460]. Contrary to SC1, the subsequent SC2 solution has no surfactant activity to remove these contaminants [460]. Therefore, one should be extremely cautious to avoid recontamination of the wafers after a HF etch. A possible way to remove the oxide and avoid electrochemical plating of some metals is to add small amounts of H_2O_2 (on the order of 1%) [467] or HCl (approximately 3%–5%) [468] to the diluted HF.

Hosoya [62] pointed out that the removal of a 20- to 30-nm surface layer from the wafer by using silicon etch such as a mixture of HNO_3, HF, and CH_3COOH (also known as CP4), before the RCA treatment is very effective in removal of iron contamination introduced by reactive ion etching. However, etching of the wafer surface may degrade the polished quality of the wafer surface.

Removal of particles and removal of surface metal contaminants are two major objectives of the RCA cleaning procedure, which unfortunately cannot be achieved by a single cleaning solution. This is because the removal of metals (as we will show below) is more efficient in acidic solutions, whereas particles are removed chiefly in alkaline solutions. The process of adsorption of particles can be quantitatively described by the electrostatic interaction between the particles and the silicon wafer. This model uses the notion of the zeta potential, which is essentially the potential of the wafer/particle interface acquired in the solution due to adsorption of ions such as OH^- or H^+ at its surface. Itano et al. [469] showed that zeta potentials of Si, SiO_2, Si_3N are all negative in the base solutions. This results in the electrostatic repulsion of SiO_2 or Si_3N particles from the Si or SiO_2 surface and makes deposition of particles improbable. On the contrary, the electrostatic attraction between the silica on the wafer surface and most of the particles is a strong driving force for deposition of particles in the solutions with pH between zero and 5 [470]. This is because the zeta potential of Si changes to positive only at $pH < 0$ (as was also shown in [471,472]), whereas the zeta potentials of SiO_2 and Si_3N_4 becomes positive at $pH < 4$ and the zeta potential of Fe_2O_3 particles is positive at $pH < 6$; the isoelectric point of alumina particles Al_2O_3 is at pH of 8.5 [473]. Note that incorporation of iron and other metals into the surface oxide, which are reportedly negatively charged in the oxide (see, for example, [183,185,186,474,475]), may also affect its zeta potential and, consequently, the probability of adsorption of particles on the wafer surface [476]. According to [477–480], standard SC2, HF/HNO_3, and HCl/HNO_3 mixtures are all in the range $0 < ph < 8.5$, favorable for particle deposition. On the contrary, SC1 has $pH \approx 10$, and H_2SO_4/H_2O_2 has $pH < 0$, which makes particle deposition less probable [477–480].

The effects of removal/deposition of metals in cleaning solutions has been a subject of intensive studies starting from the original work of Kern [481], who used radiotracer measurements to show that the most efficient removal of metals from semiconductor surfaces was achieved by the complexing dissolution in acidic H_2O_2 (such as SC2), whereas etching in spiked alkaline solutions (such as SC1) resulted in extremely high iron contamination levels of the wafer (up to $10^{14}\,cm^{-2}$). These results were later confirmed in a great number of studies. For instance, significant deposition of iron from SC1 was observed in [190,278,367,482–488].

Park et al. [489] reported that SC1 alone, or SC2 alone, or HF alone were not efficient in the removal of iron. However, the removal of iron can be successfully accomplished by a combination of a HF etch, to remove the oxide with impurities, and SC2 to desorb the residual iron remaining at bare silicon surface after HF etch [489]. The combination of all three steps (SC1, HF, SC2) was found to be most efficient [488,490,491] since this procedure first oxidizes the top surface of the substrate along with the metals, then strips the oxide, and then finally removes any remaining metal residues.

Dhanda et al. [492] studied the kinetics of the removal of Fe in a standard (1:1:5 solution at 70 °C) SC2 solution and found that the removal of Fe is complete in 10–20 s, i.e., the conventional SC2 clean (10 min or more at this temperature) is clearly "overdone" with respect to the removal of Fe. Indeed, the temperature and duration of SC2 clean was optimized by Kern [462,481] for removal of gold, which was an important impurity at that time. According to the literature reports, iron can be successfully removed by SC2 even at room temperature, and even by HCl alone without the addition of H_2O_2 [493].

Contaminated water can also deposit metals onto the silicon. As will be discussed in the next section, the $pH \approx 7$ of pure DI water favors the formation of iron oxide or iron hydroxide on the wafer surface. This phenomenon is well known in silicon cleaning technology [82,494,495], and the use of aqueous solution of Fe, Al, Cu, and Ni was even suggested as a method of intentional quantitatively controlled contamination of the surface of a silicon wafer [496].

5.2 *The electrochemistry of cleaning*

The physics and chemistry of the adsorption of metals from the solutions onto solid electrodes, such as silicon wafers, and their desorption, were established long before the beginning of the silicon era. In this section, we will briefly introduce several notions used in electrochemistry necessary to understand the mechanism of deposition and removal of iron in wet chemical solutions. More details on this subject can be found in texts on electrochemistry (for example, [497–500]).

Most salts of metals have ionic type of bonding with the electrostatic interaction energy of $U = (q_1 q_2)/(4\pi\varepsilon\varepsilon_0 r)$, where r is the distance between the ions, ε is the relative dielectric permittivity of the medium, and ε_0 is the absolute dielectric permittivity of vacuum. If a salt is introduced into the water, the attractive forces between the ions are significantly reduced due to the high dielectric permittivity of water, $\varepsilon = 78.3$ (25 °C). This decrease in the binding energy, along with the interaction of the salt molecule with the water dipoles, results in spontaneous dissociation of the salt into

ions [497]. Most chemical reactions in the solutions can thus be considered as reactions between ions. Those reactions that involve electrons leaving from a metal or other substance by metallic conduction, are referred to as *electrochemical reactions* [501]. A general form of an electrochemical reaction is $\sum \nu_i R_i + ne^- = 0$, where R_i are the reagents, ν_i are the coefficients in the reaction, and n is the number of electrons taking part in the reaction. Hence, an electrochemical reaction can proceed only if there is a supply of, or a sink for electrons. Note that the margin between the chemical and electrochemical reactions is not well defined since a *chemical* reaction, which can be expressed as $\sum \nu_i R_i = 0$, frequently consists of a sequence of two (or more) electrochemical reactions, one liberating electrons, and the other one adsorbing them. All electrochemical reactions are subdivided into oxidation reactions, if they proceed in the direction corresponding to the liberation of electrons (for example, $Fe^0 \rightarrow Fe^{2+} + 2e^-$), and reduction reactions, if they proceed in the direction corresponding to the absorption of electrons (for example, $Fe^{2+} + 2e^- \rightarrow Fe^0$).

The simplest electrochemical model of adsorption/desorption of metals neglects complexes of metals such as oxides, hydroxides, etc., and assumes that metals dissolve in the ionic form, for example, M^+, whereas deposited metals are neutral atoms, for example, M^0, where M stands for "metal". The dissolution of metals from the surface of a silicon wafer in a cleaning solution is interpreted as an oxidation reaction which consists of transfer of electrons from neutral surface metals to the silicon wafer and the desorption of the oxidized (ionized) metals into the solution. Conversely, the adsorption of metals onto the wafers from the solution is considered as a reduction reaction which involves transfer of electrons from silicon to positively charged dissolved metal ions, with their subsequent outplating as neutral species on the surface of the wafer. The first reaction will result in an accumulation of negative charge on the wafer (the charge left behind by the desorbed ions), the second one in the accumulation of a positive charge. The accumulation of the charge will result in electrostatic potential, built up between the electrolyte and the electrode. This potential will increase as the reaction progresses and will eventually stop the reaction by making it energetically unfavorable, unless the excess charge is removed by either an electric current passed through the electrolyte, or by another electrochemical reaction. It can be shown (see the texts on electrochemistry, for example, [497, 498] for more details) that the electrode potential, E, of an electrochemical reaction of the type $\sum \nu_i R_i + ne^- = 0$ is given in the general case by the Nernst equation:

$$E = E^0 + \left(\frac{RT}{nF}\right) \sum \nu_i \ln(M_i) , \tag{9}$$

where E^0 is the so-called standard electrode potential (measured when the activity of the reagents is unity), F is the Faraday constant, R is the ideal gas constant, n is the number of electrons transferred in the reaction, and M_i are the activities of the reacting species R_i. Activity of the ion is proportional to its molality, multiplied by the non-ideality coefficient which approaches unity for very dilute solutions [501]. The model described above is sufficient to describe the adsorption of noble metals, such as Au or Cu. Iron is more reactive and usually forms insoluble oxides and hydroxides rather than outplates as a neutral metal (see discussion below). However, the electrochemical mechanism is the same for all metals, the difference is primarily in the complexity of the electrochemical reactions of deposition.

The electrode potential E (also known as "redox potential", or "oxidation/reduction potential", or "half-cell potential"), formed as the result of an electrochemical reaction, is one of the major concepts in electrochemistry. This potential is a measure of the chemical driving force for the reaction to go to completion. Since it is impossible to measure the absolute value of the potential between the electrode and the electrolyte (this is because one cannot form a contact to the electrolyte without building up another unknown contact potential), all potentials are measured with respect to the standard hydrogen electrode. The standard hydrogen electrode is a platinum electrode, inserted into the electrolyte through which hydrogen gas is passed at the atmospheric pressure. The potential of the standard hydrogen electrode is determined by the oxidation reaction $1/2H_2 \rightarrow H^+ + e^-$.

One can use (9) not only to calculate the electrode potential formed by an electrochemical reaction for given concentrations (activities) of the components, but also to predict the equilibrium of several electrochemical reactions ongoing simultaneously. In the latter case, the activities of the reagents change as the reaction proceeds. The electrode potential also changes until it reaches the level at which all reactions are in equilibrium, i.e., the electrode potential of the first reaction, E_1, is equal to the electrode potential of the second reaction, E_2,

$$E^{01} + \frac{RT}{n_1 F} \sum \nu_{1,i} \ln(M_{1,i}) = E^{02} + \frac{RT}{n_2 F} \sum \nu_{2,i} \ln(M_{2,i}) . \tag{10}$$

Equation (10) enables one to predict the outcome of a pair of electrochemical reactions. The quantitative prediction of the real-life deposition/dissolution reactions is much more complicated than in the examples presented above because of the many possible chemical states that the metal, the surface of the electrode (silicon wafer), and the cleaning solution may take (see, for example, [497, 501]). Besides neutral metallic iron, Fe^0, and iron ions, Fe^{2+} and Fe^{3+}, one has to take into account such common iron compounds as FeO, Fe_2O_3, Fe_3O_4, $HFeO_2^-$, $FeOH^{2+}$, $Fe(OH)_2^+$, FeO_4^{2-}, and possible reaction between them [501]. A method to present the stability of different phases as a function of the redox potential of the solution and its pH was suggested by Pourbaix in the 1940s and is known as the Pourbaix diagram, or potential-pH diagram [501]. Since most of the reactions in aqueous solutions directly or indirectly involve hydrogen ions or OH^- radicals, pH is an important parameter which determines the outcome of the reactions along with the redox potential of each of the reactions. A typical Pourbaix diagram for iron is presented in Fig. 10. Generally, the development of such a diagram begins with assessment of all possible chemical states of iron and possible reactions between them in a particular cleaning bath. For instance, Pourbaix [501] listed 29 such reactions for iron. On the next step, the equilibrium constant for each equation is written down using Nernst equation, initial concentrations of each reagent, and oxidation potentials of the reactions involved. The obtained system of equa-

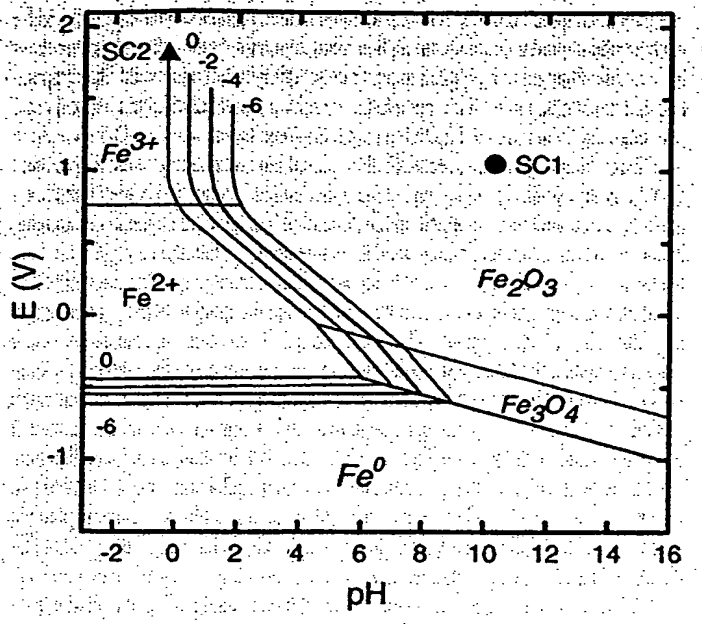

Fig. 10. The redox potential-pH (Pourbaix) diagram for the iron–water system at 25 °C (considering as solid substances only Fe, Fe_3O_4, and Fe_2O_3), for 10^{-6}, 10^{-4}, 10^{-2} and 1 molal concentrations of iron in the solution (after Pourbaix [501]). The *filled circle* and *triangle* correspond to the pair of (E, pH) of RCA SC1 and SC2 solutions, respectively (data from [477–480])

tions is solved to determine the equilibrium concentration of each iron phase for each pair of values (E, pH). Finally, the predominant phase is determined for each point of the diagram, and the boundaries between areas of stability of different phases are drawn. Although these calculations are fairly simple for two or three phases, more complicated diagrams require use of computers. A number of programs were developed and published in the 1970s [502–504]. Kern [462, 463], who used a Pourbaix diagram in his 1970 paper, was probably the first to apply E–pH diagrams to understand the chemistry of cleaning of silicon wafers. However, only in the beginning of the 1990s have these diagrams found wide application for the understanding and improvement of the cleaning techniques [477–479, 505, 506].

The interpretation of the Pourbaix diagrams is very simple. If a cleaning solution falls into the stability region of a solid phase for a given metal (for example, metal oxide), then any ions of that metal present in the cleaning solution can lower their free energy by forming the metal oxide depositions. On the contrary, if the (E, pH) point of a cleaning solution lies in the region where the ionized form is stable, then no deposition will occur, and any metal present on the wafer surface will be removed by dissolution [478]. A number of authors [478–480, 507, 508] determined the reduction potential and pH of standard cleaning solutions and plotted them on a Pourbaix diagram (Fig. 10). They showed that the position of SC1 (NH_4OH/H_2O_2), deep in the stability region of Fe_2O_3, explains why deposition of iron from contaminated SC1 solutions occurs so readily. On the contrary, SC2 gets into the region of ionic solubility of iron and can be used to remove Fe contamination from the wafers. Thus, iron will dissolve from silicon in acids, but will deposit onto a wafer in alkaline solutions. A similar diagram for copper, which can be found, for example, in [501], shows that Cu will deposit onto silicon even from acids, unless the redox potential of the solution is raised by addition of a strong oxidant, for example, hydrogen peroxide or ozone [509–513]. In most cases H_2O_2 and O_3 do not further enhance the removal of iron, yet they are important for desorption of noble metals and are also effective in oxidation of organic contaminants, which are decomposed to CO_2, H_2O, etc. [507].

To understand the real-life physics and chemistry of cleaning, one should bear in mind that contamination of wafer surfaces in solution can occur as the result of several mechanisms, which include [482, 484, 508, 514]: (i) electrochemical deposition (metal displacement); (ii) precipitation by the mechanisms of physisorption and chemisorption, and (iii) film inclusion. It is thought that metals such as Cu, Ag, and Au, which exhibit higher electronegativity than Si and have a higher redox potential than hydrogen in solutions, are adsorbed directly on the Si surface by taking electrons from Si by the mechanism of electrochemical deposition [515]. Metals that form hydroxides in alkali solutions, such as Fe and Al, deposit by mechanism (ii), i.e., by the precipitation of metal hydroxides on the substrate surface. In mechanism (iii), metallic impurities close to the Si surface are included into the oxide as the Si surface is chemically oxidized. The latter mechanism becomes important in understanding of adsorption of metals to oxidized wafers, since silicon dioxide is a dielectric, and reduction reactions at its surface are improbable [484]. Imaoka et al. [509] (see also [515]) speculated that the probability of a metal to be included in the oxide is determined by the difference in the enthalpies, ΔH, of formation of metal oxides and silicon oxide. According to their model, the metals such as Al (Al_2O_3, $\Delta H = -1675\,\mathrm{kJ/mol}$), Cr ($Cr_2O_3$, $\Delta H = -1130\,\mathrm{kJ/mol}$), and Fe ($Fe_3O_4$, $\Delta H = -1118\,\mathrm{kJ/mol}$ which can be more easily oxidized than Si (SiO_2, $\Delta H = -909\,\mathrm{kJ/mol}$), tend to get included in the SiO_2 films, whereas the inclusion of Ni (NiO, $\Delta H = -241\,\mathrm{kJ/mol}$) or Cu (CuO, $\Delta H = -155\,\mathrm{kJ/mol}$) in the growing oxide layer is much less probable. Shimizu et al. [183, 185, 186, 474, 475] reported that the incorporation of Fe into the silicon native oxide results in built-in negative charge in the oxide, which can be observed by using SPV (see also a discussion in [516]). They explained it by the formation of $(FeOSi)^-$ after a substitution of the quadrivalent Si ion in silica by a trivalent iron atom. Similarly, Loewenstein et al. [517] and Rotondaro et al. [518] explained incorporation of metals into the growing oxide by an ion exchange mechanism, in which the Si–OH groups on the hydrophilic surface act as weakly acidic ion exchangers:

$$\mathrm{Si{-}OH} + \mathrm{M}^{n+} \rightarrow \mathrm{Si\text{-}OM}^{(n-1)+} + \mathrm{H}^+ . \qquad (11)$$

The application of standard equilibrium expressions yields a relation between concentrations:

$$\frac{C(\text{outplated})}{C(\text{dissolved})} = K\frac{C(\mathrm{M}^+)}{C(\mathrm{H}^+)} , \qquad (12)$$

where K is the equilibrium constant. Equation (12) also suggests that the metals will dissolve in acids and will precipitate in alkaline solutions. Dhanda et al. [519] observed that the amount of iron deposited on the silicon surface exhibited a remarkably weak dependence on the surface clean performed prior to Fe-spiked SC1 treatment. This implies that the mechanism of iron deposition is independent of the starting sur-

face condition. They suggested that an initial rapid oxidation of the silicon wafer takes place first, followed by a preferential oxidation of the iron and its inclusion into the oxide film [519]. Rotondaro et al. [518] compared outplating of iron on bare silicon wafers and on those covered with thermal oxide and found that bare silicon wafers had two orders of magnitude lower surface Fe contamination than the thermally oxidized wafers. Norga et al. [478] pointed out that the incorporation of metals in the silicon oxide is facilitated by the fact that no nucleation step is required.

Absorption of some metals was observed to have either synergetic or competitive effect (see, for example, [520–522]). Hayami et al. [523] found that the Al contamination somewhat deteriorates the removal efficiency of Fe. Fabry [524] reported that, surprisingly, even a small increase of Na concentration by 3–5 ng/l in the rinsing water enhanced the adsorption of Fe on the native oxide of Si and doubled the surface contamination level of iron. The adsorption of Ni or Cu onto Si wafers from SC1 was found to be obstructed by Fe [487]. Although most of these effects can be explained by the electrochemical models, the examples above show that a complete model of the cleaning process should take into account a whole variety of possible contaminants, and a number of deposition mechanisms.

The final comment that is in order in this section is that the efficiency of exchange of electrons between ions and silicon depends on the energy position of ion in the solution with respect to the Fermi level in silicon wafer. Hence, the deposition of some metals onto silicon would depend on its conductivity type. For example, p-Si should be less susceptible to noble metal contamination due to its lower Fermi level position, which means that a higher energy is required to raise an electron from the Fermi level in silicon to the energy level of a metal ion dissolved in the solution [522, 525, 526]. However, no distinct difference was found between the n-type and p-type Si in terms of the absorption of Fe and Ni [509].

5.3 Challenges of the cleaning technology

Silicon cleaning technology, which has remained essentially unchanged since the middle of the 1960s, is barely adequate for today's advanced technology. The most broadly discussed challenges which cleaning technology has to face are:

(a) Traditional RCA chemistry is not well suited for the cleaning of submicron trenches and contact holes since the liquid surface tension may hamper the penetration of liquid into the very fine features of device topography. Possible solutions are the addition of fluorocarbon or hydrocarbon surfactants [527], or gas-phase cleanings (see discussion below).

(b) Ultrapure RCA cleaning is expensive since a very complicated technology is employed to obtain high-purity chemicals (see Hackett et al. [85] for a review). The efficiency of cleaning in any cleaning bath is determined by the balance between the amount of metals on the surface of the wafers to be cleaned and that in the solution [361, 482]. Jastrzebski et al. [528] presented an example of how the iron contamination level of the wafers increases as the same etching solution is repeatedly used for cleaning of wafers. They showed that the iron contamination level rose to the maximum contamination threshold after cleaning of only eight batches of wafers. Thus, one has to use ultrapure chemicals and exchange them frequently in order to maintain low contamination levels. This requirement results in the consumption of large volumes of expensive chemicals and DI water, problems of enviromental impact of the generated waste, and requires strong air flow in the wet stations to prevent chemical vapors from getting into the cleanroom [507]. The only way to reduce the cost is to develop alternative cleaning procedures, for example, those that use dilute chemicals.

(c) As insulating films used in gates and capacitors become thinner, the accuracy in controlling the etching rate must be increased from the current level of several tens of angstroms per min to several angstroms per min or even 10^{-1} Å/min [529]. This requires extremely diluted solutions, much weaker than are used in standard RCA-type cleaning. Additionally, the growth of the native oxide during DI water rinses results in an increase in the surface roughness [530, 531]. Thus, it is important to suppress native oxide growth on the silicon wafer surfaces during cleaning, which can only be done by decreasing concentration of dissolved oxygen in the water [530, 531] or by the addition of trace concentrations of HF to the water [532].

(d) Wet cleaning processes are generally incompatible with most cluster tool environments. As it was pointed out by Kitajima et al. [533], the cleanliness of the conventional cleanrooms cannot exceed the class 0.1–1 level because of the dust generated by people. This level is hardly suitable for production of DRAM chips of 1 GB and beyond, and suggests the use of mini-environment fab systems with completely automated cleaning tools, isolated from the ambient, or cluster tools, which allow single-wafer processing during which wafers are transferred under vacuum between process modules and the risk of recontamination is reduced.

(e) The microroughness of the cleaned wafer surface decreases the breakdown voltage of MOS structures [30, 513, 529, 534–536], electron channel mobility in MOSFETs [537], and yield of high aspect-ratio contact holes [467, 534]. Roughness is affected not only by the cleaning chemistry itself, but also by the metal contamination and particle density since both particles and surface metals may cause irregular etching of the silicon surface [538]. Tardif et al. [30] compared the surface roughness after about 10 different etchings and found Caro cleaning to be the best and SC1 the worst. Cleaning in a SC1 solution may result in a haze on the surface of the wafer because SC1 chemistry slightly etches the silicon surface [467, 513, 539–541]. If H_2O_2 decomposes, it does not create the protective oxide on the silicon surface, and NH_4OH attacks the bare silicon surface, causing microroughness [29, 542]. Mertens et al. [25] pointed out that the composition of SC1 may change in the process of cleaning due to the evaporation of NH_3 and the dissociation of H_2O_2, which is known to be greatly enhanced in the presence of Fe or Cu. The addition of Fe^{3+} in concentration of 1 ppb decreases the lifetime of H_2O_2 by a factor of 100 [465, 542, 543], from 19.4 h at 80 °C in clean solution (metals < 0.2 ppb) to 18 min for metal concentration of 1 ppb [542]. Helms et al. [544] suggested that the fol-

lowing reaction of decomposition of H_2O_2 takes place in the presence of Fe^{3+} ions:

$$Fe^{3+} + 1/2H_2O_2 \leftrightarrow Fe^{2+} + H^+ + 1/2O_2. \quad (13)$$

Interestingly, in SC2 solutions, the dissociation of hydrogen peroxide is only weakly affected by iron contamination [542]. This is the result of the low pH of SC2, which suppresses the flow of the reaction (13) from the left-hand to the right-hand side. Schmidt et al. [465, 542] found that the increase of the roughness during SC1 etching is to a large extent due to the formation of oxygen gas bubbles created by the decomposition of H_2O_2. These bubbles block the wafer surface from the etching action of the SC1 chemistry. From these results it can be concluded that the SC1 bath requires ultra-clean chemicals since it may cause irreversible roughness of the wafer surface if contaminated [25, 29, 543]. Besides enhancement of dissociation of H_2O_2, noble metals can increase the surface roughness by catalyzing the local oxidation of silicon. Metals such as Au, Pt, Ag, or Cu, which feature higher electronegativity than Si, attract electrons from silicon ($M^+ + e^- \rightarrow M^0$, where M stands for "Metal") and thus facilitate local Si oxidation through the reaction $Si + 2H_2O \rightarrow SiO_2 + 4H^+ + 4e^-$ ($E^0 = 0.857$ eV). Since the oxidized areas is etched by HF rapidly, irregular etching occurs and consequently the surface is roughened [484, 510, 538].

5.4 Recent developments in the cleaning technology

A significant amount of research has been done to improve the existing cleaning recipes and to find radically new cleaning solutions. Important advances in the technical implementation of the RCA cleaning method include closed system processing [460], centrifugal spray and fluid jet cleaning machines [545], and megasonic (750–980 kHz) cleaning techniques [546–552].

Diluted chemistries appear to be an interesting alternative to RCA cleaning (see, for example, [278, 553–557]) since they reduce the costs of chemicals, simplify their disposal, and reduce the rinse time and the amount of DI water used [553]. An interesting feature of dilute SC2 mixtures is that they inhibit particle deposition which is the major drawback of the standard SC2 [278, 470, 518]. This is understandable since high-pH (alkaline) solutions usually give low particle counts whereas low-pH (acidic) solutions do not. Very low concentrations of acids should behave, as far as particles are concerned, in a manner that is essentially similar to pure rinse water [278]. Another problem is that dilution of SC2 deteriorates the efficiency of removal of metals almost proportionally to the dilution ratio [30, 554]. On the other hand, Hurd et al. [470], D'Emic et al. [554], and Mertens et al. [555] suggested that the cleaning capabilities of the solution with respect to iron can be improved even above the standard SC2 recipe if the peroxide is removed from the strongly diluted SC2. This can be understood from the Pourbaix diagram for the stability of different phases of iron (Fig. 10): if an acidic solution is strongly diluted (i.e., its pH is increased from about 0 to 3–5), and if hydrogen peroxide is added to increase the redox potential, we can easily get into the area of stability of Fe_2O_3. Anttila et al. [278] suggested a cleaning sequence composed of a SC1 clean to remove particles, followed by a very dilute HCl to remove metals. They found that this sequence performs better than a standard RCA cleaning, and that the efficiency of iron removal only slightly degraded when the dilution ratio of HCl was changed from $1{:}10^3$ to $1{:}10^6$. An advantage of diluted acids is that they are usually very clean (since they consist mostly of DI water), and thus the unintentional metal contamination from the chemicals is reduced. Itano et al. [473, 557] reported that the NH_4OH content in SC1 can be decreased by a factor of 20 to $NH_4OH : H_2O_2 : H_2O = 0.05 : 1 : 5$ with degradation of neither particle removal efficiency nor surface smoothness.

During the rinse steps where pH is close to 7, a slight accidental contamination ($\ll 1$ ppb) can produce a heavy deposition of iron in the form of $Fe(OH)_3$ or iron oxide. This phenomenon can be easily avoided by adding traces (0.01%) of HCl or HNO_3 in the DI water [82, 494, 495] to keep pH in the range 4–6. Theoretically, the decrease of the pH of water to 5 should cause about 98% of the surface iron (II) hydroxide to dissociate [278].

Ohmi et al. [507, 548, 558] suggested to substitute the conventional RCA cleaning with a new wet cleaning which consists of only five steps at room temperature: ozonized Di water (to remove organics and part of the metals), $HF/H_2O_2/H_2O$/surfactant + megasonic (for removal of particles and most of metals), ozonized DI water, diluted HF, and DI water+megasonic. They claim that this cleaning procedure reduces consumption of the DI water and chemicals by 20 times. Furthermore, all cleaning steps are performed at room temperature, which greatly reduces the evaporation of water and chemicals, thus making it possible to accurately maintain chemical composition of the solutions [558]. Other alternative cleaning methods discussed in the literature include:

(a) the use of choline (trimethyl-2-hydroxyethyl ammonium hydroxide) solutions [460, 559]. A mixture of choline with a surfactant, methanol and in some cases with H_2O_2, is similar to, or more efficient than SC1 [463].
(b) chemical vapor etching (for example, HCl vapors, or H^+hfac (1,1,1,5,5,5-hexafluoro-2,4-pentanedione)), which is suitable for fine trench and contact holes with a high aspect-ratio and is capable of removing transition metals from the surface [486, 547, 560–571];
(c) remote plasma cleanings in a gas mixtures of O_2, HCl/Ar, and $NF_3/H_2/Ar$, or in H_2, which are efficient for residual oxide etching and the removal of metals [572–574];
(d) UV-excited cleanings in the presence of chlorine gas (effective for metals such as Fe or Al) or oxygen/ozone (effective for organics) [486, 564, 574–582];
(e) annealings of wafers in HCl ambient (pyrochemical cleaning) [583] (see also the section on chemical gettering, Sect. 6.6 below);
(f) the use of ozonated water (ozone is a strong oxidant which acts in wet chemistry similarly to H_2O_2 by increasing the redox potential of the mixture) [556, 584–589]. The problem of ozone is its stability. The lifetime of ozone in cleaning solutions was studied by Park et al. [588], who reported the half-life time of about 80–90 min at room temperature and about 7 min at 50 °C.
(g) the addition of chelating agents to the RCA chemistry to prevent the OH^- ions from coordinating with metal ions and to suppress metal adsorption to the silicon surface [480, 590, 591].

(h) wafer cleaning and drying in a low-pressure ambient [592].

The advantages of the gas-phase and vapor-phase cleans are mainly the reduced consumption of toxic chemicals and the ease of incorporation into the integrated processing systems [564, 593]. However, a major shortcoming of the gas-phase cleans is the comparatively inefficient metal removal. Since most metal salts are much more soluble than volatile [461], it is much easier to dissolve them than to remove them by a gas cleaning. A common application of gas cleaning is the addition of Cl-containing species into the gate-oxidation ambient. The observed increase in gate oxide breakdown yield is associated with removal of heavy metals. For example, the surface iron contamination levels were found to decrease by a factor of 4 after oxidation in a Cl-containing ambient as compared to oxidation in dry oxygen [25, 593].

6 Reducing the detrimental effect of iron on devices through gettering

Gettering is the process whereby impurity concentrations are reduced in the device region of the wafer by localizing them in separate pre-defined regions of the substrate where they cannot affect the device performance [594, 595]. Figure 11 illustrates several possible locations of intentionally introduced gettering sites: at the back surface of the wafer (mechanical damage such as sandblasting (Fig. 11a), a layer of liquid aluminum (Fig. 11b), or gettering by phosphorus diffusion (Fig. 11c)), silicon-oxide precipitates in the bulk (internal gettering, Fig. 11d), implantation-induced damage in a few μm below the wafer surface (Fig. 11e), and gettering by Fermi level effect and ion pairing in heavily doped substrates of epi-wafers (Fig. 11f). Despite the use of ultra-clean Si wafers, cleanroom technology, and hyper-pure chemicals, gettering procedures are necessary in device manufacturing to maintain high yields, especially in case of accidental contamination and/or process variations. In general, gettering can be considered a three-step process [596]: The impurity must be (i) released from its original and undesirable state to then (ii) diffuse through the crystal from the device region to the gettering sites, and (iii) be captured at the gettering site. There are three general gettering categories defined by the gettering mechanism, (a) relaxation gettering, (b) segregation gettering, and (c) phosphorus diffusion gettering.

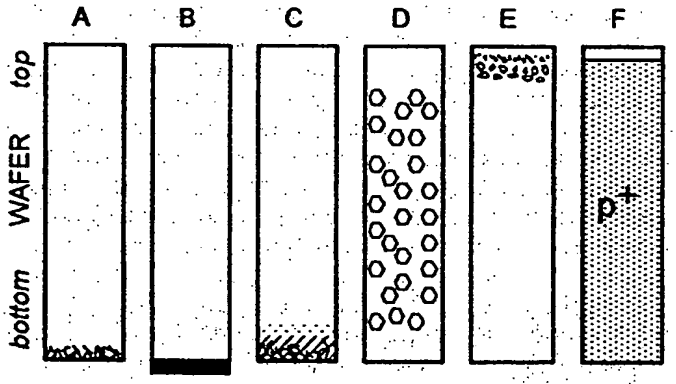

Fig. 11. Schematics of different gettering techniques, illustrating the relative location of the top of the wafers, where devices are manufactured, and the gettering sites. The drawing is not to scale

In relaxation gettering techniques, such as gettering by silicon-oxide precipitates (internal gettering), heterogeneous precipitation sites are intentionally formed in regions away from the device/surface region. The gettering process requires an impurity supersaturation, which typically occurs during a cool down from high temperatures. Any mobile and supersaturated impurity will quickly precipitate in regions of the silicon wafer, where high concentrations of precipitation sites are intentionally introduced. On the contrary, in the device/surface regions with relatively low nucleation site densities (where no precipitation sites were created intentionally), supersaturated impurities will precipitate slowly. This difference in precipitation rates creates a dissolved impurity concentration gradient, which in turn causes diffusion of supersaturated impurities away from the surface/device region and into the bulk towards the gettering sites.

Segregation gettering is driven by a gradient or a discontinuity of the impurity solubility. The region of higher solubility acts as a sink for impurities from the lower solubility region. This is because the electrochemical potential of a dissolved impurity, $\mu \propto k_B T \times \ln(c/c_0)$, for the same dissolved concentration, c, is lower in the regions with higher equilibrium solubility, c_0. The difference in electrochemical potentials is the driving force for the gettering. The advantage of segregation gettering over relaxation gettering is that no supersaturation is required. Thus, in principle, low impurity concentrations in the device region can be quickly achieved at elevated temperatures where the impurities diffuse quickly. The segregation effect can result from (a) a difference in phase, for example, between crystalline and liquid silicon during crystal growth; (b) a difference in material, for example, between silicon and aluminum layer deposited on one of the wafer surfaces; (c) difference in doping levels in different areas of the wafer, which results in a gettering effect due to the effect of Fermi level or formation of metal-acceptor pairs on solubility of metals (see, for example, [597, 598]); or (d) strain which may in some cases increase or decrease the local solubility of metal impurities (see, for example, [171, 599]).

Phosphorus diffusion gettering is a unique gettering technique which enhances the diffusion of substitutional metals towards the gettering layer through the injection of silicon self-interstitials. Additionally, the metals are trapped by a complex effect of change of solubility of metals in heavily n-type doped region and their precipitation at extended defects and precipitates formed in the diffused region. It is particularly well suited for substitutional metals, whose gettering is limited by diffusion.

Segregation and relaxation gettering mechanisms can be distinguished by examining the equilibrium metal concentration in the gettered region after prolonged anneal, sufficient to establish the equilibrium distribution of metals, and a very fast quenching of the samples to "freeze in" this distribution. Segregation gettering will decrease the metal concentration below its equilibrium solubility at the annealing temperature, whereas relaxation gettering will not. One may think that since segregation gettering is an equilibrium process that takes place at high temperatures, then the efficiency of segregation gettering would not depend on the cooling rate. However, this is true only if the segregation coefficient does not

depend on the temperature. If the segregation coefficient is a function of temperature, as it is the case with gettering of Fe by p^+ substrate (Sect. 6.3), the cooling rate will be extremely important for the efficient segregation gettering.

It should be noted that the physical mechanisms involved in gettering are very complex, and the classification of the gettering techniques given above is rather loose. Not only it is sometimes difficult to distinguish the gettering mechanisms, as it is shown in the previous paragraph, but also most gettering techniques include elements of both relaxation and segregation gettering. For instance, gettering by heavily doped substrates includes segregation gettering associated with enhancement of metal solubility in p^+-substrate and relaxation gettering by silicon-oxide precipitates in the substrate. Gettering by implantation creates damage which may provide precipitation sites for relaxation gettering, but may also change the local solubility of impurities by locally changing the strain of the lattice and the local doping level. For this reason, the discussion below will follow primarily gettering techniques rather than gettering mechanisms. It should also be noted that the authors did not attempt to give a complete account of the present understanding of gettering mechanisms in this section. Our discussion below will primarily be focused on data specifically associated with the gettering of iron. For a detailed discussion of gettering techniques and their application to gettering of Au, Cu, Ni, etc., readers are referred to our recent book chapter on gettering in silicon [600], that of McHugo et al. [601], and the review article of Myers et al. [602].

Probably the most important parameter of any gettering technique is its optimum "processing window". For segregation gettering, these are the temperatures where the impurity is mobile and the segregation effect is the strongest. For relaxation gettering, it is the range of temperatures where impurities become supersaturated, but remain sufficiently mobile to diffuse to the gettering sinks and to precipitate there. Figure 12 presents a diagram of solubility of three common contaminants, titanium (a slow diffuser with low solubility), iron (a fast diffuser with high solubility), and copper (the fastest diffuser in silicon with extremely high solubility), plotted against their diffusivity. The average diffusion lengths after 30 min anneal, calculated as $d = \sqrt{4Dt}$, which correspond to the diffusion coefficients, D, indicated at the bottom of the graph, are presented at the top of the plot. We assumed here that 30 min is a maximum reasonable duration of a gettering anneal. The dashed horizontal line corresponds to the target bulk contamination level of metals of 10^{10} cm^{-3}. For Ti, this concentration corresponds to its equilibrium solubility at 785 °C [123]. The diffusivity of Ti at this temperature is 4.3×10^{-11} cm^2/s, which implies that Ti will diffuse only 5.6 μm during 30 min. For iron and copper the supersaturation at the level of 10^{10} cm^{-3} will be achieved at about 640 °C and 275 °C, and they will diffuse during a 30-min anneal at these temperatures about 400 and 2000 μm, respectively. Note that for copper we used the intrinsic diffusion coefficient [80] since the effective diffusion coefficient in p-Si depends on the doping level. Only copper can diffuse through the whole wafer thickness within 30 min at the temperature, where its supersaturation at the level of 10^{10} cm^{-3} is reached. For all other metals the distance between the device-active region and precipitation sites is of utmost importance for effective relaxation gettering, since it is obvious that the slowly diffusing metals, such as Ti, will *not* be gettered by *relaxation* techniques down to the required levels unless the gettering sites are within a few μm from the devices. This situation is very much different from that some 10 years ago, when one had to getter metals at concentrations of 10^{13} cm^{-3}, and their supersaturation (and hence, the efficient gettering) could be achieved at much higher temperatures, corresponding to higher diffusion coefficients.

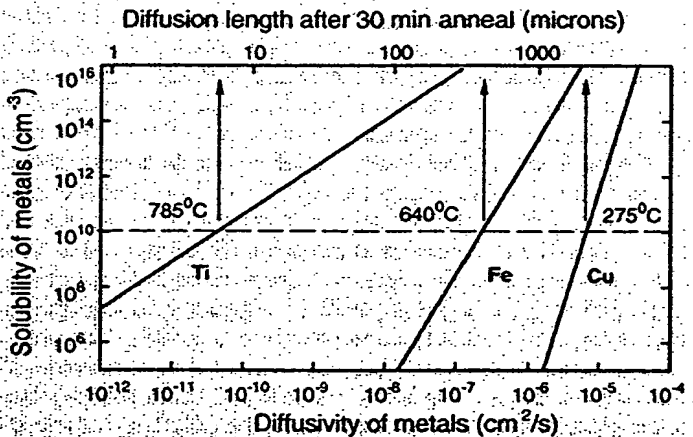

Fig. 12. Dependence on the solubility of titanium, iron, and copper on their diffusivity

This clearly shows that backside damage gettering (Fig. 11a) and aluminum gettering (Fig. 11b), which require metals to diffuse through the whole wafer, are acceptable only if the whole wafer thickness is the device, as it is the case in photovoltaics. In integrated circuit technology, backside gettering techniques would be efficient only for the fast-diffusing metals. Gettering by oxide precipitates, formed in the bulk, decreases the diffusion distance for metals to about 10–20 μm (thickness of the denuded zone). This makes it feasible to getter iron, copper, and nickel below the critical concentrations by relaxation gettering alone, if the wafers are cooled down sufficiently slowly down to temperatures as low as 300 °C [603]. However, gettering of slow-diffusing metals such as Ti remains problematic, unless the cooling is extremely slow. Gettering by implantation and heavily doped substrates brings gettering sites even closer to the devices (the average distance the impurities need to diffuse is on the order of 2–5 μm), and utilizes segregation mechanism of gettering, which is efficient at high temperatures where impurities are mobile. The techniques that form gettering sites in a very close vicinity of the devices are known as proximity gettering techniques. Although the majority of research work reported in the literature in the last few years has been focused on proximity gettering, industry relies to an equal extent on prospective new techniques and on long-established internal and backside gettering. In the next section, we will briefly discuss the most widely used and discussed gettering techniques.

6.1 Gettering of iron by silicon-oxide precipitates

Kaiser [604] and later Mets [605] were the first to establish that silicon-oxide precipitates are sinks for metal impurities. Tan et al. [606] suggested a gettering model which uses

silicon-oxide precipitates as gettering sites. Huff et al. [607] presented a convincing correlation between the amount of precipitated oxygen and DRAM refresh loss results. Studies made by Gilles et al. [148, 149, 608], Hieslmair et al. [154, 290], and Aoki et al. [150–152] confirmed that silicon-oxide precipitates are sinks for iron and proved that internal gettering is a relaxation-type gettering. Oxygen is incorporated into the silicon crystal during Czochralski-type crystal growth primarily from the SiO_2 crucible in concentrations of about 10^{17} to 10^{18} cm^{-3}. This concentration exceeds the oxygen equilibrium solubility at temperatures used for device processing and results in the precipitation of the supersaturated oxygen. Since the formation of silicon-oxide precipitates in the device region reduces device yield, much effort in the early days of the silicon era was concentrated on the engineering of oxygen precipitation. It was shown that it is possible to create a layer free of silicon-oxide precipitates near the surface/device region (denuded zone (DZ)) and to precipitate supersaturated oxygen only in the bulk of the wafer. The DZ can be formed by heating the wafer to high temperatures in order to allow the oxygen in the near-surface region to diffuse out of the wafer. After this out-diffusion, the resulting oxygen concentration in the surface region is significantly lower than the bulk concentration. Thus, during a subsequent lower temperature annealing, nucleation of silicon oxide takes place only in the bulk [606, 609–611]. The nuclei then grow during subsequent high-temperature anneals.

The only step that is required to introduce internal gettering into the technological process is the nucleation and growth of silicon-oxide precipitates, which is usually achieved by a three-step annealing. If this treatment is done before actual manufacturing of devices, then no other gettering-specific technological steps are required. Gettering occurs each time when the wafer is cooled down at the end of high-temperature annealing steps. Since internal gettering requires that metals be supersaturated and mobile at the same time, the efficiency of gettering is strongly affected by the cooling profile, particularly in the low-temperature region [603]. Additionally, the gettered iron is not stable at silicon-oxide precipitates and can be completely dissolved by re-heating the sample to sufficiently high temperatures [167, 169, 170, 612]. Hence, the *last* cooling in the technological process is the most important for efficient internal gettering.

Although internal gettering is widely used in silicon technology, not all aspects of the physics of internal gettering are completely understood. For example, the nature of the gettering sites associated with silicon-oxide precipitates has been disputed for a long time. Not only can oxygen precipitate in different morphologies depending on its initial concentration in the wafer and growth regime, but silicon-oxide precipitates also produce structural defects such as punched-out dislocations and stacking faults during precipitate growth, which could serve as precipitation sites (see, for example, [613–618]). Only recently has it become clear that each metal has different precipitation behavior and precipitates preferably at different defects [619–624]. There are indications that iron [148, 149, 154, 172, 625] and nickel [626–628] precipitate at silicon-oxide precipitates themselves and possibly at stacking faults [629, 630]. On the other hand, copper and palladium precipitate preferably at punched-out dislocations and stacking faults [624, 631]. This behavior has been related to the crystallographic structure of metal-silicides, where high silicon content silicides (such as $FeSi_2$, $NiSi_2$, $CoSi_2$, see [5, 632–634]) relieve compressive strains [171, 173] and thus would be favorable in regions of high compressive strain field such as near silicon-oxide precipitates. Additionally, it has been reported that strain fields of silicon-oxide precipitates stabilize the Fe precipitates [171]. Similar effect of trapping of iron by stress at the edges of local oxidation of silicon (LOCOS) structures was reported by Ishigami et al. [635]. In contrast, low-silicon-content silicides (such as Pd_2Si, Cu_3Si, see [5, 633, 634, 636]) require the emission of silicon interstitials and the nucleation of such a precipitate would be inhibited near an silicon-oxide precipitate. These metals precipitate at punched-out dislocations and stacking faults and, due to additional stresses, cause dislocations to move and multiply, creating additional nucleation sites [637]. Apparently, silicon-oxide precipitates with long stacking faults and punched-out dislocation networks would provide gettering sinks for both high-silicon-content and low-silicon-content metal precipitates. This was confirmed by device yield studies [638, 639] and comparative analysis of gettering of different metals [626]. Takahashi et al. [640, 641] studied the effect of size and density of silicon-oxide precipitates on the internal gettering efficiency in CZ silicon and found that, for the same amount of precipitated oxygen, the sample containing precipitates with larger size and lower density has stronger gettering efficiency than the sample containing precipitates with smaller size and higher density during cooling from the temperature of 1050 °C. They explained it by greater nr_0 products in the case of larger precipitates (n is the precipitate density, and r_0 is their radius, see [153] for details). A similar conclusion was made by Sadamitsu et al. [155], and Ogushi et al. [156], who varied the duration of the growth anneal of the precipitates and found that, for the same density of the precipitates, larger precipitates were more effective as gettering sites. On the other hand, a sample with high concentration of smaller precipitates had stronger gettering efficiency during isothermal anneal at 190 °C [640], which can be understood from the low diffusivity of iron at this temperature, and thus low probability of it being trapped if silicon-oxide precipitates are far apart.

There is no doubt that internal gettering, which is very easily incorporated into the production lines, will still play a role for the years to come, particularly with the use of optimized cooling profiles. However, although internal gettering may still be effective with the lower thermal budgets for fast-diffusing metals such as copper and nickel, there is a concern that slower diffusing metals such as iron may not be adequately gettered. Introduction of MCZ-grown wafers with lower oxygen concentration would further decrease the effectiveness of internal gettering. Therefore, alternative gettering techniques attract increasingly high attention.

6.2 *Backsurface damage and polysilicon backside gettering*

Backside damage and polysilicon backside gettering utilize gettering sites introduced at the backside of the wafer by mechanical damage of silicon (sandblasting, lapping, etc.) [605, 642, 643], by laser damage [644, 645], by deposition of a polysilicon layer [646–649], a Si_3N_4 film [649, 650], or by a layer of porous silicon [651]. TEM studies [649, 652], X-ray topography [645, 650, 653], and selective etching of

the samples [643, 654, 655] revealed that the damaged layer consists of complicated networks of dislocations, intrinsic stacking faults, and regions with intensive lattice strain. Since the structure of the damaged layer was shown to depend significantly on the type and intensity of the damage [654, 656] and could vary with high-temperature annealing [650, 655], it is very difficult to characterize the backside damage gettering mechanism in general or compare different types of damage. Likewise, the physical model of backside damage gettering remains controversial. Currently, there are three models for backside gettering: (a) backside damage gettering is relaxation gettering since backside damage provides an abundance of heterogeneous nucleation sites for precipitation of supersaturated metal impurities [648, 653, 657–660]; (b) backside gettering is segregation gettering, in which metals are trapped at defects (see, for example, discussion in Sumino [661]) by strain fields or enhanced solubility in the vicinity of structural defects [156, 599, 642, 646, 654, 655, 662–664]; and (c) backside treatments enhances internal gettering [647, 649, 665] via acceleration of growth of silicon-oxide precipitates in the bulk by absorption of silicon self-interstitials in the damaged layer [666–669].

The authors of this review believe that the actual gettering mechanism combines all three models to varying extents. Since the number of segregation trapping sites in the gettering layer is limited [670], the segregation mechanism would dominate at low impurity concentrations such as in device-yield studies. At higher impurity concentrations, such as in studies with intentional contamination, the segregation gettering sites may become saturated and the relaxation gettering mechanism becomes dominant.

Backside mechanical damage gettering may no longer be a viable gettering technique since the damage introduces particulate contaminants further into the process line [671]. However, other backside gettering techniques, such as gettering by polysilicon layers, may remain usable as a gettering technique in the future.

6.3 Gettering by heavily doped substrates

The p/p^+ structure, which consists of a moderately p-type doped epitaxial layer on a heavily p^+-doped substrate, was initially utilized to help to prevent the "latch-up" problem in CMOS devices [672]. Subsequent research revealed that the use of p/p^+ wafers provides an additional benefit of gettering iron out of the epitaxial layer and into the substrate. The enhanced solubility of iron in a heavily doped substrate [598] with respect to a moderately doped epitaxial layer is the driving force for p/p^+ segregation gettering [418, 663, 673–675]. Precipitation of metals at silicon-oxide precipitates provides an additional relaxation gettering mechanism in the substrate. The efficiency of p/p^+ gettering is characterized by segregation coefficient, which is defined as the ratio of the total equilibrium impurity (iron) concentration in the p region to that in the p^+ region. The effect of segregation of iron in the p^+-layer can be understood as follows. The total dissolved iron concentration is given by a sum of concentrations of three separate species, neutral interstitial iron, Fe_i^0, interstitial ionized iron, Fe_i^+, and iron paired with an acceptor such as boron, FeB. As discussed in the first part of our review [116], the concentration of substitutional iron can be neglected. Since iron dissolves interstitially in neutral charge state (see [116] for the details), Fe_i^0 is the species which is in actual equilibrium with the boundary phase $FeSi_2$. If significant concentrations of iron are present as Fe_i^+ or FeB pairs, the total solubility of iron will increase over its solubility in intrinsic silicon. The amount of each iron species present depends on the equilibrium of the following sequence of defect reactions:

$$FeSi_2 \leftrightarrow Fe_i^0 \leftrightarrow Fe_i^+ \leftrightarrow FeB\,. \tag{14}$$

The balance of the first reaction in (14) is given by [116]

$$N(Fe_i^0) \cong S(Fe_i) = 8.4\times10^{25}\exp(-2.86\,\mathrm{eV}/k_BT),\ \mathrm{cm}^{-3}\,, \tag{15}$$

where $N(Fe_i^0)$ is the concentration of neutral iron, and $S(Fe_i)$ is the solubility of interstitial iron. We assumed here that the solubility of iron in intrinsic silicon, given in (15), corresponds primarily to its solubility in neutral charge state. The balance of the second reaction in (14) is determined by

$$N(Fe_i^+)/N(Fe_i^0) = \frac{1}{2}\exp((E_T - E_F)/k_BT)\,, \tag{16}$$

where E_T is the energy level position of interstitial iron at the gettering temperature, and E_F is the Fermi level position. Finally, the last reaction in (14) is determined by the mass-action law [36, 116, 676]:

$$\frac{N(FeB)}{N(Fe_i^+)} = \frac{4\times N(B)}{5\times10^{22}}\exp(E_B/k_BT)\,, \tag{17}$$

where E_B is the binding energy of the FeB pairs, and $N(B)$ and $N(FeB)$ are concentrations of boron and iron-boron pairs, respectively. A simple transformation enables one to obtain the following expression for the total iron concentration:

$$\begin{aligned} N(Fe_{total}) &= N(Fe_i^0) + N(Fe_i^+) + N(FeB) \\ &= 8.4\times10^{25}\times\exp(-2.86\,\mathrm{eV}/k_BT) \\ &\quad\times\left[1+\frac{1}{2}\exp\left(\frac{E_T-E_F}{k_BT}\right)\right. \\ &\quad\left.\times\left(1+\frac{4\times N(B)}{5\times10^{22}}\exp\left(\frac{E_B}{k_BT}\right)\right)\right]. \end{aligned} \tag{18}$$

Equation (18) can be used to predict the segregation coefficient of iron in the p^+ substrate, provided the temperature dependence of the iron trap level and the pairing constants of iron with boron are known. The kinetics of gettering can be modeled if the effective diffusion coefficient of ionized iron in the presence of boron traps is available. Unfortunately, none of the required constants is known with an accuracy sufficient for accurate predictive modeling (see [116] for a detailed discussion). A simple estimate using available constants shows that the Fermi level effect and ion pairing alone can account for the segregation coefficient from 10^{-3} to 10^{-6}. Dislocation formation at the epi-substrate interface [677–680] as well as relaxation gettering by silicon-oxide precipitates in the substrate [681–683] may enhance the gettering effect even further.

There have been numerous experimental and theoretical studies on the segregation coefficient of iron [418, 663, 673,

675, 684, 685]. These studies have either observed an increase in the iron concentration in heavily doped regions [418, 686], or a decrease in the adjoining moderately doped silicon regions [663, 673, 675, 684, 685]. Tobe et al. [684] examined segregation of iron in a thin p^+ layer from p substrate to increase the sensitivity of the method. Benton et al. [418], Stolk et al. [673], and Tobe et al. [684] found that at higher temperatures (around 1000 °C) the segregation coefficient approaches unity (i.e. no segregation). Although it was not confirmed experimentally, all suggested models for temperature dependency of the segregation coefficient assume that at lower temperatures (500–600 °C) the segregation coefficient can reach 10^{-6}. The models of different authors disagree primarily in the middle-temperature range, i.e., at temperatures, where the combination of relatively high diffusivity of iron and already sufficiently high segregation coefficient makes gettering most efficient. This disagreement is associated mainly with the uncertainty in the position of iron level in the bandgap. As discussed in [116], the temperature dependence of the iron trap level, $E_T(T)$, has been investigated by Gilles et al. [598] and McHugo et al. [444] who both observed a strong decrease in the position of iron trap level measured with respect to the valence band at temperatures above 750 °C. It was found that at $T > 1100$ °C, the iron level position nearly merges with the valence band. There exist no data on the position of the iron trap level between room temperature and about 750 °C, and different interpolations were suggested. The segregation coefficient of iron, calculated for the "proportional", "step-like", and "parabolic" models from [116] using (18), and segregation coefficients of iron as predicted by Benton et al. [418] and Tobe et al. [684] are plotted in Fig. 13. Note that the doping levels of the substrate and the epi-layer, used for experimental or theoretical assessment of the segregation coefficient, varied for different groups. Therefore, to present all these models on a single plot, we had to recalculate the experimental data points and results of modeling to a p/p^+ structure with the doping levels $10^{15}/10^{18}$ cm^{-3} by using (18). The discrepancy in predicted segregation coefficient between different models is the largest at about 800 K, where it reaches more than an order of magnitude. Obviously, the p/p^+ gettering of iron cannot be quantified until the accurate measurements in the temperature range from 400 to 800 °C (and particularly in the range from 700 K (427 °C) to 900 K (627 °C), where the difference between the models shown in Fig. 13 is the largest) are carried out.

Studies of the effect of p/p^+ gettering of iron on device yield indicate that this type of gettering can efficiently protect against accidental iron contamination. In the study by Mertens et al. [25], the gate oxide yields were measured on various CZ, FZ, and p/p^+ wafers with and without intentional iron contamination. By a large margin, p/p^+ structures had the best yields with (40% to 60%) and without ($\approx$ 95%) iron contamination. In contrast, FZ wafers, which also had very good yields in the absence of any iron contamination (95%), were found to be extremely sensitive to iron (0% yield in contaminated samples). Similarly, studies by Gregor et al. [687] and Cerofolini et al. [688] have shown increased device yield when epi-wafers with heavily doped substrates were used.

Whereas p/p^+ wafers are widely used for various applications and are well studied from the point of view of gettering, very little is known about gettering of iron in n/n^+ wafers. Gilles et al. [598] have shown a solubility increase in n^+

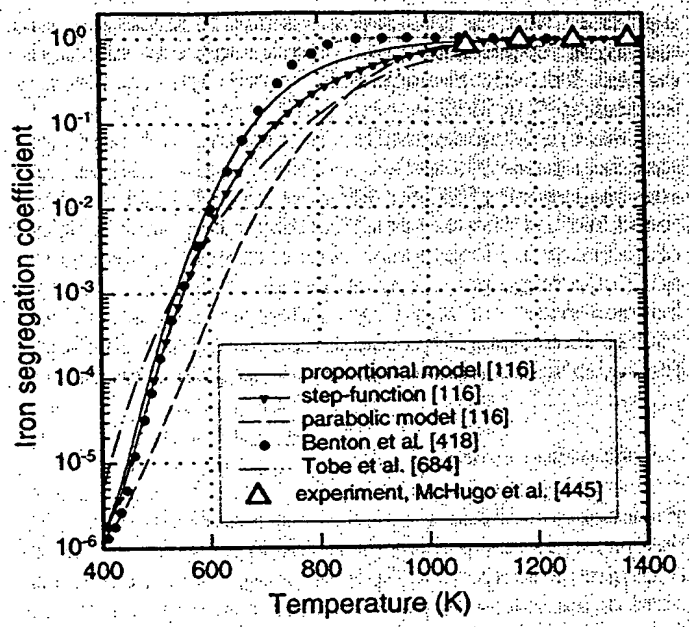

Fig. 13. The segregation coefficient as a function of temperature using three possible iron trap level dependencies according to [116] and data from McHugo et al. [445], Benton et al. [418], and Tobe et al. [684]. The *data points* shown for McHugo are derived for silicon with $N_A = 10^{18}$ B/cm^3 using their solubility measurements on silicon with a doping level of 1.5×10^{19} B/cm^3 and equations in the text

materials. Thus, in principle, n/n^+ should getter iron. Another interesting question which needs yet to be understood is whether lattice strain at epi/substrate interface [689, 690] affects the kinetics of gettering or the segregation coefficient of iron.

6.4 *Aluminum gettering*

Aluminum gettering uses a layer of Al–Si eutectic on the backside surface of a silicon wafer as a sink for impurities. Although this mechanism is incompatible with the IC industry (primarily due to Al junction spiking and the relatively high vapor pressure of Al, which can evaporate from the back surface and contaminate the front surface), it has found wide application in photovoltaics, which utilizes aluminum metallization as a part of the technological process. It has been shown that Al gettering results in a marked improvement in material properties in polycrystalline silicon and in overall increase of solar cell efficiencies by as much as 0.5% to 1% [691–699]. Experiments with Al gettering of IC-grade single-crystal silicon after intentional contamination gave similar results [697, 698, 700–704].

Aluminum gettering is accomplished by deposition and subsequent heating of a thin Al or 2% Si–Al film on the backside of a silicon substrate. The primary mechanism for Al gettering is the segregation of the impurities from the silicon to the Al–Si liquid layer. Most metal impurities, including Fe, Cu, and Ni, have a solubility of 1 to 10 atomic percent in Al over a wide temperature range [705, 706], even with a moderate concentration of silicon in the Al. Metal impurity solubilities in silicon are significantly lower and decrease with decreasing temperature. Therefore, a segregation coefficient of 10^{-3} to 10^{-9} is expected, depending on the metal impurity and temperature. Furthermore, the annealing of Al forms

the samples [643, 654, 655] revealed that the damaged layer consists of complicated networks of dislocations, intrinsic stacking faults, and regions with intensive lattice strain. Since the structure of the damaged layer was shown to depend significantly on the type and intensity of the damage [654, 656] and could vary with high-temperature annealing [650, 655], it is very difficult to characterize the backside damage gettering mechanism in general or compare different types of damage. Likewise, the physical model of backside damage gettering remains controversial. Currently, there are three models for backside gettering: (a) backside damage gettering is relaxation gettering since backside damage provides an abundance of heterogeneous nucleation sites for precipitation of supersaturated metal impurities [648, 653, 657–660]; (b) backside gettering is segregation gettering, in which metals are trapped at defects (see, for example, discussion in Sumino [661]) by strain fields or enhanced solubility in the vicinity of structural defects [156, 599, 642, 646, 654, 655, 662–664]; and (c) backside treatments enhances internal gettering [647, 649, 665] via acceleration of growth of silicon-oxide precipitates in the bulk by absorption of silicon self-interstitials in the damaged layer [666–669].

The authors of this review believe that the actual gettering mechanism combines all three models to varying extents. Since the number of segregation trapping sites in the gettering layer is limited [670], the segregation mechanism would dominate at low impurity concentrations such as in device-yield studies. At higher impurity concentrations, such as in studies with intentional contamination, the segregation gettering sites may become saturated and the relaxation gettering mechanism becomes dominant.

Backside mechanical damage gettering may no longer be a viable gettering technique since the damage introduces particulate contaminants further into the process line [671]. However, other backside gettering techniques, such as gettering by polysilicon layers, may remain usable as a gettering technique in the future.

6.3 Gettering by heavily doped substrates

The p/p^+ structure, which consists of a moderately p-type doped epitaxial layer on a heavily p^+-doped substrate, was initially utilized to help to prevent the "latch-up" problem in CMOS devices [672]. Subsequent research revealed that the use of p/p^+ wafers provides an additional benefit of gettering iron out of the epitaxial layer and into the substrate. The enhanced solubility of iron in a heavily doped substrate [598] with respect to a moderately doped epitaxial layer is the driving force for p/p^+ segregation gettering [418, 663, 673–675]. Precipitation of metals at silicon-oxide precipitates provides an additional relaxation gettering mechanism in the substrate. The efficiency of p/p^+ gettering is characterized by segregation coefficient, which is defined as the ratio of the total equilibrium impurity (iron) concentration in the p region to that in the p^+ region. The effect of segregation of iron in the p^+-layer can be understood as follows. The total dissolved iron concentration is given by a sum of concentrations of three separate species, neutral interstitial iron, Fe_i^0, interstitial ionized iron, Fe_i^+, and iron paired with an acceptor such as boron, FeB. As discussed in the first part of our review [116], the concentration of substitutional iron can be neglected. Since iron dissolves interstitially in neutral charge state (see [116] for the details), Fe_i^0 is the species which is in actual equilibrium with the boundary phase $FeSi_2$. If significant concentrations of iron are present as Fe_i^+ or FeB pairs, the total solubility of iron will increase over its solubility in intrinsic silicon. The amount of each iron species present depends on the equilibrium of the following sequence of defect reactions:

$$FeSi_2 \leftrightarrow Fe_i^0 \leftrightarrow Fe_i^+ \leftrightarrow FeB\,. \tag{14}$$

The balance of the first reaction in (14) is given by [116]

$$N(Fe_i^0) \cong S(Fe_i) = 8.4 \times 10^{25} \exp(-2.86\,\mathrm{eV}/k_B T),\ \mathrm{cm}^{-3}\,, \tag{15}$$

where $N(Fe_i^0)$ is the concentration of neutral iron, and $S(Fe_i)$ is the solubility of interstitial iron. We assumed here that the solubility of iron in intrinsic silicon, given in (15), corresponds primarily to its solubility in neutral charge state. The balance of the second reaction in (14) is determined by

$$N(Fe_i^+)/N(Fe_i^0) = \frac{1}{2}\exp((E_T - E_F)/k_B T)\,, \tag{16}$$

where E_T is the energy level position of interstitial iron at the gettering temperature, and E_F is the Fermi level position. Finally, the last reaction in (14) is determined by the mass-action law [36, 116, 676]:

$$\frac{N(FeB)}{N(Fe_i^+)} = \frac{4 \times N(B)}{5 \times 10^{22}} \exp(E_B/k_B T)\,, \tag{17}$$

where E_B is the binding energy of the FeB pairs, and $N(B)$ and $N(FeB)$ are concentrations of boron and iron-boron pairs, respectively. A simple transformation enables one to obtain the following expression for the total iron concentration:

$$\begin{aligned} N(Fe_{total}) &= N(Fe_i^0) + N(Fe_i^+) + N(FeB) \\ &= 8.4 \times 10^{25} \times \exp(-2.86\,\mathrm{eV}/k_B T) \\ &\quad \times \left[1 + \frac{1}{2}\exp\left(\frac{E_T - E_F}{k_B T}\right)\right. \\ &\quad \left. \times \left(1 + \frac{4 \times N(B)}{5 \times 10^{22}} \exp\left(\frac{E_B}{k_B T}\right)\right)\right]. \end{aligned} \tag{18}$$

Equation (18) can be used to predict the segregation coefficient of iron in the p^+ substrate, provided the temperature dependence of the iron trap level and the pairing constants of iron with boron are known. The kinetics of gettering can be modeled if the effective diffusion coefficient of ionized iron in the presence of boron traps is available. Unfortunately, none of the required constants is known with an accuracy sufficient for accurate predictive modeling (see [116] for a detailed discussion). A simple estimate using available constants shows that the Fermi level effect and ion pairing alone can account for the segregation coefficient from 10^{-3} to 10^{-6}. Dislocation formation at the epi-substrate interface [677–680] as well as relaxation gettering by silicon-oxide precipitates in the substrate [681–683] may enhance the gettering effect even further.

There have been numerous experimental and theoretical studies on the segregation coefficient of iron [418, 663, 673,

675, 684, 685]. These studies have either observed an increase in the iron concentration in heavily doped regions [418, 686], or a decrease in the adjoining moderately doped silicon regions [663, 673, 675, 684, 685]. Tobe et al. [684] examined segregation of iron in a thin p^+ layer from p substrate to increase the sensitivity of the method. Benton et al. [418], Stolk et al. [673], and Tobe et al. [684] found that at higher temperatures (around 1000 °C) the segregation coefficient approaches unity (i.e. no segregation). Although it was not confirmed experimentally, all suggested models for temperature dependency of the segregation coefficient assume that at lower temperatures (500–600 °C) the segregation coefficient can reach 10^{-6}. The models of different authors disagree primarily in the middle-temperature range, i.e., at temperatures, where the combination of relatively high diffusivity of iron and already sufficiently high segregation coefficient makes gettering most efficient. This disagreement is associated mainly with the uncertainty in the position of iron level in the bandgap. As discussed in [116], the temperature dependence of the iron trap level, $E_T(T)$, has been investigated by Gilles et al. [598] and McHugo et al. [444] who both observed a strong decrease in the position of iron trap level measured with respect to the valence band at temperatures above 750 °C. It was found that at $T > 1100$ °C, the iron level position nearly merges with the valence band. There exist no data on the position of the iron trap level between room temperature and about 750 °C, and different interpolations were suggested. The segregation coefficient of iron, calculated for the "proportional", "step-like", and "parabolic" models from [116] using (18), and segregation coefficients of iron as predicted by Benton et al. [418] and Tobe et al. [684] are plotted in Fig. 13. Note that the doping levels of the substrate and the epi-layer, used for experimental or theoretical assessment of the segregation coefficient, varied for different groups. Therefore, to present all these models on a single plot, we had to recalculate the experimental data points and results of modeling to a p/p^+ structure with the doping levels $10^{15}/10^{18}$ cm^{-3} by using (18). The discrepancy in predicted segregation coefficient between different models is the largest at about 800 K, where it reaches more than an order of magnitude. Obviously, the p/p^+ gettering of iron cannot be quantified until the accurate measurements in the temperature range from 400 to 800 °C (and particularly in the range from 700 K (427 °C) to 900 K (627 °C), where the difference between the models shown in Fig. 13 is the largest) are carried out.

Studies of the effect of p/p^+ gettering of iron on device yield indicate that this type of gettering can efficiently protect against accidental iron contamination. In the study by Mertens et al. [25], the gate oxide yields were measured on various CZ, FZ, and p/p^+ wafers with and without intentional iron contamination. By a large margin, p/p^+ structures had the best yields with (40% to 60%) and without ($\approx 95\%$) iron contamination. In contrast, FZ wafers, which also had very good yields in the absence of any iron contamination (95%), were found to be extremely sensitive to iron (0% yield in contaminated samples). Similarly, studies by Gregor et al. [687] and Cerofolini et al. [688] have shown increased device yield when epi-wafers with heavily doped substrates were used.

Whereas p/p^+ wafers are widely used for various applications and are well studied from the point of view of gettering, very little is known about gettering of iron in n/n^+ wafers. Gilles et al. [598] have shown a solubility increase in n^+

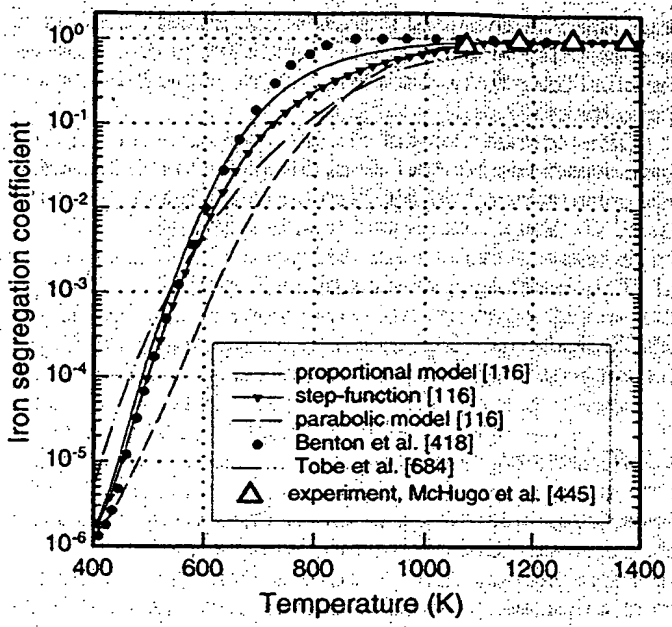

Fig. 13. The segregation coefficient as a function of temperature using three possible iron trap level dependencies according to [116] and data from McHugo et al. [445], Benton et al. [418], and Tobe et al. [684]. The *data points* shown for McHugo are derived for silicon with $Na = 10^{18}$ B/cm^3 using their solubility measurements on silicon with a doping level of 1.5×10^{19} B/cm^3 and equations in the text

materials. Thus, in principle, n/n^+ should getter iron. Another interesting question which needs yet to be understood is whether lattice strain at epi/substrate interface [689, 690] affects the kinetics of gettering or the segregation coefficient of iron.

6.4 Aluminum gettering

Aluminum gettering uses a layer of Al–Si eutectic on the backside surface of a silicon wafer as a sink for impurities. Although this mechanism is incompatible with the IC industry (primarily due to Al junction spiking and the relatively high vapor pressure of Al, which can evaporate from the back surface and contaminate the front surface), it has found wide application in photovoltaics, which utilizes aluminum metallization as a part of the technological process. It has been shown that Al gettering results in a marked improvement in material properties in polycrystalline silicon and in overall increase of solar cell efficiencies by as much as 0.5% to 1% [691–699]. Experiments with Al gettering of IC-grade single-crystal silicon after intentional contamination gave similar results [697, 698, 700–704].

Aluminum gettering is accomplished by deposition and subsequent heating of a thin Al or 2% Si–Al film on the backside of a silicon substrate. The primary mechanism for Al gettering is the segregation of the impurities from the silicon to the Al–Si liquid layer. Most metal impurities, including Fe, Cu, and Ni, have a solubility of 1 to 10 atomic percent in Al over a wide temperature range [705, 706], even with a moderate concentration of silicon in the Al. Metal impurity solubilities in silicon are significantly lower and decrease with decreasing temperature. Therefore, a segregation coefficient of 10^{-3} to 10^{-9} is expected, depending on the metal impurity and temperature. Furthermore, the annealing of Al forms

a p^+ layer, which is used in photovoltaics to reflect electrons and avoid recombination at the back surface of silicon solar cells. The reflection process is known as the back-surface field effect [707, 708].

Direct measurements of the Si–Al segregation coefficient have been made by Apel et al. [709] for Co in silicon and Hieslmair et al. [700] for Fe in silicon. Apel et al. [709] found 10^{-4} as a lower bound for the segregation coefficient of Co between silicon and an Al layer at 820 °C. Hieslmair et al. [700] found segregation coefficients of $10^{-5} - 10^{-6}$ for Fe between silicon and an Al layer at temperatures from 750 to 950 °C. Joshi et al. [698] estimated the segregation coefficient for iron in silicon/aluminum to be of the order of 10^{-4}.

6.5 *Phosphorous gettering*

Phosphorus in-diffusion gettering can be accomplished using the carrier gas $POCl_3$, PBr_3 [710, 711], P_2O_5 [628, 712–714], or a spin-on source [596, 712]. A phosphosilicate glass can form on the silicon surface when an oxidizing atmosphere is present. This glass then acts as the doping source for the phosphorus in-diffusion. The phosphorus gettering effect was confirmed by a number of researches over the last 30 years [597, 628, 710–730]. One should note, however, that most studies of phosphorus-diffusion gettering were done for gold, platinum, and palladium, whereas only limited data are available for the gettering of iron.

A layer heavily doped with phosphorus provides a number of potential mechanisms for gettering: solubility enhancement by Fermi level effects, by increase of the substitutional fraction of metals, and by ion pairing; gettering to dislocations and SiP particles generated by phosphorus diffusion, and silicon self-interstitial injection-assisted gettering [628, 723, 725, 731]. The Fermi level effect and ion pairing are expected to be active during phosphorus in-diffusion because solubility enhancements of gold and iron have been observed for heavily P- and As-doped wafers [597, 598, 719, 720] where dislocation formation and self-interstitial injection do not occur. The Fermi level effect [732–735] increases the solubility of positively or negatively charged impurities in p^{++} or n^{++} substrates, respectively, without changing the solubility of neutral impurities, thus the total impurity solubility (neutral plus charged) is increased. Dislocation formation can augment the gettering process via precipitation of the impurities (relaxation gettering) [679, 710, 718, 736, 737]. However, gettering by dislocations cannot fully explain the observed effect since the gettering enhancement has also been observed without dislocation formation [726, 738] and, moreover, some studies have shown no precipitation of the impurities at the dislocations [710, 718, 721]. Self-interstitial injection occurs during phosphorus in-diffusions as has been observed by extrinsic stacking fault growth [739], dislocation climb [740, 741], epitaxial re-growth of silicon at the phosphosilicate–silicon interface [628, 723, 731], silicon-oxide precipitate dissolution [742] and vacancy defect (D-defect) dissolution [743]. The injection of self-interstitials can enhance the diffusion of some metal impurity species, for example, Au and Pt, via the kick-out mechanism [744], which accelerates the kinetics of the gettering process [726–728]. In addition, the injection of silicon self-interstitials may increase the dissolution rate of metal precipitates with sub-critical radius in the gettered region [745]. Schröter and co-workers [628, 723, 725, 727, 729, 730] provided a theoretical model that suggests that phosphorus in-diffusion produces a flux of self-interstitials towards the phosphosilicate glass (PSG)/silicon interface. This flux is speculated to increase the diffusivity of substitutional metal impurities and to enhance their concentration in the phosphorus-doped layer above their solubility, thus driving precipitation of the impurities. Cerofolini, Polignano, et al. [688, 745] reported that the gettering by phosphorus diffusion is much more efficient than gettering by diffusion of other n-type dopants such as arsenic and antimony, which can be interpreted as an indication that formation of n^+-doping layer is only one of the components of phosphorous gettering. This conclusion is also supported by the observation that gettering is much more efficient *during* P-diffusion compared to anneals at the same temperature *after* P-diffusion.

Some further benefits are realized when phosphorous gettering is combined with another gettering technique. A combination of phosphorous and aluminum gettering has been shown to greatly improve the gettering efficiency, suggesting a synergistic effect of these two gettering techniques [699, 746–748]. Phosphorous gettering has also been successfully combined with HCl gettering. This is accomplished by adding trichloroacetic acid into the phosphorous annealing gas. Improvements have been realized for solar cells [697, 746, 748–753] and CMOS integrated-circuit devices [642, 687, 699, 712, 728, 754–757]. For polycrystalline silicon solar cells, the response of the material to the phosphorous gettering treatment depends on the concentration of structural defects [697, 752] as well as oxygen and carbon concentrations [697, 748, 751].

6.6 *Chemical gettering*

Chemical gettering consists of a high-temperature oxidation anneal (usually between 1000 °C and 1100 °C) in dry oxygen with small amounts (usually less than 1%) of chlorine-bearing species (Cl_2, HCl, $C_2H_3Cl_3$ (known as 1,1,1-trichloroethane, or TCA), $C_2H_2Cl_2$ (known as trans-1,2-dichloroethylene, or DCE), or $C_2Cl_2O_2$ (known as oxacyl-chloride, or OC) [758, 759]). The gettering effect is due to the removal of metals from the surface of the wafers through the formation of volatile chloride compounds. Additionally, the chlorine present in the gas phase reacts with the transition or alkali metals, diffusing through the walls of the quartz furnace tube before they can reach and diffuse into the silicon wafers being oxidized. Chlorine incorporated into the oxide also has a passivating effect against sodium drift [760–762]. Oxidation in the presence of chlorine species was shown to decrease the density of surface states at the Si/SiO_2 interface [763] and to improve breakdown characteristics of MOS capacitors [764]. However, the chemical gettering could only moderately decrease the total bulk concentration of metals and improve the minority carrier lifetime [753, 765, 766]. This was understood after experiments of Baginski et al. [767], Ohsawa et al. [133], and Honda et al. [7], who studied the effect of chemical gettering on intentionally contaminated wafers. They found that Cu could be easily gettered from the wafers by the addition of HCl to the oxidizing ambient, whereas Au, Fe, and Cr were not affected.

Recent investigations by Mertens et al. [188,758,759,768] showed that Cl_2 (which is formed through the reaction of the above mentioned Cl-containing gases with oxygen in the furnace ambient) is the active species in Cl-gettering and that other components such as HCl interact very little, if not at all, with the wafer [758]. They also showed that iron can be removed from the wafer only if it is trapped at the top of the surface oxide layer, which can be easily grown by introducing O_2 into the ambient during ramp up [188]. This agrees with the earlier report by Katz et al. [447], who found that HCl gettering can remove Fe and Cr only if these metals are located in the oxide, but not if they are in the substrate. Studies of Mertens et al. (Mertens, 1994 #1499; Mertens, 1997 #886) confirmed that Cl-gettering could not reduce significantly the Fe bulk concentrations. It is interesting to note that Green et al. [769], who also found that Fe and Au were not gettered by HCl at 1000 °C, reported that the average bulk concentration of Fe and Au could be reduced by a factor of 5 by a 30-min anneal at higher temperatures (1275 °C); however, such a high-temperature treatment required use of a different gas mixture, $HCl + SiH_4 + H_2$ instead of $HCl + O_2$. The removal rate was found to be much slower than would be expected from bulk-diffusion, rate-limited transport; thus, surface processes appear to be rate-limiting [769].

6.7 Gettering by implantation

The major factor that determines kinetics of gettering is the distance that metals have to diffuse from the devices to the gettering region. This is the reason why proximity gettering techniques have attracted much attention in the past few years. These techniques form gettering sites just a few μm away from the devices and allow low-temperature-budget gettering. One of the proximity techniques is gettering by ion implantation, started by the pioneering work of Buck et al. [770]. In this technique, the impurities are gettered by the implanted atoms and/or the implantation damage.

Metal impurities are gettered to implanted regions by either a relaxation- or segregation-type mechanism. Relaxation occurs either at implantation-induced damage or at clusters/precipitates of the implanted species. Segregation can occur to a separate phase formed by a high dose implant, or via the Fermi level effect or metal ion pairing with the implant species, for example, boron, arsenic or phosphorus implants, or via chemisorption to internal surfaces of cavities formed by implantation with helium or hydrogen. Metal impurities, such as Cu, Fe, Au, Cr, Ni, and Pt, have been successfully gettered to implant regions. Although most metals are gettered in the area where most of implantation damage is introduced (at projected ion range), gettering by defects at approximately half of the projected range [771–777] and beyond the projected range [778] was observed. The nature of the defects at $R = R_p/2$ and $R > R_p$ (complexes of vacancies versus complexes of interstitials) remains controversial since they cannot be directly observed by TEM.

Gettering has been observed after implantation with silicon [722,770,771,779–783], phosphorus [722,737], carbon [418,784–789], oxygen [779,789–795], helium [789, 796–807], argon [766,779,808–813], neon [811,814], krypton [808], xenon [779,808], hydrogen [780,781,815,816], boron [418,673,806,808], germanium [817,818], chlorine [810], aluminum, and chromium [819]. The implant atoms usually are light elements in order to avoid amorphization of the near-surface region. Implant energies range from 50 keV to 10 MeV with implant doses ranging from 10^{13} to 10^{17} atoms/cm^2. Helium implantation is somewhat different from the other implant types in that it results in voids (helium bubbles) in silicon rather than in implantation damage such as defect clusters or dislocations. Oxygen is another exception since implantation of oxygen to high doses forms a buried oxide layer which has many benefits in terms of radiation hardness and the reduction of device latch-up. This implantation process is known as separation by implantation of oxygen (SIMOX). Impurities such as copper, chromium, and iron can be gettered into the oxide layer [790], at the oxide/silicon interfaces [791], or at the implant damage located deeper than the oxide layer [792–794].

Implantation damage provides both segregation and relaxation gettering sites at the depth of up to 5 μm from the surface, the ratio between the two being dependent on the nature of the implant, implantation dose, and energy of the implant. For instance, Myers et al. [806] and Raineri et al. [807] observed chemisorption of iron at internal walls of cavities formed by helium implantation, and predicted that segregation gettering, at initial iron concentrations below the threshold for silicide formation, will reduce the dissolved-iron concentration by at least two orders of magnitude [806]. Saturation of the segregation effect was observed when the wall coverage of the cavities with iron reached approximately 0.01 of a monolayer [806]. Implantation of boron creates an internal p^+-layer, which getters predominantly by segregation, similarly to heavily doped substrates, and was shown to be very effective [418]. In contrast, Kononchuk et al. [771] suggested that gettering of iron by defects induced by implantation of silicon exhibits a relaxation-type behavior and is limited by diffusion from the bulk. However, a more detailed study of Koveshnikov et al. [772] showed that one should distinguish gettering by defects at ion-projected range R_p in Si-implanted silicon, which occurs predominantly by relaxation mechanism, and gettering by defects in $R_p/2$ range, which is of the segregation type. Similarly, the gettering of iron to carbon-implantation-induced defects was found to be segregation-type [795]. Different implants were shown to vary significantly in terms of the efficiency of iron gettering. Benton et al. [418,686] showed that boron implants getter more Fe than silicon implants, and that carbon implants fall in between boron and silicon in terms of Fe gettering effectiveness. Skorupa et al. [793] observed more efficient gettering of Fe and Cu by carbon implantation than He implantation-induced cavities or SIMOX-related damage structure. In fact, in Skorupa's work, Fe was observed to be gettered only by carbon implantation, in contradiction to work on Fe gettering to cavities [801,804]. Overwijk et al. [789] presented results on implantation gettering of Fe and Cu where they showed that carbon and oxygen implantation gettering is active at implant doses below 6×10^{15} atoms/cm^2 but He implantation is not. However, at doses greater than 6×10^{15} atoms/cm^2, the He implantation getters significantly more Fe and Cu than carbon or oxygen. Geipel and Tice [808] showed that B implantation requires an order of magnitude higher dose than Ar, Kr, or Xe in order to achieve effective gettering.

Implantation gettering has been shown to be highly effective. For instance, Kononchuk et al. [782] demonstrated that the efficient gettering of metallic impurities to below

10^{10} cm^{-3} is possible by MeV self-implantation with the fluence in the range of 10^{15} cm^{-2}. A similar implantation dose (about 10^{14} cm^{-2}) is required for effective gettering of iron by MeV boron implantation [686]. McHugo et al. [820] demonstrated that He implantation-induced cavities dominate as gettering sites if both cavities and internal gettering sites are present in the sample.

Difficulties that can arise from gettering by ion implantation include an increase in native point-defect concentrations, i.e., vacancies and self-interstitials, which can enhance dopant diffusion and hinder shallow-junction formation [821]. Another drawback to implantation gettering is the required high implant doses, which correspond to undesirably long implantation times.

6.8 *Predictive modeling of gettering*

Since process-yield experiments have become prohibitively expensive, computer simulations of defect reactions in silicon, and gettering in particular, is becoming an invaluable tool for process development and yield optimization. Simulations of the gettering process are achieved within a finite-differences diffusion algorithm (see for example [822–825]) by including equations that describe precipitation and/or segregation of impurities in the gettering region. Diffusion of impurities toward gettering region is described by Fick's diffusion equation. Most approaches [153, 290, 663, 826, 827] to modeling precipitation in relaxation gettering are based on Ham's fixed radius solution [289] for impurity precipitation. Ham's fixed radius solution expresses the precipitation of a supersaturated dissolved impurity as an exponential decay with a time constant, $\tau = 1/4\pi Dnr_0$, where D is the diffusivity, n is the number of precipitation sites, and r_0 is the radius of the sites. In a finite-differences simulation, the time constant in Ham's equation can be varied appropriately after each time step, Δt. In this manner, Ham's fixed radius solution can be used to simulate growing radius precipitation kinetics, effective diffusivity, changing temperature, and even a variable precipitate site density [153, 290]. Thus, experimental data can be fitted and quantified [154].

Equations for modeling segregation were suggested by Tan et al. [826, 828], who treated segregation as a result of a gradient in the chemical potential. This approach has a disadvantage that abrupt interfaces must be approximated by using a number of very closely spaced nodes. Antoniadis et al. [829] proposed a simpler approach which essentially manipulates the impurity concentration gradient (a kinetic phenomena) in order to simulate segregation (a thermodynamic phenomena). Recently, Tan et al. [830] developed a unified treatment of diffusion in chemical potentials and temperature gradients. These approaches were used in recently developed gettering simulators [290, 603, 827, 831, 832].

The major difficulty with predictive gettering simulations is to accurately obtain the material parameters such as the density and size of nucleation sites in relaxation gettering techniques, the segregation coefficients of metals in heavily doped substrates as a function of temperature, the relative contribution of segregation and relaxation gettering mechanism in each technique, the binding and dissociation energies of metal-acceptor pairs, and sometimes even the impurity diffusivity. For example, one must frequently determine *effective* diffusion coefficients, which take into account the interaction of diffusing metal ions with other impurities in the lattice, such as shallow dopants [80, 733], and the concentration of intrinsic point-defects [833, 834]. In fact, although it is clear that the equilibrium concentration of intrinsic point-defects plays an important roles in the simulations of gettering of metals [747, 835, 836], oxygen precipitation [837], and phosphorous gettering [727, 729, 747, 833, 838], their concentrations in dependence on temperature and surface conditions of the wafer are still controversial [837]. Consequently, the determination of the material parameters will become the main target of quantitative studies of gettering in the near future. Additionally, the existing simple models need to be further developed to take into account the complex gettering behaviors of different transition metals and interaction between various defects.

7 Summary

Semiconductor-grade silicon is the purest raw material produced on an industrial scale, more than 12 000 tons/year worldwide [839]. Iron has always been considered the major contaminant in silicon, partly due to its ubiquity and detrimental electrical activity, and partly because it could be detected by almost all measurement methods. Iron could therefore be readily identified as a culprit of the yield degradation. The required purity of silicon with respect to iron is astonishing. It is easy to calculate that the critical contamination level of approximately 10^{11} cm^{-3} is reached by dissolving of only 10 mg of iron in the whole yearly world production of silicon. This high level of purity became possible only after years of research, which resulted in a fairly good understanding of the predominant reaction paths of iron in silicon, and the development of technological procedures to reduce contamination levels of iron to the low level of 10^{10} to 10^{11} cm^{-3}. Some aspects of this state-of-the-art technology have been discussed in this review. Extrapolation of the trend of the increasing silicon purity for the next 10 to 15 years predicts a decrease of iron concentration by another two orders of magnitude, i.e., below the sensitivity limit of all modern analytical tools. It is not surprising that the question whether one should follow this trend or should rather learn how to tolerate the presence of some (low) concentrations of iron is being discussed more and more intensively. This discussion is strongly stimulated by the decreasing prices on the market for integrated circuits and by the increasingly high costs of ultra-pure technology and super-sensitive measurement tools. However, the physics of low iron contamination levels is not satisfactorily studied. The problem is that the predominant reaction paths of iron present in very low concentrations (10^{11} cm^{-3} and below) in the lattice may be different from intentional Fe contamination in the range of 10^{14}–10^{15} cm^{-3}. At these low concentrations, iron will not become supersaturated at temperatures where it remains mobile, and precipitation of iron is hardly possible (although little is known about the formation of small clusters of iron, such as those consisting of 2 to 4 atoms, see [116]). Therefore, the behavior of iron may be determined by other defect reactions, which could play a secondary role for high contamination levels, and were neglected in the past, such as formation of complexes of iron with the lattice defects other than boron. Furthermore, the segregation effects

in p^+ substrates, in silicon dioxide or at Si/SiO_2 interface, in the source/drain wells, or in strain fields of the devices will not saturate during gettering, unlike the case with high intentional contamination levels. Since the segregation of iron, particularly at relatively low temperatures (below 800 °C), is still poorly investigated, this area can be expected to become a field of intensive research in the near future. Similarly, the physics of the breakdown of thin gate oxides (both, SiO_2 and high-k dielectrics) in the presence of metal contaminants may receive increased attention. The questions that need to be answered are what is the mechanism of degradation of devices (particularly gate oxides with thickness below 8 nm) by low concentrations of iron, and how this damaging effect can be prevented.

Low concentrations of iron imply a new physics of contamination. For instance, the standard mechanism of iron indiffusion with formation of iron silicide at the near-surface layer may become inapplicable to surface contamination of 10^9–10^{11} cm^{-2} simply because there is not enough iron to form a silicide. However, the segregation effect of iron to the surface may become noticeable, if not dominant. An interesting illustration of this effect was reported by Nauka and Gomez [840], who reported that DLTS-measured Fe_i concentrations were twice as large as those measured by SPV on the same samples. When the Fe_i concentration exceeded approximately 5×10^{11} cm^{-2}, results obtained by both measurements matched. Additionally, it was shown that the depth profiles measured by DLTS indicated that for low iron contamination levels, concentrations of iron in the near-surface region (first 10 μm) substantially exceeded those in the bulk [840, 841]. It was explained by a competitive processes of out-diffusion of Fe from the bulk towards the surface, and indiffusion of Fe from the surface into the bulk, mediated by the Si oxidation [841]. Furthermore, at low iron concentrations one may expect to observe effects of native point-defects, oxygen, and carbon on defect reaction of iron. These reactions take place at any iron concentrations, but are usually masked by agglomeration/complexing reactions caused by high supersaturation of iron. Hence, the differences between CZ, MCZ, and FZ-grown silicon, as well as between different areas of CZ wafers (inside/outside of the stacking fault ring) may become visible, and can be studied.

The sets of analytical tools, used by the semiconductor industry, has adequate sensitivity for monitoring the concentration of metal impurities at or below the present threshold for device yield. Figure 14 summarizes the sensitivity of different techniques to the bulk and surface iron contamination levels. According to the statistics reported in [294], both wafer- and device-makers are employing primarily TXRF, lifetime/diffusion length measurement techniques, VPD-AAS, and DLTS for routine assessment of contamination level of silicon wafers. These techniques, along with NAA and mass spectrometry, provide a complex of methods suitable to monitor iron contamination in the bulk, in the near-surface region, and on the surface. These methods are in good quantitative agreement with each other as is confirmed by numerous research groups. A good agreement (usually within 30%, but often even within 10%) was achieved between TXRF and RBS [338], TXRF and NAA [842], ICP-MS and AAS [425], TXRF and TOF-SIMS [337, 416, 843], NAA, AAS, and DLTS [443], TXRF and DLTS after diffusion anneal [174], TXRF and SPV after diffusion anneal [177, 279, 296, 844, 845], DLTS and SPV [111, 840, 841, 845], μ-PCD and SPV [279], TXRF and VPD-AAS [298, 344], VPD-AAS and SPV after indiffusion [296], VPD-AAS and SPV, μ-PCD, and DLTS after anneal [846], and surface SIMS and ELYMAT after indiffusion [261, 298].

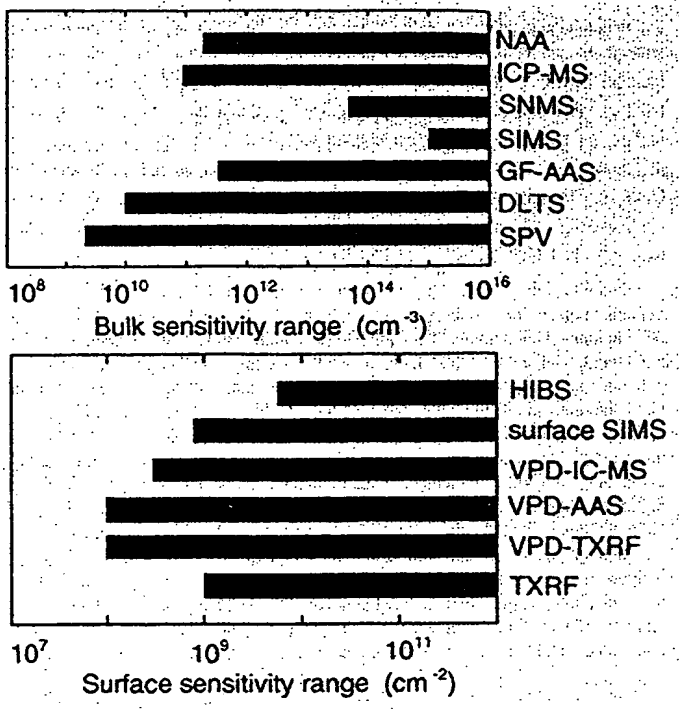

Fig. 14. Comparative diagram of bulk and surface detection limits of analytical techniques discussed in this study. Actual detection limits may be different depending on details of the experimental equipment

An increase in the sensitivity of analytical tools to the iron contamination level of 10^8 cm^{-3} in the next years represents an unprecedented challenge for silicon metrology. Furthermore, the necessity to understand the chemical state of iron in silicon requires techniques that combine high sensitivity with the capability to distinguish different types of chemical bonding. Parallel to this development in metrology, a number of relevant physical problems should be addressed and solved in order to gain a better understanding of the physics of low contamination levels of iron. These problems include, but are not limited to, (a) the iron diffusivity in the ionized/neutral charge state; (b) the temperature dependence of the energy level of iron; (c) the existence and properties of substitutional iron; (d) accurate values of pairing constants of iron with boron; (e) the reactions of iron with Si native defects; (f) the complexes of iron with oxygen, carbon, hydrogen; (g) the effect of cross-contamination with other metals on the reaction paths of iron; (h) the analysis of the physics of iron contamination during silicon crystal growth and processing of the wafers; (i) competitive gettering of iron by gettering sites and devices; (j) the segregation coefficient of iron in p/p^+ epi-wafers at intermediate temperatures; (k) the stability of iron at gettering sites; (l) gettering for low-thermal-budget processing; (m) "how clean is clean enough?" – how far should the cleaning technology be pushed?; (n) the development of metrology of iron to measure even lower Fe concentrations; and (o) the quantification of the influence of iron on device yield. This list, along with the discussion of various aspects of iron contamination-related issues presented in this study,

convincingly shows that the problems associated with unintentional iron contamination on a production line can be traced back to the fundamental physics of iron in silicon, and that a process engineer can greatly benefit from the knowledge of the physical properties and reaction paths of iron in silicon. This series of two reviews on iron in silicon was the first, to the best of our knowledge, attempt to combine the knowledge from the areas of fundamental science and technology, for the benefit of the both.

Acknowledgements. The authors are grateful to L.V.C. Assali, M. Aoki, J.S. Becker, A. Buczkowski, P.K. Chu, D. Ballutaud, J.D'Amico, L. Fabry, E. Gaubas, H. Huff, J.-P. Joly, L.C. Kimerling, J. Knapp, J. Lagowski, P. Mertens, Y. Mori, H. Nakashima, K. Nauka, T. Ohmi, A. Ohsawa, M.L. Polignano, A. Schnieders, A.L. Smith, H. Tsuya, and E. Yakimov for sending us reprints of their papers. The content of this review was influenced by valuable discussions with M. Brohl, A. Buczkowski, L. Fabry, R. Falster, D. Gilles, W. Henley, A. Huber, H. Huff, F.G. Kirscht, J. Knapp, S. Koveshnikov, K.V. Ravi, G. Rozgonyi, W. Schröter, M. Seibt, M. Seacrist, M.B. Shabani, L. Shive, and B.L. Sopori. We would like to thank P. Taylor, S. Rouvimov, S. Koveshnikov, A. Aivazov, L. Shive, Y. Bonan, and H. Kohno for critical reading of the manuscript. The contribution of S.A. McHugo to the collection of data for the gettering section is gratefully acknowledged. This work was supported by the National Renewable Energy Laboratory (NREL) under subcontract number XAF-8-17607-04.

References

1. SIA, International technology roadmap for semiconductors, http://www.itrs.net/ntrs/publntrs.nsf, http://www.sematech.org
2. L. Jastrzebski, J. Lagowski, W. Henley, P. Edelman: In *Beam-Solid Interactions for Materials Synthesis and Characterization*, ed. by D.C. Jacobson, D.E. Luzzi, T.F. Heinz, M. Iwaki (Mater. Res. Soc., Pittsburgh 1995) p. 405
3. W. Bergholz, G. Zoth, F. Gelsdorf, B. Kolbesen: In *Defects in Silicon II*, ed. by W.M. Bullis, U. Gösele (The Electrochem. Soc., Pennington 1991) p. 21
4. W. Schröter, M. Seibt, D. Gilles: In *Materials Science and Technology: A Comprehensive Treatment*, ed. by R.W. Cahn, P. Haasen, E.J. Kramer (VCH, New York 1991) p. 576
5. M. Ronay, R.G. Schad: Phys. Rev. Lett. **64**, 2042 (1990)
6. J. Wong-Leung, D.J. Eaglesham, J. Sapjeta, D.C. Jacobson, J.M. Poate, J.S. Williams: J. Appl. Phys. **83**, 580 (1998)
7. K. Honda, A. Ohsawa, T. Nakanishi: J. Electrochem. Soc. **142**, 3486 (1995)
8. K. Honda, T. Nakanishi, A.W. Ohsawa, N. Toyokura: J. Appl. Phys. **62**, 1960 (1987)
9. N. Nishio, T. Taketomi, M. Morita, S. Ohi, H. Mikoshiba: In *Diagnostic Techniques for Semiconductor Materials and Devices*, ed. by J.L. Benton, G.N. Maracas, P. Rai-Choudhury (The Electrochem. Soc., Pennington 1992) p. 164
10. A.G. Cullis, L.E. Katz: Philos. Mag. **30**, 1419 (1974)
11. H. Mikoshiba, N. Nishio, T. Matsumoto, H. Kikuchi, T. Kitano, H. Kaneko: In *Defect Engineering in Semiconductor Growth, Processing and Device Technology*, ed. by S. Ashok, J. Chevallier, K. Sumino, E. Weber (Mater. Res. Soc, Pittsburgh 1992) p. 629
12. S. Sadamitsu, A. Sasaki, M. Hourai, S. Sumita, N. Fujino: Jpn. J. Appl. Phys. **30**, 1591 (1991)
13. K. Honda, A. Ohsawa, N. Toyokura: Appl. Phys. Lett. **46**, 582 (1985)
14. W.B. Henley, L. Jastrzebski, N.F. Haddad: J. Non-Cryst. Solids **187**, 134 (1995)
15. J. D'Amico, L. Jastrzebski, M. Wilson, A. Savtchouk: In *In-line Methods and Monitors for Process and Yield Improvement*, ed. by S. Ajuria, J.F. Jakubczak (SPIE, Bellingham 1999) p. 124
16. M. Wilson, J. Lagowski, A. Savtchouk, L. Jastrzebski, D. D'Amico, D.K. DeBusk, A. Buczkowski: In *Diagnostic Techniques for Semiconductor Materials and Devices*, ed. by B.O. Kolbesen, C.L. Claeys, P. Stallhofer, F. Tardif, J. Benton, T.J. Shaffner, D.K. Schroder, S. Kishino, P. Rai-Choudhury (The Electrochem. Soc., Pennington 1999) p. 373
17. G. Kamoulakos, C. Kelaidis, C. Papadas, E. Vincent, S. Bruyere, G. Ghibaudo, G. Pananakakis, P. Mortini, G. Ghidini: J. Appl. Phys. **86**, 5131 (1999)
18. M. Liehr, H. Dallaporta, J.E. Lewis: Appl. Phys. Lett. **53**, 589 (1988)
19. M. Takiyama, S. Ohtsuka, S. Hayashi, M. Tachimori: In *Semiconductor Silicon-1994*, ed. by H.R. Huff, W. Bergholz, K. Sumino (The Electrochem. Soc., Pennington 1994) p. 346
20. W.B. Henley, L. Jastrzebski, N.F. Haddad: In *Surface Chemical Cleaning and Passivation for Semiconductor Processing*, ed. by G.S. Higashi, E.A. Irene, T. Ohmi (Mater. Res. Soc., Pittsburg 1993) p. 299
21. L. Jastrzebski, W. Henley, C.J. Nuese: Solid State Technol. **35**(12), 27 (1992)
22. W.B. Henley, L. Jastrzebski, N.F. Haddad: In *Cleaning Technology in Semiconductor Device Manufacturing*, ed. by J. Ruzyllo, R.E. Novak (The Electrochem. Soc., Pennington 1994) p. 487
23. E.P. Burte, W. Aderhold: Solid State Electron. **41**, 1021 (1997)
24. M. Miyazaki, S. Miyazaki, T. Kitamura, T. Aoki, Y. Nakashima, M. Hourai, T. Shigematsu: Jpn. J. Appl. Phys. **34**, 409 (1995)
25. P.W. Mertens, M. Meuris, H.F. Schmidt, S. Verhaverbeke, M.M. Heyns, P. Carr, D. Gräf, A. Schnegg, M. Kubota, K. Dillenbeck, R. de Blank: In *Crystalline Defects and Contamination: Their Impact and Control in Device Manufacturing*, ed. by B.O. Kolbesen, C. Claeys, P. Stallhofer, F. Tardif (The Electrochem. Soc., Grenoble, France 1993) p. 87
26. A. Ohsawa, K. Honda, R. Takizawa, T. Nakanishi, M. Aoki, N. Toyokura: In *Semiconductor Silicon-1990*, ed. by H.R. Huff, K.G. Barraclough, J.I. Chikawa (The Electrochem. Soc., Pennington 1990) p. 601
27. K. Hiramoto, M. Sano, S. Sadamitsu, N. Fujino: Jpn. J. Appl. Phys. (Letters) **28**, L2109 (1989)
28. W. Rieger: In *Crystalline Defects and Contamination: Their Impact and Control in Device Manufacturing*, ed. by B.O. Kolbesen, C. Claeys, P. Stallhofer, F. Tardif (The Electrochem. Soc., Grenoble 1993) p. 103
29. S. De Gendt, D.M. Knotter, K. Kenis, P.W. Mertens, M.M. Heyns: J. Electrochem. Soc. **145**, 2589 (1998)
30. F. Tardif, T. Lardin, C. Paillet, D. Bremond, J.P. Joly, F. Martin, P. Mur, L. Mouche, P. Patruno, A. Tonti, D. Levy, K. Barla, W. Sievert: In *Ultra-Clean Processing of Silicon Surfaces-II*, ed. by M. Heyns (Acco, Leuven, Belgium 1994) p. 309
31. F.G. Kirscht, N.R. Kanungo: In *Contamination Control and Defect Reduction in Semiconductor Manufacturing II*, ed. by R. Novak, D.N. Schmidt, T. Ito, D. Reedy (The Electrochem. Soc., Pennington 1994) p. 38
32. S. Saito, K. Hamada, D.J. Eaglesham, Y. Shiramizu, J.L. Benton, H. Kitajima, S.D.C. Jacobson, J.M. Poate: In *Science and Technology of Semiconductor Surface Preparation*, ed. by G.S. Higashi, M. Hirose, S. Raghavan, S. Verhaverbeke (Mater. Res. Soc., Pittsburgh 1997) p. 81
33. W.C. McColgin, J.P. Lavine, C.V. Stancampiano, J.B. Russel: In *Defect & Impurity Engineered Semiconductors & Devices II*, ed. by S. Ashok, J. Chevallier, W. Goetz, B. Sopori, K. Sumino (Mater. Res. Soc., Pittsburgh 1998) p. 475
34. G. Obermeier, D. Huber: J. Appl. Phys. **81**, 7345 (1997)
35. D. Walz, J.P. Joly, F. Tardif: In *Ultraclean Processing of Si Surfaces-94*, ed. by M. Heyns (Acco, Leuven 1994) p. 139
36. H. Lemke: Phys. Status Solidi A **76**, 223 (1983)
37. W. Shockley, W.T. Read: Phys. Rev. **87**, 835 (1952)
38. R.F. Pierret: *Semiconductor Device Fundamentals* (Addison-Wesley, New York 1996)
39. H.H. Busta, H.A. Waggener: J. Electrochem. Soc. **124**, 1424 (1977)
40. M. Miyazaki, M. Sano, S. Sumita, N. Fujino: Jpn. J. Appl. Phys. (Letters) **30**, L295 (1991)
41. M. Morita, Y. Muramatsu, K. Watanabe, N. Nishio, T. Taketomi, T. Shimono: In *Diagnostic Techniques for Semiconductor Materials and Devices*, ed. by J.L. Benton, G.N. Maracas, P. Rai-Choudhury (The Electrochem. Soc., Pennington 1992) p. 152
42. O.V. Bogorodskii, T.P. Vorontsova, O.S. Zhgutova, V.A. Zlobin, L.A. Kirdyashkina, V.A. Kuz'min, A.S. Kyuregyan, Y.M. Loktaev, L.S. Rybachuk, Y.G. Sorokin, P.N. Shlygin, V.V. Fedorov: Sov. Phys. Techn. Phys. **30**, 818 (1985)
43. Y. Dai: Solid-State Electron. **32**, 439 (1989)
44. H.J. Schulze, B.O. Kolbesen: In *Power Semiconductor Materials and Devices*, ed. by S.J. Pearton, R.J. Shul, E. Wolfgang, F. Ren, S. Tenconi (Mater. Res. Soc., Warrendale 1998) p. 381
45. B.O. Kolbesen, W. Bergholz, H. Wendt: Mat. Sci. Forum **38-41**, 1 (1989)
46. L. Jastrzebski: IEEE Trans. Electron. Devices **ED-29**, 475 (1982)

47. P.J. Ward: J. Electrochem. Soc. **129**, 2573 (1982)
48. G. Zoth, W. Bergholz: J. Appl. Phys. **67**, 6764 (1990)
49. J.H. Reiss, R.R. King, K.W. Mitchell: Appl. Phys. Lett. **68**, 3302 (1996)
50. M. Kittler, W. Seifert, M. Stemmer, J. Palm: J. Appl. Phys. **77**, 3725 (1995)
51. A. Ihlal, R. Rizk: J. Phys. D **29**, 3096 (1996)
52. W. Seifert, M. Kittler, J. Vanhellemont, E. Simoen, C. Claeys, F.G. Kirscht: In *Defect Recognition and Image Processing in Semiconductors 1995*, ed. by A.R. Mickelson (Institute of Physics, Bristol 1996) p. 319
53. M. Kittler, W. Seifert: Scanning Microsc. **9**, 677 (1995)
54. W. Seifert, M. Kittler, J. Vanhellemont: Mater. Sci. Eng. B **42**, 260 (1996)
55. B.L. Sopori: Mater. Sci. Forum **258-63**, 527 (1997)
56. J. Bailey, E.R. Weber: Phys. Status Solidi A **137**, 515 (1993)
57. B.K. Miremadi, S.R. Morrison: J. Appl. Phys. **55**, 3658 (1984)
58. R. Klockenkämper: *Total-Reflection X-ray Fluorescence Analysis* (Wiley, New York 1997)
59. S. Saito, K. Hamada, D.J. Eaglesham, Y. Shiramizu, J.L. Benton, H. Kitajima, S.D.C. Jacobson, J.M. Poate: In *Materials Reliability in Microelectronics VII*, ed. by J.J. Clement, R.R. Keller, K.S. Krisch, J.E. Sanchez, Jr., Z. Suo (Mater. Res. Soc., Pittsburgh 1997) p. 141
60. M.L. Verheijke, H.J.J. Jaspers, J.M.G. Hanssen, M.J.J. Theunissen: J. Radioanal. Nucl. Chem. **113**, 397 (1987)
61. L.A. Files, T. Orent, M. Hammerbacher, J. Arch, J. Butterbaugh: In *Diagnostic Techniques for Semiconductor Materials and Devices*, ed. by D.K. Schroder, J.L. Benton, P. Rai-Choudhury (The Electrochem. Soc., Pennington 1994) p. 322
62. T. Hosoya, Y. Ozaki, K. Hirata: J. Electrochem. Soc. **132**, 2436 (1985)
63. S. Krishnan, O. Laparra: IEEE Trans. Semicond. Manuf. **10**, 273 (1997)
64. G. Zoth, S. Geyer, H.-J. Schulze: In *Analytical and Diagnostic Techniques for Semiconductor Materials, Devices, and Processes*, ed. by B.O. Kolbesen, C. Claeys, P. Stallhofer, F. Tardif, J. Benton, T.J. Shaffner, D.K. Schroder, S. Kishino, P. Rai-Choudhury (The Electrochem. Soc., Pennington 1999) p. 5
65. J.A. James, D.H. Richards: J. Electron. Control **3**, 500 (1957)
66. S. Niese: J. Radioanal. Chem. **28**, 171 (1975)
67. S. Niese: J. Radioanal. Chem. **38**, 37 (1976)
68. A. Huber, G. Böhm, S. Pahlke: J. Radioanal. Nucl. Chem. **169**, 93 (1993)
69. P.F. Schmidt, C.W. Pearce: J. Electrochem. Soc. **128**, 630 (1981)
70. F.A. Trumbore: Bell Syst. Techn. J. **39**, 205 (1960)
71. A.A. Bugay, V.E. Kosenko, E.G. Miseliuk: Zh. Techn. Phys. **27**, 210 (1957)
72. K. Mishra, M. Banan, J. Moody, S. Chandrasekhar: In *Diagnostic Techniques for Semiconductor Materials and Devices*, ed. by D.K. Schroder, J.L. Benton, P. Rai-Choudhury (The Electrochem. Soc., Pennington 1994) p. 131
73. C.B. Collins, R.O. Carlson: Phys. Rev. **108**, 1409 (1957)
74. E.R. Weber: Appl. Phys. A **30**, 1 (1983)
75. E.R. Weber: In *Properties of Silicon (EMIS Datareviews Series No.4)* (INSPEC, London 1988) p. 442
76. K. Harada, H. Tanaka, J. Matsubara, Y. Shimanuki, H. Furuya: J. Cryst. Growth **154**, 47 (1995)
77. R. Falster, G. Borionetti: In *Recombination Lifetime Measurements in Silicon*, ed. by D.C. Gupta, F.R. Bacher, W.M. Hughes (ASTM, West Conshohocken 1998) p. 226
78. D. Gilmore, T. Arahori, M. Ito, H. Murakami, S.I. Miki: In *High Purity Silicon IV*, ed. by C.L. Claeys, P. Stallhofer, P. Rai-Choudhury, J.E. Maurtis (The Electrochem. Soc., Pennington 1996) p. 102
79. D. Gilmore, T. Arahori, M. Ito, H. Murakami, S.I. Miki: J. Electrochem. Soc. **145**, 621 (1998)
80. A.A. Istratov, C. Flink, H. Hieslmair, E.R. Weber, T. Heiser: Phys. Rev. Lett. **81**, 1243 (1998)
81. W.T. Stacy, D.F. Allison, T.C. Wu: J. Electrochem. Soc. **129**, 1128 (1982)
82. J.P. Joly: Microelectron. Eng. **40**, 285 (1998)
83. F. Tardif, J.P. Joly, D. Walz: In *Analytical Techniques for Semiconductor Materials and Process Characterization II*, ed. by B.O. Kolbesen, C. Claeys, P. Stallhofer (The Electrochem. Soc., Pennington 1995) p. 299
84. J. Fucsko, S.S. Tan, M.K. Balazs: J. Electrochem. Soc. **140**, 1105 (1993)
85. T. Hackett, K. Dillenbeck: In *Contamination Control and Defect Reduction in Semiconductor Manufacturing I*, ed. by D.N. Schmidt (The Electrochem. Soc., Pennington 1992) p. 254
86. L. Fabry, S. Pahlke, L. Kotz, P. Blöchl, T. Ehmann, K. Bachmann: In *Ultra Clean Processing of Silicon Surfaces*, ed. by M. Heyns, M. Meuris, P. Mertens (Acco, Leuven 1996) p. 163
87. Y.H. Lee, R.L. Kleinhenz, J.W. Corbett: Inst. Phys. Conf. Ser. **46**, 521 (1979)
88. J.D. Gerson, L.J. Cheng, J.W. Corbett: J. Appl. Phys. **48**, 4821 (1977)
89. E. Weber: Appl. Phys. Lett. **33**, 433 (1978)
90. M.L. Swanson: Phys. Status Solidi **33**, 721 (1969)
91. H.J. Rijks, J. Bloem, L.J. Giling: J. Appl. Phys. **50**, 1370 (1979)
92. M. Stojic: Fizika **15**, 353 (1983)
93. H. Feichtinger, A. Gschwandtner, J. Waltl: Phys. Status Solidi A **53**, K71 (1979)
94. N. Fujino, K. Hiramoto, M. Sano, K. Murakami, H. Horiye, Y. Oka, S. Sumita: In *Semiconductor Silicon 1990*, ed. by H.R. Huff, K.G. Barraclough, J.I. Chikawa (The Electrochem. Soc., Pennington 1990) p. 709
95. T. Boone, G.S. Higashi, J.L. Benton, R.C. Kistler, G.R. Weber, R.C. Keller, G. Makris: In *Surface Chemical Cleaning and Passivation for Semiconductor Processing*, ed. by G.S. Higashi, E.A. Irene, T. Ohmi (Mater. Res. Soc., Pittsburgh 1993) p. 359
96. Y. Takano: In *Defect Control in Semiconductors*, ed. by K. Sumino (North-Holland, Amsterdam 1990) p. 311
97. H. Daio, K. Yakushiji, A. Buczkowski, F. Shimura: Mater. Sci. Forum **196-201**, 1817 (1995)
98. E. Weber, H.G. Riotte: J. Appl. Phys. **51**, 1484 (1980)
99. D.K. DeBusk, A.M. Hoff: Solid State Technol. **4**, 67 (1999)
100. P.F. Schmidt: J. Electrochem. Soc. **130**, 196 (1983)
101. P.F. Schmidt: Solid State Technol. **26**(6), 147 (1983)
102. J. Yoshikawa, R. Takeda, K. Hayashi, H. Shirai, Y. Matsushita: In *High purity silicon IV*, ed. by C.L. Claeys, P. Stallhofer, P. Rai-Choudhury, J.E. Maurtis (The Electrochem. Soc., Pennington 1996) p. 250
103. G.K. Kirov, H.N. Neykov: Cryst. Res. Technol. **26**, 591 (1991)
104. M. Kobayashi, K. Yamazaki, Y. Okui, T. Ogawa: In *Cleaning Technology in Semiconductor Device Manufacturing*, ed. by J. Ruzyllo, R.E. Novak (The Electrochem. Soc., Pennington 1992) p. 313
105. D.E. Voigt, S.L. Brantley: J. Cryst. Growth **113**, 527 (1991)
106. W. Kern: J. Electrochem. Soc. **109**, 700 (1962)
107. H. Feichtinger: Acta Phys. Austr. **51**, 161 (1979)
108. G. Borchardt, E. Weber, N. Wiehl: J. Appl. Phys. **52**, 1603 (1981)
109. T. Hattori: In *Ultraclean Surface Processing of Silicon Wafers*, ed. by H. Hattori (Springer, Berlin 1998) p. 3
110. J. Sugiura: In *Ultraclean Surface Processing of Silicon Wafers*, ed. by H. Hattori (Springer, Berlin 1998) p. 29
111. G. Zoth, W. Bergholz: In *Diagnostic Techniques for Semiconductor Materials and Devices*, ed. by J.L. Benton, G.N. Maracas, P. Rai-Choudhury (The Electrochem. Soc., Pennington 1992) p. 88
112. W. Bergholz, D. Landsmann, P. Schauberger, B. Schoepperl: In *Crystalline Defects and Contamination: Their Impact and Control in Device Manufacturing*, ed. by B.O. Kolbesen, C. Claeys, P. Stallhofer, F. Tardif (The Electrochem. Soc., Pennington 1993) p. 69
113. M.L. Polignano, C. Bresolin, F. Cazzaniga, A. Sabbadini, G. Queirolo: In *Optical characterization techniques for high-performance microelectronic device manufacturing II*, ed. by J.K. Lowell, R.T. Chen, J.P. Mathur (SPIE, Bellingham, WA, USA 1995) p. 14
114. O. Joubert, D. Mathiot, J. Pelletier: Appl. Phys. Lett. **54**, 2241 (1989)
115. K. Tomita, T. Migita, S. Shimonishi, T. Shibata, T. Ohmi, T. Nitta: J. Electrochem. Soc. **142**, 1692 (1995)
116. A.A. Istratov, H. Hieslmair, E.R. Weber: Appl. Phys. A **69**, 13 (1999)
117. A.A. Istratov, H. Hedemann, M. Seibt, O.F. Vyvenko, W. Schröter, T. Heiser, C. Flink, H. Hieslmair, E.R. Weber: J. Electrochem. Soc. **145**, 3889 (1998)
118. A.A. Istratov, O.F. Vyvenko, C. Flink, T. Heiser, H. Hieslmair, E.R. Weber: In *Defect & Impurity Engineered Semiconductors & Devices, II*, ed. by S. Ashok, J. Chevallier, W. Goetz, B. Sopori, K. Sumino (Mater. Res. Soc., Pittsburgh 1998) p. 313
119. M. Seibt, W. Schröter: Philos. Mag. A **59**, 337 (1989)
120. N.R. Baldwin, D.G. Ivey: J. Phase Equilibria **16**, 300 (1995)
121. T.B. Massalski, H. Okamoto, P.R. Subramanian, L. Kacprzak: *Binary Alloy Phase Diagrams* (ASM International, Materials Park 1990)
122. P. Augustus: Semicond. Int. **8**(11), 88 (1985)
123. K. Graff: *Metal Impurities in Silicon-Device Fabrication* (Springer, Berlin 1995)

124. M.D. De Coteau, P.R. Wilshaw, R. Falster: Solid State Phenom. **19-20**, 27 (1991)
125. K. Radermacher, R. Carius, S. Mantl: Nuclear Instrum. Methods Phys. Res. B **84**, 163 (1994)
126. H. Katsumata, Y. Makita, N. Kobayashi, H. Shibata, M. Hasegawa, I. Aksenov, S. Kimura, A. Obara, S. Uekusa: J. Appl. Phys. **80**, 5955 (1996)
127. X.W. Lin, J. Desimoni, H. Bernas, Z. Liliental-Weber, J. Washburn: In *Phase Transformations in Thin Films – Thermodynamics and Kinetics*, ed. by M. Atzmon, A.L. Greer, J.M.E. Harper, M.R. Libera (Mater. Res. Soc., Pittsburgh 1993) p. 293
128. X.W. Lin, M. Behar, J. Desimoni, H. Bernas, W. Swider, Z. Liliental-Weber, J. Washburn: In *Beam Solid Interactions: Fundamentals and Applications*, ed. by M. Nastasi, L.R. Harriott, N. Herbots, R.S. Averback (Mater. Res. Soc., Pittsburgh 1993) p. 535
129. R.L. Maltez, M. Behar, L. Amaral, P.F.P. Fichtner, X.W. Lin: Nucl. Instrum. Methods Phys. Res. B **96**, 366 (1995)
130. C.W.T. Bulle-Lieuwma, D.J. Oostra, D.E.W. Vandenhoudt: In *Microcrystalline Semiconductors: Materials Science and Devices*, ed. by P.M. Fauchet, C.C. Tsai, L.T. Canham, I. Shimizu, Y. Aoyagi (Mater. Res. Soc., Pitsburgh 1993) p. 885
131. J. Desimoni, H. Bernas, M. Behar, X.W. Lin, J. Washburn, Z. Liliental-Weber: Appl. Phys. Lett. **62**, 306 (1993)
132. R.L. Maltez, L. Amaral, M. Behar, A. Vantomme, G. Langouche, X.W. Lin: Phys. Rev. B **54**, 11659 (1996)
133. A. Ohsawa, K. Honda, N. Toyokura: J. Electrochem. Soc. **131**, 2964 (1984)
134. J. Desimoni, F.H. Sánchez, M.B. Fernandez van Raap, H. Bernas, C. Clerc, X.W. Lin: Phys. Rev. B **51**, 86 (1995)
135. D.N. Leong, M.A. Harry, K.J. Reeson, K.P. Homewood: Appl. Phys. Lett. **68**, 1649 (1996)
136. K. Lefki, P. Muret: J. Appl. Phys. **74**, 1138 (1993)
137. D. Leong, M. Harry, K.J. Reeson, K.P. Homewood: Nature **387**, 686 (1997)
138. D.M. Lee, G.A. Rozgonyi: Appl. Phys. Lett. **65**, 350 (1994)
139. C. Hässler, G. Pensl, M. Schulz, A. Voigt, H.P. Strunk: Phys. Status Solidi A **137**, 463 (1993)
140. X. Portier, A. Ihlal, R. Rizk: Phys. Status Solidi A **161**, 75 (1997)
141. B. Shen, T. Sekiguchi, Z. Rong, Y. Shi, H. Shi, Y. Kai, Z. Youdou, K. Sumino: Jpn. J. Appl. Phys. **35**, 3301 (1996)
142. P.S.D. Lin, R.B. Marcus, T.T. Sheng: J. Electrochem. Soc. **130**, 1878 (1983)
143. P.M. Petroff, G.A. Rozgonyi, T.T. Sheng: J. Electrochem. Soc. **123**, 565 (1976)
144. K.V. Ravi, C.J. Varker, C.E. Volk: J. Electrochem. Soc. **120**, 533 (1973)
145. M. Kageyama, N. Tsuchiya, Y. Matsushita: In *Contamination Control and Defect Reduction in Semiconductor Manufacturing II*, ed. by R. Novak, D.N. Schmidt, T. Ito, D. Reedy (The Electrochem. Soc., Pennington 1994) p. 202
146. K. Schmalz, F.G. Kirscht, S. Niese, H. Richter, M. Kittler, W. Seifert, I. Babanskaya, H. Klose, K. Tittelbach-Helmrich, J. Schoneich: Phys. Status Solidi A **100**, 69 (1987)
147. M. Hourai, K. Murakami, T. Shigematsu, N. Fujino, T. Shiraiwa: Jpn. J. Appl. Phys. **28**, 2413 (1989)
148. D. Gilles, E.R. Weber, S. Hahn, O.R. Monteiro, K. Cho: In *Semiconductor Silicon 1990*, ed. by H.R. Huff, K.G. Barraclough, J.I. Chikawa (The Electrochem. Soc., Pennington 1990) p. 697
149. D. Gilles, E.R. Weber, S.K. Hahn: Phys. Rev. Lett. **64**, 196 (1990)
150. M. Aoki, A. Hara, A. Ohsawa: Jpn. J. Appl. Phys. **30**, 3580 (1991)
151. M. Aoki, A. Hara, A. Ohsawa: J. Appl. Phys. **72**, 895 (1992)
152. M. Aoki, A. Hara: Jpn. J. Appl. Phys. (Letters) **35**, L1231 (1996)
153. H. Hieslmair, A.A. Istratov, T. Heiser, E.R. Weber: J. Appl. Phys. **84**, 713 (1998)
154. H. Hieslmair, A.A. Istratov, S.A. McHugo, C. Flink, T. Heiser, E.R. Weber: Appl. Phys. Lett. **72**, 1460 (1998)
155. S. Sadamitsu, S. Ogushi, Y. Koike, N. Reilly, T. Nagashima, M. Sano, H. Tsuya: Solid State Phenom. **57-58**, 53 (1997)
156. S. Ogushi, S. Sadamitsu, K. Marsden, Y. Koike, M. Sano: Jpn. J. Appl. Phys. **36**, 6601 (1997)
157. O. Kononchuk, K.G. Korablev, N. Yarykin, G.A. Rozgonyi: Appl. Phys. Lett. **73**, 1206 (1998)
158. M.B. Shabani, T. Yoshimi, S. Okuuchi, H. Abe: Solid State Phenom. **57-58**, 81 (1997)
159. Y. Kamiura, F. Hashimoto, M. Iwami: Appl. Phys. Lett. **53**, 1711 (1988)
160. Y. Kamiura, F. Hashimoto, M. Iwami: Appl. Surf. Sci. **41-42**, 447 (1989)
161. T. Yoshimi, M.B. Shabani, S. Okuuchi, H. Abe: In *Diagnostic Techniques for Semiconductor Materials and Devices*, ed. by P. Rai-Choudhury, J.L. Benton, D.K. Schroder, T.J. Shaffner (Mater. Res. Soc., Pennington 1997) p. 452
162. X. Ding, M.F. Chiah, W.Y. Cheung, S.P. Wong, J.B. Xu, I.H. Wilson, W. Hui-min, C. Li-zhi, L. Xiang-huai: J. Appl. Phys. **86**, 2550 (1999)
163. T. Heiser, A. Mesli: Appl. Phys. Lett. **58**, 2240 (1991)
164. T. Heiser, A. Mesli: Phys. Rev. Lett. **68**, 978 (1992)
165. X. Gao, H. Mollenkopf, S. Yee: Appl. Phys. Lett. **59**, 2133 (1991)
166. H. Hieslmair (1999): unpublished
167. D.A. Ramappa, W.B. Henley: J. Electrochem. Soc. **144**, 4353 (1997)
168. E.G. Colas, E.R. Weber: Appl. Phys. Lett. **48**, 1371 (1986)
169. M. Aoki, A. Hara, A. Ohsawa: In *Defect Engineering in Semiconductor Growth, Processing and Device Technology*, ed. by S. Ashok, J. Chevallier, K. Sumino, E. Weber (Mater. Res. Soc., Pittsburgh 1992) p. 963
170. M. Aoki, A. Hara: J. Appl. Phys. **74**, 1440 (1993)
171. S.A. McHugo, E.R. Weber, M. Mizuno, F.G. Kirscht: Appl. Phys. Lett. **66**, 2840 (1995)
172. W. Wijaranakula: J. Appl. Phys. **79**, 4450 (1996)
173. B. Shen, J. Jablonski, T. Sekiguchi, K. Sumino: Jpn. J. Appl. Phys. **35**, 4187 (1996)
174. B. Hackl, K.J. Range, P. Stallhofer, L. Fabry: J. Electrochem. Soc. **139**, 1495 (1992)
175. K. Graff, H. Pieper: J. Electrochem. Soc. **128**, 669 (1981)
176. S.E. Beck, M.A. George, D.A. Bohling, B.J. Shemanski, R.G. Ridgeway, G.A. Hames, J.J. Wortman, W.A. Lanford: Solid State Technol. **38**(6), 69 (1995)
177. A.L.P. Rotondaro, T.Q. Hurd, A. Kaniava, J. Vanhellemont, E. Simoen, M.M. Heyns, C. Claeys, G. Brown: In *Analytical Techniques for Semiconductor Materials and Process Characterization II*, ed. by B.O. Kolbesen, C. Claeys, P. Stallhofer (The Electrochem. Soc., Pennington 1995) p. 54
178. H.C. Swart, G.L.P. Berning: Appl. Surf. Sci. **78**, 77 (1994)
179. T. Kitano: J. Electron. Mat. **21**, 1027 (1992)
180. S.A. McHugo, A.C. Thompson, G. Lamble, A. MacDowell, R. Celestre, H. Padmore, M. Imaizumi, M. Yamaguchi, I. Périchaud, S. Martinuzzi, M. Werner, M. Rinio, H.J. Möller, B. Sopori, H. Hieslmair, C. Flink, A.A. Istratov, E.R. Weber: In *Applications of Synchrotron Radiation Techniques to Materials Science IV*, ed. by S.M. Mini, S.R. Stock, D.L. Perry, L.J. Terminello (Mater. Res. Soc., Warrendale 1998) p. 297
181. S.A. McHugo, A.C. Thompson, G. Lamble, C. Flink, E.R. Weber: Physica B **273–273**, 371 (1999)
182. R. Takizawa, T. Nakanishi, A. Ohsawa: J. Appl. Phys. **62**, 4933 (1987)
183. H. Shimizu: J. Electrochem. Soc. **144**, 4335 (1997)
184. H. Shimizu, H. Uchida, S. Ishiwari: Jpn. J. Appl. Phys. **33**, 5690 (1994)
185. H. Shimizu, S. Saitou: Jpn. J. Appl. Phys. **34**, 3071 (1995)
186. H. Shimizu, S. Ishiwari: Materials Transactions, JIM **36**, 1271 (1995)
187. T. Abe, T. Itoh, Y. Hayamizu, K. Sunagawa, S. Yokota, H. Yamagishi: In *Defect Control in Semiconductors*, ed. by K. Sumino (Elsevier Science Publishers B. V. 1990) p. 297
188. P.W. Mertens, A.L.P. Rotondaro, M. Meuris, H.F. Schmidt, M.M. Heyns, D. Gräf: In *1994 Proceedings of the Institute of Enviromental Sciences*, Vol. 1 *(ISBN 1-877862-45-2)* (IES, Mount Prospect, IL, USA 1994) p. 325
189. P.W. Mertens, T. Bearda, M. Houssa, L.M. Loewenstein, I. Cornelissen, S. DeGendt, K. Kenis, I. Teerlinck, R. Vos, M. Meuris, M.M. Heyns: Microelectron. Eng. **48**, 199 (1999)
190. F. Tardif, J.P. Joly, T. Lardin, A. Tonti, P. Patruno, D. Levy, W. Sievert: In *Crystalline Defects and Contamination: Their Impact and Control in Device Manufacturing*, ed. by B.O. Kolbesen, C. Claeys, P. Stallhofer, F. Tardif (The Electrochem. Soc., Grenoble, France 1993) p. 114
191. F. Tardif, J.P. Joly, T. Lardin: In *Cleaning Technology in Semiconductor Device Manufacturing*, ed. by J. Ruzyllo, R.E. Novak (The Electrochem. Soc., Pennington 1994) p. 85
192. R.S. Hockett, D. Hymes: In *Chemical Surface Preparation, Passivation and Cleaning for Semiconductor Growth and Processing*, ed. by R.J. Nemanich, C.R. Helms, M. Hirose, G.W. Rubloff (Mater. Res. Soc., Pittsburgh 1992) p. 173

193. L. Zhong, F. Shimura: Appl. Phys. Lett. **61**, 1078 (1992)
194. G.H. Frischat: *Ionic diffusion in oxide glasses* (Trans Tech Publications, Aedermannsdorf 1975)
195. A. Atkinson, J.W. Gardner: Corros. Sci. **21**, 49 (1981)
196. D.A. Ramappa, W.B. Henley: J. Electrochem. Soc. **146**, 3773 (1999)
197. A.R. Smith, R.J. McDonald, H. Manini, D.L. Hurley, E.B. Norman, M.C. Vella, R.W. Odom: J. Electrochem. Soc. **143**, 339 (1996)
198. E.R. Weber, A.A. Istratov, S.A. McHugo, H. Hieslmair, C. Flink: In *Recombination Lifetime Measurements in Silicon*, ed. by D.C. Gupta, F.R. Bacher, W.M. Hughes (ASTM, West Conshohocken 1998) p. 18
199. M. Werner, E.R. Weber, S. McHugo, K.L. Chapman: Solid State Phenom. **51-2**, 81 (1996)
200. M. Werner, E.R. Weber, S. McHugo, H. Hieslmair, K.L. Chapman: Solid State Phenom. **47-8**, 449 (1996)
201. D.K. Schroder: IEEE Trans. Electron. Devices **ED-29**, 1336 (1982)
202. D.K. Schroder: Solid State Phenom. **6-7**, 383 (1989)
203. D.K. Schroder: In *Recombination lifetime measurements in silicon*, ed. by D.C. Gupta, F.R. Bacher, W.M. Hughes (ASTM, West Conshohocken 1998) p. 5
204. J.W. Orton, P. Blood: *The Electrical Characterization of Semiconductors: Measurement of Minority Carrier Properties* (Academic Press, London 1990)
205. J.S. Blakemore: *Semiconductor Statistics* (Dover, New York 1987)
206. D.K. Schroder: *Semiconductor Material and Device Characterization* (Wiley, New York 1998)
207. R.N. Hall: Phys. Rev. **87**, 387 (1952)
208. P. Eichinger, M. Rommel: In *Crystalline Defects and Contamination: Their Impact and Control in Device Manufacturing II*, ed. by B.O. Kolbesen, C. Claeys, P. Stallhofer, F. Tardiff (The Electrochem. Soc., Pennington 1997) p. 363
209. A.C. Diebold, P. Maillot, M. Gordon, J. Baylis, J. Chacon, R. Witowski, H.F. Arlinghaus, J.A. Knapp, B.L. Doyle: J. Vac. Sci. Technol. A **10**, 2945 (1992)
210. J. Lagowski, P. Edelman, M. Dexter, W. Henley: Semicond. Sci. Technol. **7**, A185 (1992)
211. J. Lagowski, P. Edelman, R. Erickson: In *Defect Recognition and Image Processing in Semiconductors 1995*, ed. by A.R. Mickelson (Institute of Physics, Bristol 1996) p. 91
212. D.R. Frankl, E.A. Ulmer: Surf. Sci. **6**, 115 (1966)
213. J. Lagowski, A.M. Kontkiewicz, L. Jastrzebski, P. Edelman: Appl. Phys. Lett. **63**, 2902 (1993)
214. O.J. Anttila, S.K. Hahn: J. Appl. Phys. **74**, 558 (1993)
215. J. Lagowski, V. Faifer, P. Edelman: In *High purity silicon IV*, ed. by C.L. Claeys, P. Stallhofer, P. Rai-Choudhury, J.E. Maurtis (The Electrochem. Soc., Pennington 1996) p. 512
216. V. Faifer, P. Edelman, A. Kontkiewicz, J. Lagowski, A. Hoff, V. Dyukov, A. Pravdivtsev, I. Kornienko: In *Analytical Techniques for Semiconductor Materials and Process Characterization II*, ed. by B.O. Kolbesen, C. Claeys, P. Stallhofer (The Electrochem. Soc., Pennington 1995) p. 73
217. J. Lagowski, P. Edelman: In *Materials Reliability in Microelectronics VI*, ed. by W.F. Filter, J.J. Clement, A.S. Oates, R. Rosenberg, P.M. Lenahan (Mater. Res. Soc., Pittsburgh 1996) p. 449
218. J. Lagowski, P. Edelman, A.M. Kontkiewicz, O. Milic, W. Henley, M. Dexter, L. Jastrzebski, A.M. Hoff: Appl. Phys. Lett. **63**, 3043 (1993)
219. J. Lagowski, P. Edelman: In *High purity silicon IV*, ed. by C.L. Claeys, P. Stallhofer, P. Rai-Choudhury, J.E. Maurtis (The Electrochem. Soc., Pennington 1996) p. 523
220. A.P. Ramsa, H. Jacobs, F.A. Brand: J. Appl. Phys. **30**, 1054 (1959)
221. V. Lehmann, H. Föll: J. Electrochem. Soc. **135**, 2831 (1988)
222. J. Carstensen, W. Lippik, H. Föll: Mater. Sci. Forum **173-174**, 159 (1995)
223. H. Föll: Appl. Phys. A **53**, 8 (1991)
224. J. Carstensen, W. Lippik, H. Föll: In *Semiconductor Silicon-1994*, ed. by H.R. Huff, W. Bergholz, K. Sumino (The Electrochem. Soc., Pennington 1994) p. 1105
225. D. Walz, G. Le Carval, J.P. Joly, G. Kamarinos: Semicond. Sci. Technol. **10**, 1022 (1995)
226. H. Föll, V. Lehmann, G. Zoth, F. Gelsdorf, B. Gottinger: In *Analytical techniques for semiconductor materials and process characterization*, ed. by B.O. Kolbesen, D.V. McCaughan, W. Vandervorst (The Electrochem. Soc., Pennington 1990) p. 44
227. H. Föll, V. Lehmann, W. Lippik: In *Crystalline Defects and Contamination: Their Impact and Control in Device Manufacturing*, ed. by B.O. Kolbesen, C. Claeys, P. Stallhofer, F. Tardif (The Electrochem. Soc., Pennington 1993) p. 252
228. T. Tiedje, J.I. Haberman, R.W. Francis, A.K. Ghosh: J. Appl. Phys. **54**, 2499 (1983)
229. A. Buczkowski, Z.J. Radzimski, G.A. Rozgonyi, F. Shimura: J. Appl. Phys. **69**, 6495 (1991)
230. A. Buczkowski, Z.J. Radzimski, G.A. Rozgonyi, F. Shimura: J. Appl. Phys. **72**, 2873 (1992)
231. K.L. Luke, C. Li-Jen: J. Appl. Phys. **61**, 2282 (1987)
232. V. Grivickas, E. Gaubas, A. Kaniava, J. Linnros, A.R. Salmanov, A.E. Zemko, G.N. Travleyev, L.A. Kazakevich, V.I. Kuznecov, I.M. Filippov: Lithuanian: J. Phys. **32**, 307 (1992)
233. T.S. Horányi, T. Pavelka, P. Tüttő: Appl. Surf. Sci. **63**, 306 (1993)
234. W.M. Bullis, H.R. Huff: J. Electrochem. Soc. **143**, 1399 (1996)
235. A.B. Fedortsov, D.G. Letenko, Y.V. Churkin, L.M. Tsentsiper, J. Vedde: In *High Purity Silicon*, ed. by C.L. Claeys, P. Stallhofer, P. Rai-Choudhury, J.E. Maurtis (The Electrochem. Soc., Pennington 1996) p. 481
236. T. Yoshida, Y. Kitagawara: In *High Purity Silicon*, ed. by C.L. Claeys, P. Stallhofer, P. Rai-Choudhury, J.E. Maurtis (The Electrochem. Soc., Pennington 1996) p. 455
237. S. Eranen, M. Blomberg: J. Appl. Phys. **56**, 2372 (1984)
238. S.K. Pang, A. Rohatgi: J. Appl. Phys. **74**, 5554 (1993)
239. H. M'saad, J. Michel, J.J. Lappe, L.C. Kimerling: J. Electron. Mat. **23**, 487 (1994)
240. E. Yablonovitch, D.L. Allara, C.C. Chang, T. Gmitter, T.B. Bright: Phys. Rev. Lett. **57**, 249 (1986)
241. A.W. Stephens, A.G. Aberle, M.A. Green: J. Appl. Phys. **76**, 363 (1994)
242. H. M'saad, G.J. Norga, J. Michel, L.C. Kimerling: AIP Conf. Proc. **306**, 471 (1994)
243. J.P. Joly: In *Crystalline Defects and Contamination: Their Impact and Control in Device Manufacturing II*, ed. by B.O. Kolbesen, C. Claeys, P. Stallhofer, F. Tardiff (The Electrochem. Soc., Pennington 1997) p. 259
244. K.L. Luke, C. Li-Jen: J. Electrochem. Soc. **135**, 957 (1988)
245. M. Schöfthaler, R. Brendel, G. Langguth, J.H. Werner: In *Conference Record of the 1994 IEEE First World Converence on Photovoltaic Energy Conversion* (IEEE, New York 1994) p. 1509
246. K. Katayama, Y. Kirino, K. Iba, F. Shimura: Jpn. J. Appl. Phys. (Letters) **30**, L1907 (1991)
247. A. Buczkowski, G.A. Rozgonyi, F. Shimura: Jpn. J. Appl. Phys. (Letters) **32**, L218 (1993)
248. K. Katayama, F. Shimura: Jpn. J. Appl. Phys. (Letters) **31**, L1001 (1992)
249. L. Zhong, A. Buczkowski, K. Katayama, F. Shimura: Appl. Phys. Lett. **61**, 931 (1992)
250. T.S. Horányi, P. Tüttő, C. Kovacsics: J. Electrochem. Soc. **143**, 216 (1996)
251. L. Köster, P. Blöchl, L. Fabry: Jpn. J. Appl. Phys. **34**, 932 (1995)
252. K. Kurita, T. Shingyouji: Jpn. J. Appl. Phys. **37**, 5861 (1998)
253. G. Ferenczi, T. Pavelka, P. Tüttő: Jpn. J. Appl. Phys. **30**, 3630 (1991)
254. A. Kaniava, E. Gaubas, J. Vaitkus, J. Vanhellemont, A.L.P. Rotondaro: Mater. Sci. Technol. **11**, 670 (1995)
255. A. Kaniava, A.L.P. Rotondaro, J. Vanhellemont, U. Menczigar, E. Gaubas: Appl. Phys. Lett. **67**, 3930 (1995)
256. M.L. Polignano, F. Cazzaniga, A. Sabbadini, G. Queirolo, A. Cucciato, A. Di Bartolo: Mater. Sci. Engin. B **42**, 157 (1996)
257. R.K. Ahrenkiel, S. Johnston: In *Defect and Impurity Engineered Semiconductors II*, ed. by S. Ashok, J. Chevallier, K. Sumino, B.L. Sopori, W. Götz (Mater. Res. Soc., Warrendale 1998) p. 575
258. T. Pavelka: In *Recombination lifetime measurements in silicon*, ed. by D.C. Gupta, F.R. Bacher, W.M. Hughes (ASTM, West Conshohocken 1998) p. 206
259. P. Eichinger: In *Recombination Lifetime Measurements in Silicon*, ed. by D.C. Gupta, F.R. Bacher, W.M. Hughes (ASTM, West Conshohocken 1998) p. 101
260. D.C. Gupta: In *Diagnostic Techniques for Semiconductor Materials and Devices*, ed. by P. Rai-Choudhury, J.L. Benton, D.K. Schroder, T.J. Shaffner (The Electrochem. Soc., Pennington 1997) p. 267
261. M.L. Polignano, F. Cazzaniga, A. Sabbadini, F. Zanderigo, F. Priolo: Mater. Sci. Semicond. Process. **1**, 119 (1998)
262. Y. Kirino, A. Buczkowski, Z.J. Radzimski, G.A. Rozgonyi, F. Shimura: Appl. Phys. Lett. **57**, 2832 (1990)
263. F. Shimura, T. Okui, T. Kusama: J. Appl. Phys. **67**, 7168 (1990)

264. A. Buczkowski, G.A. Rozgonyi, F. Shimura: In *Contamination Control and Defect Reduction in Semiconductor Manufacturing II*, ed. by R. Novak, D.N. Schmidt, T. Ito, D. Reedy (The Electrochem. Soc., Pennington 1994) p. 1
265. M. Itsumi: Appl. Phys. Lett. **63**, 1095 (1993)
266. M. Itsumi, Y. Sato, K. Imai, N. Yabumoto: J. Appl. Phys. **82**, 3250 (1997)
267. A.G. Aberle, S. Glunz, W. Warta: J. Appl. Phys. **71**, 4422 (1992)
268. E.E. Fisch, R.H. Gaylord, S.A. Estes: In *Cleaning Technology in Semiconductor Device Manufacturing*, ed. by J. Ruzyllo, R.E. Novak (The Electrochem. Soc., Pennington 1994) p. 514
269. D. Walz, J.P. Joly, R. Falster, G. Kamarinos: Jpn. J. Appl. Phys. **34**, 4091 (1995)
270. D. Walz, J.P. Joly, M. Suarez, J. Palleau, G. Kamarinos: In *Analytical Techniques for Semiconductor Materials and Process Characterization II*, ed. by B.O. Kolbesen, C. Claeys, P. Stallhofer (The Electrochem. Soc., Pennington 1995) p. 64
271. L. Jastrzebski, O. Milic, M. Dexter, J. Lagowski, D. DeBusk, K. Nauka, R. Witowski, M. Gordon, E. Persson: In *Cleaning Technology in Semiconductor Device Manufacturing*, ed. by J. Ruzyllo, R.E. Novak (The Electrochem. Soc., Pennington 1992) p. 294
272. J. Wittmann, W. Bergholz, H. Hoffmann: J. Electrochem. Soc. **146**, 313 (1999)
273. C. Fujihira, M. Morin, H. Hashizume, J. Friedt, Y. Nakai, M. Hirose: Jpn. J. Appl. Phys. (Letters) **32**, L1362 (1993)
274. H. Hashizume, S. Sumie, Y. Nakai: In *Recombination Lifetime Measurements in Silicon*, ed. by D.C. Gupta, F.R. Bacher, W.M. Hughes (ASTM, West Conshohocken 1998) p. 47
275. D. Walz, J.P. Joly, G. Kamarinos, K. Barla: In *Analytical Techniques for Semiconductor Materials and Process Characterization II*, ed. by B.O. Kolbesen, C. Claeys, P. Stallhofer (The Electrochem. Soc., Pennington 1995) p. 35
276. A. Kempf, P. Blöchl, A. Huber, L. Fabry, L. Meinecke: In *Recombination Lifetime Measurements in Silicon*, ed. by D.C. Gupta, F.R. Bacher, W.M. Hughes (ASTM, West Conshohocken 1998) p. 259
277. M.R. Seacrist: In *Recombination Lifetime Measurements in Silicon*, ed. by D.C. Gupta, F.R. Bacher, W.M. Hughes (ASTM, West Conshohocken 1998) p. 318
278. O.J. Anttila, M.V. Tilli: J. Electrochem. Soc. **139**, 1751 (1992)
279. A.L.P. Rotondaro, T.Q. Hurd, A. Kaniava, J. Vanhellemont, E. Simoen, M.M. Heyns, C. Claeys, G. Brown: J. Electrochem. Soc. **143**, 3014 (1996)
280. D. Walz, J.P. Joly, G. Kamarinos: Appl. Phys. A **62**, 345 (1996)
281. H. Lemke: Phys. Status Solidi A **64**, 215 (1981)
282. J. Lagowski, P. Edelman, V. Faifer: In *Recombination Lifetime Measurements in Silicon, ASTM STP 1340*, ed. by D.C. Gupta, F.R. Bacher, W.M. Hughes (ASTM, West Conshohocken 1998) p. 125
283. H. Conzelmann, K. Graff, E.R. Weber: Appl. Phys. A **30**, 169 (1983)
284. W.B. Henley, D.A. Ramappa: Appl. Phys. Lett. **74**, 278 (1999)
285. S.W. Glunz, S. Rein, W. Warta, J. Knobloch, W. Wettling: In *Proceedings of Ninth Workshop on Crystalline Silicon Solar Cell Materials and Processes*, ed. by B.L. Sopori (NREL, Breckenridge, CO, USA, 1999) p. 51
286. L.C. Kimerling, M.T. Asom, J.L. Benton, P.J. Drevinsky, C.E. Caefer: Mater. Sci. Forum **38-41**, 141 (1989)
287. J. Schmidt, A.G. Aberle, R. Hezel: In *Proceedings of Twenty Sixth IEEE Photovoltaic Specialists Conference*, (Anaheim, CA, New York, NY, USA IEEE 1997) p. 13
288. J. Schmidt, A. Cuevas: J. Appl. Phys. **86**, 3175 (1999)
289. F.S. Ham: J. Phys. Chem. Solids **6**, 335 (1958)
290. H. Hieslmair, A.A. Istratov, S.A. McHugo, C. Flink, E.R. Weber: J. Electrochem. Soc. **145**, 4259 (1998)
291. A. Romanowski, A. Buczkowski, A. Karoui, G.A. Rozgonyi: J. Appl. Phys. **83**, 7730 (1998)
292. A. Romanowski, A. Buczkowski, A. Karoui, G.A. Rozgonyi: In *Recombination lifetime measurements in silicon*, ed. by D.C. Gupta, F.R. Bacher, W.M. Hughes (ASTM, West Conshohocken 1998) p. 68
293. E. Gaubas, A. Kaniava: Rev. Sci. Instrum. **67**, 2339 (1996)
294. P. Eichinger, J. Hage, D. Huber, R. Falster: In *Crystalline Defects and Contamination: Their Impact and Control in Device Manufacturing*, ed. by B.O. Kolbesen, C. Claeys, P. Stallhofer, F. Tardif (The Electrochem. Soc., Pennington 1993) p. 240
295. K. Mishra, M. Banan, J. Moody, S. Chandrasekhar: In *Optical Characterization Techniques for High-Performance Microelectronic Device Manufacturing*, Vol. 2337 ed. by J.P. Mathur, J. Lowell, R.T. Chen (The Proc. of SPIE, 1994) p. 143
296. G. Zoth: In *Recombination Lifetime Measurements in Silicon*, ed. by D.C. Gupta, F.R. Bacher, W.M. Hughes (ASTM, West Conshohocken 1998) p. 30
297. A. Buczkowski, G. Rozgonyi, F. Shimura, K. Mishra: J. Electrochem. Soc. **140**, 3240 (1993)
298. M.L. Polignano, E. Bellandi, D. Lodi, F. Pipia, A. Sabbadini, F. Zanderigo, G. Queirolo, F. Priolo: Mater. Sci. Eng. B **B55**, 21 (1998)
299. Y. Ogita: Semicond. Sci. Technol. **7**, A175 (1992)
300. T. Kitamura, F. Tamura, T. Hara, M. Hourai, H. Tsuya: In *High Purity Silicon*, ed. by C.L. Claeys, P. Stallhofer, P. Rai-Choudhury, J.E. Maurtis (The Electrochem. Soc., Pennington 1996) p. 533
301. Y.I. Ogita, N. Tate, H. Masumura, M. Miyazaki, K. Yakushiji: In Recombination Lifetime Measurements in Silicon, ed. by D.C. Gupta, F.R. Bacher, W.M. Hughes (ASTM, West Conshohocken 1998) p. 168
302. J. Lowell, V. Wenner, D. Debusk: In *Ultraclean Semiconductor Processing Technology and Surface Chemical Cleaning and Passivation*, ed. by M. Liehr, M. Heyns, M. Hirose, H. Parks (Mater. Res. Soc., Pittsburgh 1995) p. 207
303. T. Pavelka, Z. Batari: In *Analytical and Diagnostic Techniques for Semiconductor Materials, Devices, and Processes*, ed. by B.O. Kolbesen, C. Claeys, P. Stallhofer, F. Tardif, J. Benton, T.J. Shaffner, D.K. Schroder, S. Kishino, P. Rai-Choudhury (The Electrochem. Soc., Pennington 1999) p. 48
304. A. Buczkowski, A. Romanowski, F.G. Kirscht: In *Analytical and Diagnostic Techniques for Semiconductor Materials, Devices, and Processes*, ed. by B.O. Kolbesen, C. Claeys, P. Stallhofer, F. Tardif, J. Benton, T.J. Shaffner, D.K. Schroder, S. Kishino, P. Rai-Choudhury (The Electrochem. Soc., Pennington 1999) p. 400
305. D.V. Lang: J. Appl. Phys. **45**, 3023 (1974)
306. D.V. Lang: J. Appl. Phys. **45**, 3014 (1974)
307. G.L. Miller, D.V. Lang, L.C. Kimerling: In *Annual Review of Materials Science*, Vol. 7, ed. by R.A. Huggins (Annual Reviews, Palo Alto 1977) p. 377
308. D.V. Lang: In *Thermally Stimulated Relaxation in Solids*, ed. by P. Bräunlich (Springer-Verlag, Berlin, West Germany 1979) p. 92
309. P. Blood, J.W. Orton: *The electrical characterization of semiconductors: majority carriers and electron states* (Academic press, London 1992)
310. A.A. Istratov, O.F. Vyvenko: Sov. Phys. Semicond. **29**, 340 (1995)
311. S. Koveshnikov, Y. Pan, H. Mollenkopf: In *High Purity Silicon IV*, ed. by C.L. Claeys, P. Stallhofer, P. Rai-Choudhury, J.E. Maurtis (The Electrochem. Soc., Pennington 1996) p. 473
312. A.A. Istratov: Rev. Sci. Instrum. **68**, 3861 (1997)
313. A.A. Istratov, O.F. Vyvenko, H. Hieslmair, E.R. Weber: Meas. Sci. Technol. **9**, 477 (1998)
314. L. Dobaczewski, P. Kaminski, R. Kozlowski, M. Surma: Mater. Sci. Forum **196-201**, 669 (1995)
315. A. Chantre, G. Vincent, D. Bois: Phys. Rev. B **23**, 5335 (1981)
316. A. Mitonneau, G.M. Martin, A. Mircea: In proc. of the 6th international symposium on Gallium Arsenide and Related Compounds, ed. by C. Hilsum (Institute of Physics, Bristol, 1977) p. 73
317. R. Brunwin, B. Hamilton, P. Jordan, A.R. Peaker: Electron. Lett. **15**, 349 (1979)
318. P. Stallhofer, A. Huber, P. Blöchl, H. Schwenk: In *Semiconductor Silicon-1990*, ed. by H.R. Huff, K.G. Barraclough, J.I. Chikawa (The Electrochem. Soc., Pennington 1990) p. 1016
319. P. Wobrauschek, H. Aiginger: Anal. Chem. **47**, 852 (1975)
320. C. Streli, H. Aiginger, P. Wobrauschek: Spectrochimica Acta B **44**, 491 (1989)
321. J.A. Sees, L.H. Hall: J. Electrochem. Soc. **142**, 1238 (1995)
322. H. Kondo, J. Ryuta, E. Morita, T. Yoshimi, Y. Shimanuki: Jpn. J. Appl. Phys. (Letters) **31**, L11 (1992)
323. J. Knoth, H. Schwenke: Fresenius Z. Anal. Chem. **291**, 200 (1978)
324. H. Aiginger, P. Wobrauschek: Nucl. Instrum. Methods **114**, 157 (1974)
325. Y. Yoneda, T. Horiuchi: Rev. Sci. Instrum. **42**, 1069 (1971)
326. P. Wobrauschek, H. Aiginger: X-Ray Spectrom. **8**, 57 (1979)
327. R. Jenkins, R.W. Gould, D. Gedcke: *Quantitative X-ray spectrometry* (Marcel Dekker, Inc., New York 1995)
328. G.R. Lachance, F. Claisse: *Quantitative X-ray Fluorescence Analysis: Theory and Application* (Wiley, Chichester 1995)
329. R.S. Hockett, J.M. Metz, S. Tan: In *Ultra-Clean Processing of Silicon Surfaces*, ed. by M. Heyns, M. Meuris, P. Mertens (Acco, Leuven 1994) p. 171

330. J. Knoth, H. Schwenke, P. Eichinger: In *Ultra-Clean Processing of Silicon Surfaces*, ed. by M. Heyns, M. Meuris, P. Mertens (Acco, Leuven 1994) p. 107
331. D.C. Jacobson, J.M. Poate, G.S. Higashi, T. Boone, D.J. Eaglesham, R. Hockett: In *Surface Chemical Cleaning and Passivation for Semiconductor Processing*, ed. by G.S. Higashi, E.A. Irene, T. Ohmi (Mater. Res. Soc., Pittsburgh 1993) p. 347
332. R.S. Hockett: In *Contamination Control and Defect Reduction in Semiconductor Manufacturing III*, ed. by D.N. Schmidt, D. Reedy, R.L. Guldi, J.V. Martinez de Pinillos (The Electrochem. Soc., Pennington 1994) p. 241
333. Y. Mori, K. Shimanoe, T. Sakon: Anal. Sci. **11**, 499 (1995)
334. W. Berneike: Spectrochim. Acta B **48**, 269 (1993)
335. U. Reus: Spectrochim. Acta B **44**, 533 (1989)
336. R. Klockenkämper, M. Becker, H. Bubert: Spectrochim. Acta B **46**, 1379 (1991)
337. S.P. Smith, J. Metz: In *Science and Technology of Semiconductor Surface Preparation*, ed. by G.S. Higashi, M. Hirose, S. Raghavan, S. Verhaverbeke (Mater. Res. Soc., Pittsburgh 1997) p. 305
338. V. Penka, W. Hub: Spectrochim. Acta B **44**, 483 (1989)
339. U. Weisbrod, R. Gutschke, J. Knoth, H. Schwenke: Fresenius J. Anal. Chem. **341**, 83 (1991)
340. A. Iida, K. Sakurai, A. Yoshinaga, Y. Gohshi: Nucl. Instrum. Methods Phys. Res. A **246**, 736 (1986)
341. P. Eichinger, H.J. Rath, H. Schwenke: In *Semiconductor Fabrication: Technology and Metrology*, ed. by D.C. Gupta (ASTM, Philadelphia 1989) p. 305
342. N. Streckfuss, L. Frey, P. Pichler, M. Kugel, G. Zielonka, H. Ryssel: In *Crystalline Defects and Contamination: Their Impact and Control in Device Manufacturing*, ed. by B.O. Kolbesen, C. Claeys, P. Stallhofer, F. Tardif (The Electrochem. Soc., Pennington 1993) p. 222
343. R.S. Hockett, W. Katz: J. Electrochem. Soc. **136**, 3481 (1989)
344. P. Eichinger: In *Analytical techniques for semiconductor materials and process characterization*, ed. by B.O. Kolbesen, D.V. McCaughan, W. Vandervorst (The Electrochem. Soc., Pennington 1990) p. 227
345. R.S. Hockett: In *Cleaning Technology in Semiconductor Device Manufacturing*, ed. by J. Ruzyllo, R.E. Novak (The Electrochem. Soc., Pennington 1992) p. 350
346. T. Ohmi, T. Imaoka, T. Kezuka, J. Takano, M. Kogure: J. Electrochem. Soc. **140**, 811 (1993)
347. R.S. Hockett: In *Beam-Solid Interactions for Materials Synthesis and Characterization*, ed. by D.C. Jacobson, D.E. Luzzi, T.F. Heinz, M. Iwaki (Mater. Res. Soc., Pittsburgh 1995) p. 377
348. L. Fabry, L. Köster, S. Pahlke, L. Kotz, J. Hage: IEEE Trans. Semicond. Manufact. **9**, 428 (1996)
349. T. Mori, K. Kubota, T. Sakon: Analytical Sciences **14**, 275 (1998)
350. K. Tsuji, T. Sato, K. Wagatsuma: Jpn. J. Appl. Phys. **37**, 5821 (1998)
351. K. Tsuji, T. Sato, K. Wagatsuma, M. Claes, R. Van Grieken: Rev. Sci. Instrum. **70**, 1621 (1999)
352. V.B. Baryshev, G.N. Kulipanov, A.N. Skrinsky: Nucl. Instrum. Methods Phys. Res. A **246**, 739 (1986)
353. L. Fabry, S. Pahlke, L. Kotz: In *Analytical Techniques for Semiconductor Materials and Process Characterization II*, ed. by B.O. Kolbesen, C. Claeys, P. Stallhofer (The Electrochem. Soc., Pennington 1995) p. 217
354. A. Fischer-Colbrie, S.S. Laderman, S. Brennan, N. Takaura, P. Pianetta, A. Shimazaki, K. Miyazaki, J. Kortright, D.C. Wherry: In *Ultra-Clean Processing of Silicon Surfaces*, ed. by M. Heyns, M. Meuris, P. Mertens (Acco, Leuven 1994) p. 57
355. P. Pianetta, N. Takaura, S. Brennan, W. Tompkins, S.S. Laderman, A. Fischer-Colbrie, A. Shimazaki, K. Miyazaki, M. Madden, D.C. Wherry, J.B. Kortright: Rev. Sci. Instrum. **66**, 1293 (1995)
356. A. Bayoumi, A. Fischer-Colbrie, R. Parker, M. Cox, W. Greene: In *Science and Technology of Semiconductor Surface Preparation*, ed. by G.S. Higashi, M. Hirose, S. Raghavan, S. Verhaverbeke (Mater. Res. Soc., Pittsburgh 1997) p. 247
357. A. Fischer-Colbrie, S.S. Laderman, S. Brennan, S. Ghosh, N. Takaura, P. Pianetta, A. Shimazaki, A. Waldhauer, D. Wherry, S. Barkan: In *Science and Technology of Semiconductor Surface Preparation*, ed. by G.S. Higashi, M. Hirose, S. Raghavan, S. Verhaverbeke (Mater. Res. Soc., Pittsburgh 1997) p. 403
358. F. Comin: In *Analytical and Diagnostic Techniques for Semiconductor Materials, Devices, and Processes*, ed. by B.O. Kolbesen, C. Claeys, P. Stallhofer, F. Tardif, J. Benton, T.J. Shaffner, D.K. Schroder, S. Kishino, P. Rai-Choudhury (The Electrochem. Soc., Pennington 1999) p. 134
359. S. Brennan, W. Tompkins, N. Takaura, P. Pianetta, S.S. Laderman, A. Fischer-Colbrie, J.B. Kortright, M.C. Madden, D.C. Wherry: Nucl. Instrum. Methods Phys. Res. A **417** (1994)
360. A. Shimazaki, H. Hiraisuka, Y. Matsushita, S. Yoshii: In Proceedings of Extended Abstracts of the 16th (1984 International) Conference on Solid State Devices and Materials, Kobe, Japan, 1984 (Tokyo, Japan: Business Centre for Acad. Sci. Japan) p. 281
361. T. Shiraiwa, N. Fujino, S. Sumita, Y. Tanizoe: In *Semiconductor Fabrication: Technology and Metrology*, ed. by D.C. Gupta (ASTM, Philadelphia 1989) p. 314
362. C. Neumann, P. Eichinger: Spectrochim. Acta B **46**, 1369 (1991)
363. Y. Mizokami, T. Ajioka, N. Terada: IEEE Trans. Semicond. Manufact. **7**, 447 (1994)
364. L. Fabry, S. Pahlke, L. Kotz: Advances in X-ray chemical analysis (Japan) **27**, 345 (1996)
365. A. Huber, H.J. Rath, P. Eichinger, T. Bauer, L. Kotz, R. Staudigl: In *Diagnostic Techniques for Semiconductor Materials and Devices*, ed. by T.J. Shaffner, D.T. Schroder (The Electrochem. Soc., Pennington 1988) p. 109
366. L. Fabry, S. Pahlke, L. Kotz, E. Schemmel, W. Berneike: In *Crystalline Defects and Contamination: Their Impact and Control in Device Manufacturing*, ed. by B.O. Kolbesen, C. Claeys, P. Stallhofer, F. Tardif (The Electrochem. Soc., Pennington 1993) p. 232
367. O.J. Anttila, M.V. Tilli, M. Schaekers, C.L. Claeys: J. Electrochem. Soc. **139**, 1180 (1992)
368. M.A. Lavoie, E.D. Adams, G.L. Miles: J. Vac. Sci. Technol. A **14**, 1924 (1996)
369. A. Walsh: Spectrochim. Acta **7**, 108 (1955)
370. B.V. L'vov: Spectrochim. Acta **17**, 761 (1961)
371. A. Syty: CRC Critical Rev. Anal. Chem. **4**, 155 (1974)
372. R. Woodgriff: Appl. Spectrosc. **28**, 413 (1974)
373. D.R. Thomerson, K.C. Thompson: Chem. in Britain **11**, 316 (1975)
374. G.F. Kirkbright, M. Sargent: *Atomic Absorption and Fluorescence Spectroscopy* (Academic Press, London 1974)
375. J. Ramirez-Munoz: *Atomic-absorption spectroscopy* (Elsevier Publishing Co., Amsterdam 1968)
376. B. Welz: *Atomic Absorption Spectroscopy* (Verlag Chemie, Weinheim 1976)
377. K.C. Thompson, R.J. Reynolds: *Atomic Absorption, Fluorescence and Flame Emission Spectroscopy: Apractical Approach* (Wiley, New York 1978)
378. A. Varma: *CRC Handbook of Inductively Coupled Plasma Atomic Emission Spectroscopy* (CRC press, Boca Raton 1991)
379. S. Okuuchi, M.B. Shabani, T. Yoshimi, H. Abe: In *Diagnostic Techniques for Semiconductor Materials and Devices*, ed. by P. Rai-Choudhury, J.L. Benton, D.K. Schroder, T.J. Shaffner (The Electrochem. Soc., Pennington 1997) p. 39
380. M.B. Shabani, T. Yoshimi, H. Abe: J. Electrochem. Soc. **143**, 2025 (1996)
381. S.H. Tan: Nucl. Instrum. Methods Phys. Res. B **99**, 458 (1995)
382. M. Takenaka, M. Hayashi, Y. Honma, A. Kubota, Y. Matsushita: In *Ultra-clean Processing of Silicon Surfaces '94*, ed. by M. Heyns (Acco, Leuven, Belgium 1994) p. 61
383. P. Gupta, S.H. Tan, Z. Pournotamed, F. Cristobal, N. Oshiro, B. McDonald: In *Contamination Control and Defect Reduction in Semiconductor Manufacturing III*, ed. by D.N. Schmidt, D. Reedy, R.L. Guldi, J.V. Martinez de Pinillos (The Electrochem. Soc., Pennington 1994) p. 200
384. J. Roboz: *Mass Spectrometry Instrumentation and Techniques* (Interscience, New York 1968)
385. R. Stuck, P. Siffert: Prog. Cryst. Growth Charact. **8**, 11 (1984)
386. J.C. Vickerman, A. Brown, N.M. Reed (Ed.): *Secondary Ion Mass Spectrometry: Principles and Applications* (Clarendon Press, Oxford 1989)
387. A. Benninghoven, F.G. Rudenauer, H.W. Werner: *Secondary Ion Mass Spectrometry: Basic Concepts, Instrumental Aspects, Applications and Trends* (Wiley-Interscience, New York 1987)
388. D. Briggs, M.P. Seah (Ed.): *Practical Surface Analysis* (Wiley, Chichister 1992)
389. K. Wittmaack: Vacuum **32**, 65 (1982)
390. J.S. Becker, H.J. Dietze: Spectrochim. Acta B **53**, 1475 (1998)

391. H.W. Werner: Surf. Interf. Anal. **2**, 56 (1980)
392. A. Brown, J.C. Vickerman: Surf. Interf. Anal. **6**, 1 (1984)
393. P.K. Chu, V.K.F. Chia, S.P. Smith, C.W. Magee: Mater. Chem. Phys. **52**, 60 (1998)
394. P.K. Chu, S.P. Smith, R.J. Bleiler: J. Vac. Sci. Technol. B **14**, 3321 (1996)
395. P.G. Harris, A.D. Trigg: GEC J. Res. Incorporating Marconi Rev. **5**, 88 (1987)
396. G.E. McGuire, L.B. Church, D.L. Jones, K.K. Smith, D.T. Tuenge: J. Vac. Sci. Technol. A **1**, 732 (1983)
397. P.C. Zalm: Philips J. Res. **47**, 287 (1993)
398. K. Iltgen, C. Bendel, A. Benninghoven, E. Niehuis: J. Vac. Sci. Technol. A **15**, 460 (1997)
399. A. Wucher, F. Novak, W. Reuter: J. Vac. Sci. Technol. A **6**, 2265 (1988)
400. A. Wucher: J. Vac. Sci. Technol. A **6**, 2287 (1988)
401. M. Anderle, L. Moro: Surf. Interf. Anal. **15**, 525 (1990)
402. H. Oechsner, W. Gerhard: Phys. Lett. A **40A**, 211 (1972)
403. H. Oechsner, W. Gerhard: Surf. Sci. **44**, 480 (1974)
404. O. Ganschow: In *Analytical Techniques for Semiconductor Materials and Process Characterization*, ed. by B.O. Kolbesen, D.V. McCaughan, W. Vandervorst (The Electrochem. Soc., Pennington 1990) p. 190
405. M.J. Pellin, C.E. Young, W.F. Calaway, J.W. Burnett, B. Jorgensen, E.L. Schweitzer, D.M. Gruen: Nucl. Instrum. Methods Phys. Res. B **18**, 446 (1987)
406. M.J. Pellin, C.E. Young, W.F. Calaway, D.M. Gruen: Nucl. Instrum. Methods Phys. Res. B **13**, 653 (1986)
407. S.M. Daiser: IEEE Circuits Devices Mag. **7**, 27 (1991)
408. M.J. Pellin, C.E. Young, W.F. Calaway, J.W. Burnett, D.M. Gruen: In *Diagnostic Techniques for Semiconductor Materials and Devices*, ed. by T.J. Shaffner, D.T. Schroder (The Electrochem. Soc., Pennington 1988) p. 73
409. A. Schnieders, R. Mollers, M. Terhorst, H.G. Cramer, E. Niehuis, A. Benninghoven: J. Vac. Sci. Technol. B **14**, 2712 (1996)
410. J.C. Riviere, S. Myhra (Ed.): *Handbook of Surface and Interface Analysis* (Marcel Dekker, Inc., New York 1998)
411. P.K. Chu, B.W. Schueler, F. Reich, P.M. Lindley: J. Vac. Sci. Technol. B **15**, 1908 (1997)
412. M. Terhorst, R. Mollers, A. Schnieders, E. Niehuis, A. Benninghoven: In *Secondary Ion Mass Spectrometry SIMS IX*, ed. by A. Benninghoven, Y. Nihei, R. Shimizu, H.W. Werner (Wiley, Chichister 1994) p. 13
413. H.G. Cramer, U. Jurgens, E. Niehuis, M. Terhorst, Z. Zhang, A. Benninghoven: In *Secondary Ion Mass Spectrometry SIMS IX*, ed. by A. Benninghoven, Y. Nihei, R. Shimizu, H.W. Werner (Wiley, Chichister 1994) p. 33
414. A.C. Diebold: J. Vac. Sci. Technol. B **12**, 2768 (1994)
415. S.P. Smith, C.J. Hitzman, R.S. Hockett: In *Cleaning Technology in Semiconductor Device Manufacturing*, ed. by R.E. Novak, J. Ruzyllo (The Electrochem. Soc., Pennington 1996) p. 308
416. B. Schueler, R.C. Hockett: In *Cleaning Technology in Semiconductor Device Manufacturing*, ed. by J. Ruzyllo, R.E. Novak (The Electrochem. Soc., Pennington 1994) p. 554
417. A.L. Gray: Spectrochim. Acta **40B**, 1525 (1985)
418. J.L. Benton, P.A. Stolk, D.J. Eaglesham, D.C. Jacobson, J.Y. Cheng, J.M. Poate, N.T. Ha, T.E. Haynes, S.M. Myers: J. Appl. Phys. **80**, 3275 (1996)
419. F.D. McDaniel, J.M. Anthony, J.F. Kirchhoff, D.K. Marble, Y.D. Kim, S.N. Renfrow, E.C. Grannan, E.R. Reznik, G. Vizkelethy, S. Matteson: Nucl. Instrum. Methods Phys. Res. B **242-249**, 242 (1994)
420. J.M. Anthony, J. Thomas: Nucl. Instrum. Methods Phys. Res. **218**, 463 (1983)
421. M. Dobeli, P.W. Nebiker, M. Suter, H.A. Synal, D. Vetterli: Nucl. Instrum. Methods Phys. Res. B **85**, 770 (1994)
422. R.S. Houk, V.A. Fassel, G.D. Flesch, H.J. Svec, A.L. Gray, C.E. Taylor: Anal. Chem. **52**, 2283 (1980)
423. M. Thompson, J.N. Walsh: *Handbook of Inductively Coupled Plasma Spectroscopy* (Blackie, Glasgow 1989)
424. R.S. Houk: Anal. Chem. **58**, 97A (1986)
425. K. Ruth, P. Schmidt, J. Coria, E. Mori: In *Cleaning technology in semiconductor device manufacturing*, ed. by J. Ruzyllo, R.E. Novak (The Electrochem. Soc., Pennington 1994) p. 565
426. J.M. Hollander, I. Perlman, G.T. Seaborg: Reviews of modern physics **25**, 469 (1953)
427. I.E. Makasheva, I.A. Maslov, A.P. Obukhov: Z. Anal. Khim. **15**, 329 (1960)
428. S. Niese: Isotopenpraxis **16**, 133 (1980)
429. A. Kant, J.P. Cali, H.D. Thompson: Anal. Chem. **28**, 1867 (1956)
430. R.J. McDonald, A.R. Smith, D.L. Hurley, E.B. Norman, M.C. Vella: In *High purity silicon IV*, ed. by C.L. Claeys, P. Stallhofer, P. Rai-Choudhury, J.E. Maurtis (The Electrochem. Soc., Pennington 1996) p. 554
431. P.F. Schmidt, D.J. McMillan: Anal. Chem. **48**, 1962 (1976)
432. P.F. Schmidt, J.E. Riley, Jr., and D.J. McMillan: Anal. Chem. **51**, 189 (1979)
433. W. Helbig, S. Niese: Nucl. Instrum. Methods Phys. Res. B **17**, 431 (1986)
434. G.W. Leddicotte, S.A. Reynolds: Nucleonics **8**, 62 (1951)
435. D. Lafeuille, D. Roche: Analysis **2**, 207 (1973)
436. J. Hoste: J. Radioanal. Chem. **19**, 7 (1974)
437. F. De Corte, A. Speecke, J. Hoste: J. Radioanal. Chem. **9**, 9 (1971)
438. M.L. Bouger, S. Niese, D. Birnstein, W. Helbig: J. Radioanal. Nucl. Chem. **130**, 417 (1989)
439. W. Heinze, S. Niese: Isotopenpraxis **8**, 41 (1972)
440. S. Niese: J. Radioanal. Chem. **58**, 195 (1980)
441. J.A. Keenan, B.E. Gnade, J.B. White: J. Electrochem. Soc. **132**, 2232 (1985)
442. R.S. Hockett, S.M. Baumann, E. Schemmel: In *Diagnostic Techniques for Semiconductor Materials and Devices*, ed. by T.J. Shaffner, D.K. Schroder (The Electrochem. Soc., Pennington 1988) p. 113
443. H.J. Rath, P. Stallhofer, D. Huber, P. Eichinger, I. Ruge: In *Impurity Diffusion and Gettering in Silicon*, ed. by R.B. Fair, C.W. Pearce, J. Washburn (Mater. Res. Soc., Pittsburgh 1985) p. 13
444. S.A. McHugo, R.J. McDonald, A.R. Smith, D.L. Hurley, A.A. Istratov, H. Hieslmair, E.R. Weber: In *Defect and impurity engineered semiconductors and devices II*, ed. by S. Ashok, J. Chevallier, K. Sumino, B.L. Sopori, W. Götz (Mater. Res. Soc., Warrendale 1998) p. 361
445. S.A. McHugo, R.J. McDonald, A.R. Smith, D.L. Hurley, E.R. Weber: Appl. Phys. Lett. **73**, 1424 (1998)
446. N. Wiehl, U. Herpers, E. Weber: J. Radioanal. Chem. **72**, 69 (1982)
447. L.E. Katz, P.F. Schmidt, C.W. Pearce: J. Electrochem. Soc. **128**, 620 (1981)
448. B.L. Doyle, J.A. Knapp, D.L. Buller: Nucl. Instrum. Methods Phys. Res. B **42**, 295 (1989)
449. J.A. Knapp, B.L. Doyle: Nucl. Instrum. Methods Phys. Res. B **45**, 143 (1990)
450. J.A. Knapp, D.K. Brice, J.C. Banks: Nucl. Instrum. Methods Phys. Res. B **108**, 324 (1996)
451. J.A. Knapp, J.C. Banks, D.K. Brice: In *Beam-Solid Interactions for Materials Synthesis and Characterization*, ed. by D.C. Jacobson, D.E. Luzzi, T.F. Heinz, M. Iwaki (Mater. Res. Soc., Pittsburgh 1995) p. 389
452. J.A. Knapp, J.C. Banks, B.L. Doyle: Nucl. Instrum. Methods Phys. Res. B **85**, 20 (1994)
453. J.A. Knapp, J.C. Banks: Nucl. Instrum. Methods Phys. Res. B **79**, 457 (1993)
454. J.A. Knapp, J.C. Barbour, B.L. Doyle: J. Vac. Sci. Technol. A **10**, 2685 (1992)
455. R.R. Hart, H.L. Dunlap, A.J. Mohr, O.J. Marsch: Thin Solid Films **19**, 137 (1973)
456. F.M. Jacobsen, M.J. Zarcone, D. Steski, K. Smith, P. Thieberger, K.G. Lynn, J. Throwe, M. Cholewa: Semicond. Int. **19**(6), 243 (1996)
457. J.C. Banks, B.L. Doyle, J.A. Knapp, D. Werho, R.B. Gregory, M. Anthony, T.Q. Hurd, A.C. Diebold: Nucl. Instrum. Methods Phys. Res. B **136-138**, 1223 (1998)
458. E.L. Principe, R.W. Odom, A.L. Johnson, G.D. Ackermann, Z. Hussain, H. Padmore: In *Applications of synchrotron radiation techniques to materials science IV*, ed. by S.M. Mini, S.R. Stock, D.L. Perry, L.J. Terminello (Mater. Res. Soc., Warrendale 1998) p. 221
459. LBNL, ALS technical specifications, http://www-als.lbl.gov/als/techspec.html
460. W. Kern: J. Electrochem. Soc. **137**, 1887 (1990)
461. M. Liehr: In *Chemical Surface Preparation, Passivation and Cleaning for Semiconductor Growth and Processing*, ed. by R.J. Nemanich,

C.R. Helms, M. Hirose, G.W. Rubloff (Mater. Res. Soc., Pittsburgh 1992) p. 3
462. W. Kern, D. Puotinen: RCA Rev. 31, 187 (1970)
463. W. Kern: *Handbook of Semiconductor Wafer Cleaning Technology:Science, Technology, and Applications* (Noyes Publications, Park Ridge 1993)
464. M. Meuris, S. Verhaverbeke, P.W. Mertens, H.F. Schmidt, A.L.P. Rotondaro, M.M. Heyns: In *Cleaning technology in semiconductor device manufacturing*, ed. by J. Ruzyllo, R.E. Novak (The Electrochem. Soc., Pennington 1994) p. 15
465. H.F. Schmidt, M. Meuris, P.W. Mertens, A.L.P. Rotondaro, M.M. Heyns, T.Q. Hurd, Z. Hatcher: In *Ultra-Clean Processing of Silicon Surfaces*, ed. by M. Heyns (Acco, Leuven, Belgium 1994) p. 259
466. C.R. Helms, H.S. Park, S. Dhanda, P. Gupta, M. Tran: In *Ultra-Clean Processing of Silicon Surfaces*, ed. by M. Heyns (Acco, Leuven/Amersdorf 1994) p. 205
467. M. Meuris, M. Heyns, P. Mertens, S. Verhaverbeke, A. Philipossian: In *Cleaning Technology in Semiconductor Device Manufacturing*, ed. by J. Ruzyllo, R.E. Novak (The Electrochem. Soc., Pennington 1992) p. 144
468. I. Oki, H. Shibayama, A. Kagisawa: In *Cleaning Technology in Semiconductor Device Manufacturing*, ed. by J. Ruzyllo, R.E. Novak (The Electrochem. Soc., Pennington 1994) p. 206
469. M. Itano, T. Kezuka, M. Ishii, I. Unemoto, M. Kubo, T. Ohmi: J. Electrochem. Soc. 142, 971 (1995)
470. T.Q. Hurd, P.W. Mertens, L.H. Hall, M.M. Heyns: In *Ultra-Clean Processing of Silicon Surfaces-II*, ed. by M. Heyns (Acco, Leuven, Belgium 1994) p. 41
471. M. Alessandri, E. Bellandi, F. Pipia, B. Crivelli, K. Wolke, M. Schenkl: In *Cleaning Technology in Semiconductor Device Manufacturing V*, ed. by J. Ruzyllo, R.E. Novak, C.M. Appel, T. Hattori, M. Heyns (The Electrochem. Soc., Pennington 1998) p. 523
472. D.J. Riley, R.G. Carbonell: In *Cleaning Technology in Semiconductor Device Manufacturing*, ed. by J. Ruzyllo, R.E. Novak (The Electrochem. Soc., Pennington 1992) p. 223
473. M. Itano, F.W. Kern, Jr., R.W. Rosenberg, M. Miyashita, I. Kawanabe, T. Ohmi: IEEE Trans. Semicond. Manufact. 5, 114 (1992)
474. H. Shimizu, C. Munakata: In *Diagnostic Techniques for Semiconductor Materials and Devices*, ed. by D.K. Schroder, J.L. Benton, P. Rai-Choudhury (The Electrochem. Soc., Pennington 1994) p. 120
475. H. Shimizu, C. Munadata: Appl. Phys. Lett. 62, 276 (1993)
476. L.W. Shive: (1999) private communications
477. G.J. Norga, K.A. Black, H. M'saad, J. Michel, L.C. Kimerling: In *Ultraclean Processing of Si Surfaces UCPSS-94*, ed. by M. Heyns (Acco, Leuven, Belgium 1994) p. 221
478. G.J. Norga, L.C. Kimerling: J. Electron. Mater. (USA) 24, 397 (1995)
479. G.J. Norga, K.A. Black, H. M'saad, J. Michel, L.C. Kimerling: Mater. Sci. Technol. 11, 90 (1995)
480. H. Morinaga, M. Aoki, T. Maeda, M. Fujisue, H. Tanaka, M. Toyoda: In *Science and Technology of Semiconductor Surface Preparation*, ed. by G.S. Higashi, M. Hirose, S. Raghavan, S. Verhaverbeke (Mater. Res. Soc, Pittsburgh 1997) p. 35
481. W. Kern: RCA Rev. 31, 234 (1970)
482. J. Ryuta, T. Yoshimi, H. Kondo, H. Okuda, Y. Shimanuki: Jpn. J. Appl. Phys. 31, 2338 (1992)
483. G. Maeda, I. Takahashi, H. Kondo, J. Ryuta, T. Shingyouji: In *Ultraclean Semiconductor Processing Technology and Surface Chemical Cleaning and passivation*, ed. by M. Liehr, M. Heyns, M. Hirose, H. Parks (Mater. Res. Soc., Pittsburgh 1995) p. 195
484. L. Mouche, F. Tardif, J. Derrien: J. Electrochem. Soc. 142, 2395 (1995)
485. Y. Mori, K. Uemvra, K. Shimanoe, T. Sakon: J. Electrochem. Soc. 142, 3104 (1995)
486. R. Sugino, Y. Okui, M. Okuno, M. Shigeno, Y. Sato, A. Ohsawa, T. Ito: IEICE Trans. Electron. (Japan) E75-C, 829 (1992)
487. H. Okuda, J. Ryuta, E. Morita, Y. Shimanuki: In *Chemical Surface Preparation, Passivation and Cleaning for Semiconductor Growth and Processing*, ed. by R.J. Nemanich, C.R. Helms, M. Hirose, G.W. Rubloff (Mater. Res. Soc., Pittsburgh 1992) p. 399
488. H. Park, C.R. Helms, K. Daehong: J. Electrochem. Soc. 145, 1724 (1998)
489. H. Park, C.R. Helms: In *Cleaning technology in semiconductor device manufacturing*, ed. by J. Ruzyllo, R.E. Novak (The Electrochem. Soc., Pennington 1994) p. 50
490. M.L. Kniffin, T.E. Beerling, C.R. Helms: J. Electrochem. Soc. 139, 1195 (1992)
491. M.L. Kniffin, C.R. Helms: In *Cleaning Technology in Semiconductor Device Manufacturing*, ed. by J. Ruzyllo, R.E. Novak (The Electrochem. Soc., Pennington 1992) p. 197
492. S. Dhanda, R.P. Chiarello, C.R. Helms, P. Gupta: In *Cleaning Technology in Semiconductor Device Manufacturing V*, ed. by J. Ruzyllo, R.E. Novak, C.M. Appel, T. Hattori, M. Heyns (The Electrochem. Soc., Pennington 1998) p. 113
493. S. Verhaverbeke, R. Messoussi, H. Morinaga, T. Ohmi: In *Ultraclean Semiconductor Processing Technology and Surface Chemical Cleaning and Passivation*, ed. by M. Liehr, M. Heyns, M. Hirose, H. Parks (Mater. Res. Soc., Pittsburgh 1995) p. 3
494. F. Tardif, T. Lardin, C. Paillet, J.P. Joly, A. Fleury, P. Patruno, D. Levy, K. Barla: In *Cleaning Technology in Semiconductor Device Manufacturing*, ed. by R.E. Novak, J. Ruzyllo (The Electrochem. Soc., Pennington 1995) p. 49
495. L.M. Loewenstein, P.W. Mertens: In *Cleaning Technology in Semiconductor Device Manufacturing V*, ed. by J. Ruzyllo, R.E. Novak, C.M. Appel, T. Hattori, M. Heyns (The Electrochem. Soc., Pennington 1998) p. 89
496. M. Hourai, T. Naridomi, Y. Oka, K. Murakami, S. Sumita, N. Fujino, T. Shiraiwa: Jpn. J. Appl. Phys. (Letters) 27, L2361 (1988)
497. C.H. Hamann, A. Hamnett, W. Vielstich: *Electrochemistry* (Wiley-VCH, Weinheim, New York 1998)
498. L. Michaelis, L.B. Flexner: *Oxidation-reduction potentials* (J.B. Lippincott company, Philadelphia 1930)
499. S. Glasstone: *An introduction to electrochemistry* (D. van Nostrand Co., Princeton 1942)
500. W.M. Latimer: *The Oxidation States of the Elements and Their Potentials in Aqueous Solutions* (Prentice Hall, New York 1938)
501. M. Pourbaix: *Atlas of electrochemical equilibria in aqueous solutions* (National Association of Corrosion Engineers, Houston 1974)
502. K. Osseo-Asare: Hydrometallurgy 4, 217 (1979)
503. P.A. Brook: Corrosion Sci. 11, 389 (1971)
504. M.H. Froning, M.E. Shanley, E.D. Verink: Corrosion Sci. 16, 371 (1976)
505. K. Osseo-Asare, D. Wei: In *Cleaning technology in semiconductor device manufacturing*, ed. by J. Ruzyllo, R.E. Novak (The Electrochem. Soc., Pennington 1994) p. 34
506. K. Osseo-Asare, W. Dawei, K.K. Mishra: J. Electrochem. Soc. 143, 749 (1996)
507. T. Ohmi: In *Cleaning Technology in Semiconductor Device Manufacturing*, ed. by R.E. Novak, J. Ruzyllo (The Electrochem. Soc., Pennington 1996) p. 1
508. J.S. Kim, H. Morita, J.D. Joo, T. Ohmi: J. Electrochem. Soc. 144, 3275 (1997)
509. T. Imaoka, T. Kezuka, J. Takano, I. Sugiyama, T. Ohmi: IEICE Trans. Electron. (Japan) E75-C, 816 (1992)
510. H. Morinaga, T. Ohmi: In *Cleaning Technology in Semiconductor Device Manufacturing*, ed. by R.E. Novak, J. Ruzyllo (The Electrochem. Soc., Pennington 1996) p. 257
511. T. Shimono, M. Tsuji: In *Defects in Silicon II*, ed. by W.M. Bullis, U. Gösele (The Electrochem. Soc., Pennington 1991) p. 361
512. Y. Fukazawa, K. Sanpei, K. Nakijama, K. Takase, K. Miyazaki: In *Ultra-Clean Processing of Silicon Surfaces II*, ed. by M. Heyns, M. Meuris, P. Mertens (Acco, Leuven, Belgium 1994) p. 378
513. M. Miyashita, T. Tusga, K. Makihara, T. Ohmi: J. Electrochem. Soc. 139, 2133 (1992)
514. H. Morinaga, M. Suyama, M. Nose, S. Verhaverbeke, T. Ohmi: IEICE Trans. Electron. (Japan) E79-C, 343 (1996)
515. T. Ohmi, T. Imaoka, I. Sugiyama, T. Kezuka: J. Electrochem. Soc. 139, 3317 (1992)
516. A.F. Wells: *Structural inorganic chemistry* (Clarendon Press, Oxford University Press, Oxford England New York 1990)
517. L.M. Loewenstein, P.W. Mertens: J. Electrochem. Soc. 145, 2841 (1998)
518. A.L.P. Rotondaro, T.Q. Hurd, H.F. Schmidt, I. Teerlinck, M.M. Heyns, C. Claeys: In *Ultraclean Semiconductor Processing Technology and Surface Chemical Cleaning and Passivation*, ed. by M. Liehr, M. Heyns, M. Hirose, H. Parks (Mater. Res. Soc., Pittsburgh 1995) p. 183

519. S. Dhanda, C.R. Helms, P. Gupta, B.B. Triplett, M. Tran: In *Ultraclean Semiconductor Processing Technology and Surface Chemical Cleaning and Passivation*, ed. by M. Liehr, M. Heyns, M. Hirose, H. Parks (Mater. Res. Soc., Pittsburgh 1995) p. 201
520. H.G. Parks, J.B. Hiskey, K. Yoneshige: In *Interface Control of Electrical, Chemical, and Mechanical Properties*, ed. by S.P. Murarka, K. Rose, T. Ohmi, T. Seidel (Mater. Res. Soc., Pittsburgh 1994) p. 245
521. E. Hsu, H.G. Parks, R. Craigin, S. Tomooka, J.S. Ramberg, R.K. Lowry: J. Electrochem. Soc. **139**, 3659 (1992)
522. Y.S. Obeng: In *Cleaning technology in semiconductor device manufacturing*, ed. by J. Ruzyllo, R.E. Novak (The Electrochem. Soc., Pennington 1994) p. 42
523. Y. Hayami, Y. Okui, H. Ogawa, S. Fujimura: In *Cleaning Technology in Semiconductor Device Manufacturing V*, ed. by J. Ruzyllo, R.E. Novak, C.M. Appel, T. Hattori, M. Heyns (The Electrochem. Soc., Pennington 1998) p. 97
524. L. Fabry: Fresenius J. Anal. Chem. **357**, 148 (1997)
525. G.J. Norga, M. Platero, K.A. Black, A.J. Reddy, J. Michel, L.C. Kimerling: J. Electrochem. Soc. **144**, 2801 (1997)
526. H. Cachet, M. Froment, E. Souteyrand, C. Dennig: J. Electrochem. Soc. **139**, 2920 (1992)
527. H. Kikuyama, N. Miki, K. Saka, J. Takano, I. Kawanabe, M. Miyashita, T. Ohmi: IEEE Trans. Semicond. Manufact. **3**, 99 (1990)
528. L. Jastrzebski, W. Henley, D. DeBusk, N. Haddad, J. Lowell, V. Wenner, K. Nauka, E. Persson: In *Cleaning Technology in Semiconductor Device Manufacturing*, ed. by J. Ruzyllo, R.E. Novak (The Electrochem. Soc., Pennington 1994) p. 530
529. H. Kikuyama, M. Waki, M. Miyashita, T. Yabune, N. Miki, J. Takano, T. Ohmi: J. Electrochem. Soc. **141**, 366 (1994)
530. Y. Yagi, T. Imaoka, Y. Ksama, T. Ohmi: IEEE Trans. Semicond. Manufact. **5**, 121 (1992)
531. M. Morita, T. Ohmi, E. Hasegawa, M. Kawakami, M. Ohwada: J. Appl. Phys. **68**, 1272 (1990)
532. T. Hattori: In *Ultraclean Surface Processing of Silicon Wafers*, ed. by H. Hattori (Springer, Berlin 1998) p. 437
533. H. Kitajima, Y. Shiramizu: IEEE Trans. Semicond. Manufact. **10**, 267 (1997)
534. M. Heyns, C. Hasenack, R. De Keersmaecker, R. Falster: Microelectron. Eng. **10**, 235 (1991)
535. T. Ohmi, M. Miyashita, M. Itano, T. Imaoka, I. Kawanabe: IEEE Trans. Electron. Devices **39**, 537 (1992)
536. T. Ohmi: Proc. IEEE **81**, 716 (1993)
537. T. Ohmi, K. Kotani, A. Teramoto, M. Miyashita: IEEE Electron. Device Lett. **12**, 652 (1991)
538. H. Morinaga, T. Futatsuki, T. Ohmi, E. Fuchita, M. Oda, C. Hayashi: J. Electrochem. Soc. **142**, 966 (1995)
539. J.E.A.M. Van den Meerakker, M.H.M. Van der Straaten: J. Electrochem. Soc. **137**, 1239 (1990)
540. S. Pirooz, J.C. Coria-Garcia, L.W. Shive: In *Cleaning Technology in Semiconductor Device Manufacturing*, ed. by J. Ruzyllo, R.E. Novak (The Electrochem. Soc., Pennington 1992) p. 162
541. H. Mishima, T. Yasui, T. Mizuniwa, M. Abe, T. Ohmi: IEEE Trans. Semicond. Manufact. **2**, 69 (1989)
542. H.F. Schmidt, M. Meuris, P.W. Mertens, A.L.P. Rotondaro, T.Q. Hurd, M.M. Heyns, Z. Hatcher: Jpn. J. Appl. Phys. **34**, 727 (1995)
543. P.W. Mertens, M. Baeyens, G. Moyaerts, H.F. Okorn-Schmidt, R. Vos, R. De Waele, Z. Hatcher, W. Hub, S. De Gendt, M. Knotter, M. Meuris, M.M. Heyns: In *Cleaning Technology in Semiconductor Device Manufacturing V*, ed. by J. Ruzyllo, R.E. Novak, C.M. Appel, T. Hattori, M. Heyns (The Electrochem. Soc., Pennington 1998) p. 176
544. C.R. Helms, H. Park: In *Cleaning Technology in Semiconductor Device Manufacturing*, ed. by J. Ruzyllo, R.E. Novak (The Electrochem. Soc., Pennington 1994) p. 26
545. I. Kanno, N. Yokoi, K. Sato: In *Cleaning Technology in Semiconductor Device Manufacturing V*, ed. by J. Ruzyllo, R.E. Novak, C.M. Appel, T. Hattori, M. Heyns (The Electrochem. Soc., Pennington 1998) p. 54
546. S. Shwartzman, A. Mayer, W. Kern: RCA review **46**, 81 (1985)
547. A. Mayer, S. Shwartzman: J. Electron. Mat. **8**, 855 (1979)
548. S. Ojima, K. Kubo, M. Kato, M. Toda, T. Ohmi: J. Electrochem. Soc. **144**, 1482 (1997)
549. W.A. Syverson, M.J. Fleming, P.J. Schnbring: In *Cleaning Technology in Semiconductor Device Manufacturing*, ed. by J. Ruzyllo, R.E. Novak (The Electrochem. Soc., Pennington 1992) p. 10
550. C.J. Gow, R.E. Smith, W.A. Syverson, R.F. Kunesh, E.D. Buker, K.B. Albaugh, L.S. Whittingham: In *Cleaning Technology in Semiconductor Device Manufacturing*, ed. by J. Ruzyllo, R.E. Novak (The Electrochem. Soc., Pennington 1992) p. 366
551. K. Kubo, S. Ojima, M. Toda, T. Ohmi: In *Cleaning Technology in Semiconductor Device Manufacturing*, ed. by R.E. Novak, J. Ruzyllo (The Electrochem. Soc., Pennington 1995) p. 107
552. P.J. Resnick, C.L.J. Adkins, P.J. Clews, E.V. Thomas, S.T. Cannaday: In *Cleaning Technology in Semiconductor Device Manufacturing*, ed. by J. Ruzyllo, R.E. Novak (The Electrochem. Soc., Pennington 1994) p. 450
553. T. Dhayagude, W. Chen, M. Shenasa, D. Nelms, M. Olesen: In *Science and Technology of Semiconductor Surface Preparation*, ed. by G.S. Higashi, M. Hirose, S. Raghavan, S. Verhaverbeke (Mater. Res. Soc., Pittsburgh 1997) p. 217
554. C.p. D'Emic, S. Cohen, M.A. Zaitz: In *Science and Technology of Semiconductor Surface Preparation*, ed. by G.S. Higashi, M. Hirose, S. Raghavan, S. Verhaverbeke (Mater. Res. Soc., Pittsburgh 1997) p. 233
555. P.W. Mertens, T.Q. Hurd, D. Gräf, M. Meuris, H.F. Schmidt, M.M. Heyns, L. Kwakman, M. Hendriks, M. Kubota: In *Contamination Control and Defect Reduction in Semiconductor Manufacturing III*, ed. by D.N. Schmidt, D. Reedy, R.L. Guldi, J.V. Martinez de Pinillos (The Electrochem. Soc., Pennington 1994) p. 241
556. F. Tardif, T. Lardin, B. Sandrier, P. Boelen, R. Matthews, I. Kashkoush, R. Novak: In *Cleaning Technology in Semiconductor Device Manufacturing V*, ed. by J. Ruzyllo, R.E. Novak, C.M. Appel, T. Hattori, M. Heyns (The Electrochem. Soc., Pennington 1998) p. 15
557. M. Itano, F.W. Kern, Jr., M. Miyashita, T. Ohmi: IEEE Trans. Semicond. Manufact. **6**, 258 (1993)
558. T. Ohmi: J. Electrochem. Soc. **143**, 2957 (1996)
559. U. Keller, W. Aderhold, E.P. Burte: In *Ultra-Clean Processing of Silicon Surfaces*, ed. by M. Heyns (Acco, Leuven/Amersfoort 1994) p. 111
560. D.B. Kao, B.R. Cairns, B.E. Deal: In *Cleaning Technology in Semiconductor Device Manufacturing*, ed. by J. Ruzyllo, R.E. Novak (The Electrochem. Soc., Pennington 1992) p. 251
561. A. Izumi, T. Matsuka, T. Takeuchi, A. Yamano: In *Cleaning Technology in Semiconductor Device Manufacturing*, ed. by J. Ruzyllo, R.E. Novak (The Electrochem. Soc., Pennington 1992) p. 260
562. C.R. Helms, B.E. Deal: In *Cleaning Technology in Semiconductor Device Manufacturing*, ed. by J. Ruzyllo, R.E. Novak (The Electrochem. Soc., Pennington 1992) p. 267
563. S. O'Brien, B. Bohannon, M.H. Bennett, C. Tipton, A. Bowling: In *Cleaning Technology in Semiconductor Device Manufacturing*, ed. by J. Ruzyllo, R.E. Novak (The Electrochem. Soc., Pennington 1994) p. 233
564. S.E. Beck, D.A. Bohling, B.S. Felker, M.A. George, A.G. Gilicinski, J.C. Ivankovits, J.G. Langan, S.W. Rynders, J.A.T. Norman, D.A. Roberts, G. Voloshin, D.M. Hess, A. Lane: In *Cleaning Technology in Semiconductor Device Manufacturing*, ed. by J. Ruzyllo, R.E. Novak (The Electrochem. Soc., Pennington 1994) p. 254
565. M.A. George, D.W. Hess, S.E. Beck, K.M. Young, D.A. Roberts, R. Vrtis, G. Voloshin, D.A. Bohling, A.P. Lane: In *Cleaning Technology in Semiconductor Device Manufacturing*, ed. by R.E. Novak, J. Ruzyllo (The Electrochem. Soc., Pennington 1996) p. 175
566. S.E. Beck, M.A. George, K.M. Young, D.A. Moniot, D.A. Bohling, A.A. Badowski, A.P. Lane: In *Cleaning Technology in Semiconductor Device Manufacturing*, ed. by R.E. Novak, J. Ruzyllo (The Electrochem. Soc., Pennington 1996) p. 166
567. C. Elsmore, T.Q. Hurd, J. Clarke, M. Meuris, P.W. Mertens, M.M. Heyns: In *Cleaning Technology in Semiconductor Device Manufacturing*, ed. by R.E. Novak, J. Ruzyllo (The Electrochem. Soc., Pennington 1996) p. 142
568. J.C. Ivankovits, D.A. Bohling, A. Lane, D.A. Roberts: In *Cleaning Technology in Semiconductor Device Manufacturing*, ed. by J. Ruzyllo, R.E. Novak (The Electrochem. Soc., Pennington 1992) p. 105
569. S.E. Beck, E.A. Robertson, III, M.A. George, D.A. Moniot, J.L. Waskiewicz, D.A. Bohling, K.M. Young, A.A. Badowski: In *Cleaning Technology in Semiconductor Device Manufacturing V*, ed. by J. Ruzyllo, R.E. Novak, C.M. Appel, T. Hattori, M. Heyns (The Electrochem. Soc., Pennington 1998) p. 336

570. M.A. George, S.E. Beck, D.A. Moniot, K.M. Young, D.A. Bohling, G. Voloshin, D.W. Hess: In *Structure and Evolution of Surfaces*, ed. by R.C. Cammarata, E.H. Chason, T.L. Einstein, E.D. Williams (Mater. Res. Soc., Pittsburgh 1997) p. 443
571. E.A. Robertson, III, S.E. Beck, M.A. George, D.A. Bohling, J.L. Waskiewicz: Electrochem. Solid-State Lett. **2**, 91 (1999)
572. D.C. Frystak, J. Ruzyllo: In *Cleaning Technology in Semiconductor Device Manufacturing*, ed. by J. Ruzyllo, R.E. Novak (The Electrochem. Soc., Pennington 1992) p. 58
573. A. Tasch, S. Banerjee, B. Anthony, T. Hsu, R. Qian, J. Irby, D. Kinosky: In *Cleaning Technology in Semiconductor Device Manufacturing*, ed. by J. Ruzyllo, R.E. Novak (The Electrochem. Soc., Pennington 1992) p. 418
574. J. Ruzyllo, A.M. Hoff, D.C. Frystak, S.D. Hossain: J. Electrochem. Soc. **136**, 1474 (1989)
575. J.R. Vig: J. Vac. Sci. Technol. A **3**, 1027 (1985)
576. R. Sugino, M. Okuno, N. Shigeno, Y. Sato, A. Ohsawa, T. Ito, Y. Okui: In *Cleaning Technology in Semiconductor Device Manufacturing*, ed. by J. Ruzyllo, R.E. Novak (The Electrochem. Soc., Pennington 1992) p. 72
577. D.K. Hwang, J. Ruzyllo: In *Cleaning Technology in Semiconductor Device Manufacturing*, ed. by J. Ruzyllo, R.E. Novak (The Electrochem. Soc., Pennington 1994) p. 401
578. J. Ruzyllo, G.T. Duranko, A.M. Hoff: J. Electrochem. Soc. **134**, 2052 (1987)
579. A.S. Lawing, H.H. Sawin, T. Fayfield: In *Cleaning Technology in Semiconductor Device Manufacturing V*, ed. by J. Ruzyllo, R.E. Novak, C.M. Appel, T. Hattori, M. Heyns (The Electrochem. Soc., Pennington 1998) p. 299
580. R. Sugino, Y. Okui, M. Shigeno, S. Ohkubo, K. Takasaki, T. Ito: In *Cleaning Technology in Semiconductor Device Manufacturing V*, ed. by J. Ruzyllo, R.E. Novak, C.M. Appel, T. Hattori, M. Heyns (The Electrochem. Soc., Pennington 1998) p. 291
581. R. Sugino, Y. Tada, T. Ito, Y. Okui, J. Sakuma: J. Electrochem. Soc. **144**, 4059 (1997)
582. T. Ito, R. Sugino, Y. Sato, M. Okuno, A. Osawa, T. Aoyama, T. Yamazaki, Y. Arimuto: In *Chemical Surface Preparation, Passivation and Cleaning for Semiconductor Growth and Processing*, ed. by R.J. Nemanich, C.R. Helms, M. Hirose, G.W. Rubloff (Mater. Res. Soc., Pittsburgh 1992) p. 195
583. Y. Limb, B.Y. Nguyen, P. Tobin: In *Cleaning Technology in Semiconductor Device Manufacturing*, ed. by J. Ruzyllo, R.E. Novak (The Electrochem. Soc., Pennington 1994) p. 409
584. J.K. Tong, D.C. Grant, C.A. Peterson: In *Cleaning Technology in Semiconductor Device Manufacturing*, ed. by J. Ruzyllo, R.E. Novak (The Electrochem. Soc., Pennington 1992) p. 18
585. J.G. Park, M.F. Pas: In *Cleaning Technology in Semiconductor Device Manufacturing*, ed. by R.E. Novak, J. Ruzyllo (The Electrochem. Soc., Pennington 1996) p. 82
586. T. Ohmi, T. Isagawa, M. Kogure, T. Imaoka: J. Electrochem. Soc. **140**, 804 (1993)
587. Y. Fukazawa, K. Miyazaki, Y. Ogawa: In *Cleaning Technology in Semiconductor Device Manufacturing V*, ed. by J. Ruzyllo, R.E. Novak, C.M. Appel, T. Hattori, M. Heyns (The Electrochem. Soc., Pennington 1998) p. 264
588. J.G. Park, J.H. Han: In *Cleaning Technology in Semiconductor Device Manufacturing V*, ed. by J. Ruzyllo, R.E. Novak, C.M. Appel, T. Hattori, M. Heyns (The Electrochem. Soc., Pennington 1998) p. 231
589. J.D. Joo, J.S. Kim, H. Morita, T. Ohmi: In *Cleaning Technology in Semiconductor Device Manufacturing V*, ed. by J. Ruzyllo, R.E. Novak, C.M. Appel, T. Hattori, M. Heyns (The Electrochem. Soc., Pennington 1998) p. 280
590. M. Miyashita, H. Kubota, Y. Matsushita, R. Yoshimur, T. Tada: Jpn. J. Appl. Phys. (Letters) **34**, L288 (1995)
591. T.Q. Hurd, A.L.P. Rotondaro, J. Sees, A. Misra, C. Appel: In *Cleaning Technology in Semiconductor Device Manufacturing V*, ed. by J. Ruzyllo, R.E. Novak, C.M. Appel, T. Hattori, M. Heyns (The Electrochem. Soc., Pennington 1998) p. 105
592. I. Oki, T. Biwa, J. Kudo, T. Ashida: In *Cleaning Technology in Semiconductor Device Manufacturing*, ed. by J. Ruzyllo, R.E. Novak (The Electrochem. Soc., Pennington 1992) p. 215
593. Y. Ma, M.L. Green, L.C. Feldman, J. Sapjeta, K.J. Hanson, T.W. Weidman: J. Vac. Sci. Technol. B **13**, 1460 (1995)
594. E.R. Weber, D. Gilles: In *Semiconductor Silicon-1990*, ed. by H.R. Huff, K.G. Barraclough, J.I. Chikawa (The Electrochem. Soc., Pennington 1990) p. 585
595. D. Gilles: Solid State Phenom. **32-33**, 57 (1993)
596. J.S. Kang, D.K. Schroder: J. Appl. Phys. **65**, 2974 (1989)
597. R.N. Hall, J.H. Racette: J. Appl. Phys. **35**, 379 (1964)
598. D. Gilles, W. Schröter, W. Bergholz: Phys. Rev. B **41**, 5770 (1990)
599. A. Ihlal, R. Rizk, O.B.M.H. Duparc: J. Appl. Phys. **80**, 2665 (1996)
600. H. Hieslmair, S.A. McHugo, A.A. Istratov, E.R. Weber: In *Properties of Crystalline Silicon*, ed. by R. Hull (INSPEC, Short Run Press, Exeter 1999) p. 775
601. S.A. McHugo, H. Hieslmair: In *Wiley Encyclopedia of Electrical and Electronics Engineering*, ed. by J.G. Webster (Wiley, New York 1999) p. 388
602. S.M. Myers, M. Seibt, W. Schröter: J. Appl. Phys. to be published (2000)
603. H. Hieslmair, A.A. Istratov, E.R. Weber: Semicond. Sci. Technol. **13**, 1401 (1998)
604. W. Kaiser: Phys. Rev. **105**, 1751 (1957)
605. E.J. Mets: J. Electrochem. Soc. **112**, 420 (1965)
606. T.Y. Tan, E.E. Gardner, W.K. Tice: Appl. Phys. Lett. **30**, 175 (1977)
607. H.R. Huff, H.F. Schaake, J.T. Robinson, S.C. Baber, D. Wong: J. Electrochem. Soc. **130**, 1551 (1983)
608. D. Gilles, E.R. Weber, S. Hahn: In Proceedings of 20th International Conference on the Physics of Semiconductors, ed. by E.M. Anastassakis, J.D. Joannopoulos (Singapore World Scientific, Thessaloniki Greece 6–10 Aug. 1990) p. 537
609. H. Tsuya, K. Ogawa, F. Shimura: Jpn. J. Appl. Phys. **20**, L31 (1981)
610. G.Z. Nemtsev, A.I. Pekarev, Y.D. Chistyakov: Mikroelektronika (USSR) **12**, 432 (1983)
611. K. Nagasawa, Y. Matsushita, S. Kishino: Appl. Phys. Lett. **37**, 622 (1980)
612. E.G. Colas, E.R. Weber, S. Hahn: In *Oxygen, Carbon, Hydrogen and Nitrogen in Crystalline Silicon*, ed. by J.C. Mikkelsen, Jr., S.J. Pearton, J.W. Corbett, S.J. Pennycook (Mater. Res. Soc., Pittsburgh 1986) p. 341
613. F. Shimura, R.K. Willardson, A.C. Beer, E.R. Weber (Ed.): *Oxygen in Silicon, in series: Semiconductors and Semimetals*, Series ed. by R.K. Willardson, E.R. Weber (Academic Press, New York 1994)
614. H. Fujimori: J. Electrochem. Soc. **144**, 3180 (1997)
615. K.L. Enisherlova, T.F. Rusak, M.G. Mil'vidskii, V.J. Reznick: Mater. Sci. Eng. B **36**, 120 (1996)
616. L. Rivaud, C.N. Anagnostopoulos, G.R. Erikson: J. Electrochem. Soc. **135**, 437 (1988)
617. A. Bourret, J. Thibault-Desseaux, D.N. Seidman: J. Appl. Phys. **55**, 825 (1984)
618. A. Borghesi, B. Pivac, A. Sassella, A. Stella: J. Appl. Phys. **77**, 4169 (1995)
619. M. Miyazaki, M. Sano, S. Sadamitsu, S. Sumita, N. Fujino, T. Shiraiwa: Jpn. J. Appl. Phys. (Letters) **28**, L519 (1989)
620. K. Graff, H.A. Hefner, H. Pieper: In *Impurity Diffusion and Gettering in Silicon*, ed. by R.B. Fair, C.W. Pearce, J. Washburn (Mater. Res. Soc., Pittsburgh 1985) p. 19
621. K. Graff, H.A. Hefner, W. Hennerici: J. Electrochem. Soc. **135**, 952 (1988)
622. R. Falster, W. Bergholtz: J. Electrochem. Soc. **137**, 1548 (1990)
623. M. Seibt, K. Graff: J. Appl. Phys. **63**, 4444 (1988)
624. B. Shen, T. Sekiguchi, J. Jablonski, K. Sumino: J. Appl. Phys. **76**, 4540 (1994)
625. J. Jablonski: In *Crystalline Defects and Contamination: Their Impact and Control in Device Manufacturing II*, ed. by B.O. Kolbesen, C. Claeys, P. Stallhofer, F. Tardiff (The Electrochem. Soc., Pennington 1997) p. 295
626. A.R. Bhatti, R. Falster, G.R. Booker: Solid State Phenom. **19-20**, 51 (1991)
627. R. Falster, Z. Laczik, G.R. Booker, A.R. Bhatti, P. Török: In *Defect Engineering in Semiconductor Growth, Processing and Device Technology*, ed. by S. Ashok, J. Chevallier, K. Sumino, E. Weber (Mater. Res. Soc., Pittsburgh 1992) p. 945
628. A. Ourmazd, W. Schröter: Appl. Phys. Lett. **45**, 781 (1984)
629. B. Shen, X.Y. Zhang, K. Yang, P. Chen, R. Zhang, Y. Shi, Y.D. Zheng, T. Sekiguchi, K. Sumino: Appl. Phys. Lett. **70**, 1876 (1997)

630. R.K. Sinha, W.S. Glaunsinger: In *Semiconductor Fabrication: Technology and Metrology*, ed. by D.C. Gupta (ASTM, Philadelphia 1989) p. 339
631. B. Shen, T. Sekiguchi, R. Zhang, Y. Shi, Y.D. Zheng, K. Sumino: Phys. Status Solidi A **155**, 321 (1996)
632. I. Vanhellemont, C. Claeys: Mater. Sci. Forum **38-41**, 171 (1989)
633. M. Seibt: In *Crystalline Defects and Contamination: Their Impact and Control in Device Manufacturing II*, ed. by B.O. Kolbesen, C. Claeys, P. Stallhofer, F. Tardif (The Electrochem. Soc., Pennington 1997) p. 243
634. A.A. Istratov, E.R. Weber: Appl. Phys. A **66**, 123 (1998)
635. S. Ishigami, S. Ishii, H. Shinyashiki, H. Furuya, T. Shingyouji: Jpn. J. Appl. Phys. **33**, 1728 (1994)
636. S. Krieger-Kaddour, N.E. Chabane-Sari, D. Barbier: J. Electrochem. Soc. **140**, 495 (1993)
637. R. Falster, Z. Laczik, G.R. Booker, P. Török: Solid State Phenom. **19-20**, 33 (1991)
638. L. Jastrzebski, R. Soydan, J. McGinn, R. Kleppinger, M. Blumenfeld, G. Gillespie, N. Armour, B. Goldsmith, W. Henry, S. Vecrumba: J. Electrochem. Soc. **134**, 1018 (1987)
639. L. Jastrzebski, R. Soydan, B. Goldsmith, J.T. McGinn: J. Electrochem. Soc. **131**, 2944 (1984)
640. H. Takahashi, H. Yamada-Kaneta, M. Suezawa: Solid State Phenom. **57-58**, 75 (1997)
641. H. Takahashi, H. Yamada-Kaneta, M. Suezawa: Jpn. J. Appl. Phys. **37**, 1689 (1998)
642. L. Baldi, G. Cerofolini, G. Ferla: J. Electrochem. Soc. **127**, 164 (1980)
643. C.L. Reed, K.M. Mar: J. Electrochem. Soc. **127**, 2058 (1980)
644. C.W. Pearce, V.J. Zaleckas: J. Electrochem. Soc. **126**, 1436 (1979)
645. K.H. Yang, G.H. Schwuttke: Phys. Status Solidi A **58**, 127 (1980)
646. Y. Hayamizu, S. Ushio, T. Takenaka: In *Defect Engineering in Semiconductor Growth, Processing and Device Technology*, ed. by S. Ashok, J. Chevallier, K. Sumino, E. Weber (Mater. Res. Soc., Pittsburgh 1992) p. 1005
647. K.K. Mishra: In *Defect and Impurity Engineered Semiconductors and Devices*, ed. by S. Ashok, J. Chevallier, I. Akasaki, N.M. Johnson, B.L. Sopori (Mater. Res. Soc., Pittsburgh 1995) p. 321
648. R.B.M. Girisch: In *Crystalline Defects and Contamination: Their Impact and Control in Device Manufacturing*, ed. by B.O. Kolbesen, C. Claeys, P. Stallhofer, F. Tardif (The Electrochem. Soc., Pennington 1993) p. 170
649. J. Partanen, T. Tuomi, M. Tilli, S. Hahn, C.C.D. Wong, F.A. Ponce: J. Mater. Res. **4**, 623 (1989)
650. C. Jourdan, J. Gastaldi, J. Derrien, M. Bienfait, J.M. Layet: Appl. Phys. Lett. **41**, 259 (1982)
651. S. Roorda, B. Morin, E. Soudée, S.C. Gujrathi: Can. J. Phys. **73**, 45 (1995)
652. M. Sano, M. Horai, M. Miyazaki, N. Fujino, T. Shiraiwa: Jpn. J. Appl. Phys. **27**, 1220 (1988)
653. P.M. Rice, M.J. Kim, R.W. Carpenter: In *Defects in Materials*, ed. by P.D. Bristowe, J.E. Epperson, J.E. Griffith, Z. Liliental-Weber (Mater. Res. Soc., Pittsburgh 1991) p. 385
654. R. Sawada, T. Karaki, J. Watanabe: Jpn. J. Appl. Phys. **20**, 2097 (1981)
655. R. Sawada: Jpn. J. Appl. Phys. **23**, 959 (1984)
656. S.E. Lindo, K.M. Matney, M.S. Goorsky: In *Defect and Impurity Engineered Semiconductors and Devices*, ed. by S. Ashok, J. Chevallier, I. Akasaki, N.M. Johnson, B.L. Sopori (Mat. Res. Soc, Pittsburgh 1995) p. 315
657. D. Gilles: In *Defect Engineering in Semiconductor Growth, Processing and Device Technology*, ed. by S. Ashok, J. Chevallier, K. Sumino, E. Weber (Mater. Res. Soc., Pittsburgh 1992) p. 917
658. D. Gilles, H. Ewe: In *Semiconductor Silicon-1994*, ed. by H.R. Huff, W. Bergholz, K. Sumino (The Electrochem. Soc., Pennington 1994) p. 772
659. M. Seibt, M. Apel, A. Döller, H. Ewe, E. Spiecker, W. Schröter, A. Zozime: In *Semiconductor Silicon-1998*, ed. by H. Huff, U. Gösele, H. Tsuya (The Electrochem. Soc., San Diego 1998) p. 1064
660. M.B. Shabani, T. Yoshimi, S. Okuuchi, T. Shingyoji, F. Kirscht: In *Crystalline Defects and Contamination: Their Impact and Control in Device Manufacturing II*, ed. by B.O. Kolbesen, C. Claeys, P. Stallhofer, F. Tardiff (The Electrochem. Soc., Pennington 1997) p. 318
661. K. Sumino: Mater. Sci. Forum **105-110**, 139 (1992)
662. G.E.J. Eggermont, R.J. Falster, S.K. Hahn: Solid State Technol. **26**, 171 (1983)
663. Y. Hayamizu, S. Tobe, H. Takeno, Y. Kitagawara: In *Semiconductor Silicon-1998*, ed. by H. Huff, U. Gösele, H. Tsuya (The Electrochem. Soc., Pennington 1998) p. 1080
664. M.C. Chen, V.J. Silvestri: J. Electrochem. Soc. **129**, 1294 (1982)
665. F.G. Kirscht, E.R. Weber, I. Babanskaya: Solid State Phenom. **19-20**, 137 (1991)
666. H. Shirai, A. Yamaguchi, F. Shimura: Appl. Phys. Lett. **54**, 1748 (1989)
667. B. Pichaud, G. Mariani: J. Phys. III **2**, 295 (1992)
668. S. Hahn, C.C.D. Wong, F.A. Ponce, Z.U. Rek: In *Oxygen, Carbon, Hydrogen and Nitrogen in Crystalline Silicon*, ed. by J.C. Mikkelsen, Jr., S.J. Pearton, J.W. Corbett, S.J. Pennycook (Mater. Res. Soc., Pittsburgh 1986) p. 353
669. V.V. Voronkov: Semicond. Sci. Technol. **8**, 2037 (1993)
670. V.A. Gusev, N.V. Bogach: Mikroelektronika (USSR) **19**, 374 (1990)
671. S.J. Brunkhorst, D.W. Sloat: Solid State Technol. **41**, 87 (1998)
672. R.R. Troutman: IEEE Electron. Device Lett. **EDL-4**, 438 (1983)
673. P.A. Stolk, J.L. Benton, D.J. Eaglesham, D.C. Jacobson, J.Y. Cheng, J.M. Poate, S.M. Myers, T.E. Haynes: Appl. Phys. Lett. **68**, 51 (1996)
674. M. Sano, S. Sumita, T. Shigematsu, N. Fujino: In *Semiconductor Silicon 1994*, ed. by H.R. Huff, W. Bergholz, K. Sumino (The Electrochem. Soc., Pennington 1994) p. 784
675. M. Aoki, T. Itakura, N. Sasaki: Appl. Phys. Lett. **66**, 2709 (1995)
676. L.C. Kimerling, J.L. Benton: Physica B & C **116**, 297 (1983)
677. D.P. Miller, J.E. Moore, C.R. Moore: J. Appl. Phys. **33**, 2648 (1962)
678. M.L. Joshi, F. Wilhelm: J. Electrochem. Soc. **112**, 185 (1965)
679. T.H. Yeh, M.L. Joshi: J. Electrochem. Soc. **116**, 73 (1969)
680. H. Kikuchi, M. Kitakata, F. Toyokawa, M. Mikami: Appl. Phys. Lett. **54**, 463 (1989)
681. H. Tsuya, Y. Kondo, M. Kanamori: Jpn. J. Appl. Phys. (Letters) **22**, L16 (1983)
682. S. Matsumoto, I. Ishihara, H. Kaneko, H.H. Harada, T. Abe: In *Impurity Diffusion and Gettering in Silicon*, ed. by R.B. Fair, C.W. Pearce, J. Washburn (Mater. Res. Soc., Pittsburgh 1984) p. 263
683. H. Takeno, M. Mizuno, S. Ushio, T. Takenaka: Mater. Sci. Forum **196-200**, 1865 (1995)
684. S. Tobe, Y. Hayamizu, Y. Kitagawara: J. Appl. Phys. **84**, 1279 (1998)
685. M. Miyazaki, S. Miyazaki, S. Ogushi, T. Ochiai, M. Sano, T. Shigematsu: Jpn. J. Appl. Phys. (Letters) **36**, L380 (1997)
686. J.L. Benton, P.A. Stolk, D.J. Eaglesham, D.C. Jacobson, J.Y. Cheng, J.M. Poate, S.M. Myers, T.E. Haynes: J. Electrochem. Soc. **143**, 1406 (1996)
687. R.W. Gregor, W.H. Stinebaugh, Jr.: J. Appl. Phys. **64**, 2079 (1988)
688. G.F. Cerofolini, M.L. Polignano, H. Bender, C. Claeys: Phys. Status Solidi A **103**, 643 (1987)
689. F. Kirscht, B. Snegirev, P. Zaumseil, G. Kissinger, K. Takashima, P. Wildes, J. Hennessy: In *Diagnostic Techniques for Semiconductor Materials and Devices*, ed. by P. Rai-Choudhury, J.L. Benton, D.K. Schroder, T.J. Shaffner (The Electrochem. Soc., Pennington 1997) p. 60
690. F.G. Kirscht, T. Shabani, T. Yoshimi, S.B. Kim, B. Snegirev, C. Wang, L. Willamson, K. Takashima, P. Taylor, D. Lange: Solid State Phenom. **56-57**, 355 (1997)
691. W.A. Orr, M. Arienzo: IEEE Trans. Electron. Devices **ED-29**, 1151 (1982)
692. R.D. Thompson, K.N. Tu: Appl. Phys. Lett. **41**, 440 (1982)
693. R. Sundaresan, D.E. Burk, J.G. Fossum: J. Appl. Phys. **55**, 1162 (1984)
694. S. Martinuzzi, H. Poitevin, M. Zehaf, C. Zurletto: Rev. Phys. Appl. (France) **22**, 645 (1987)
695. L.A. Verhoef, P.P. Michiels, S. Roorda, W.C. Sinke, R.J.C. Van Zolingen: Mater. Sci. Eng. B **7**, 49 (1990)
696. P. Sana, A. Rohatgi, J.P. Kalejs, R.O. Bell: Appl. Phys. Lett. **64**, 97 (1994)
697. S.A. McHugo, H. Hieslmair, E.R. Weber: Appl. Phys. A **64**, 127 (1997)
698. S.M. Joshi, U.M. Gösele, T.Y. Tan: J. Appl. Phys. **77**, 3858 (1995)
699. B. Hartiti, A. Slaoui, J.C. Muller, P. Siffert: Appl. Phys. Lett. **63**, 1249 (1993)

700. H. Hieslmair, S.A. McHugo, E.R. Weber: In Proceedings of 25th IEEE Photovoltaic Specialists Conference, (Washington D.C. 1996) p. 441
701. A. Luque, A. Moehlecke, R. Lagos, C. Del Canizo: Phys. Status Solidi A **155**, 43 (1996)
702. S. Martinuzzi, I. Périchaud, J.J. Simon: Appl. Phys. Lett. **70**, 2744 (1997)
703. N. Gay, S. Martinuzzi: Appl. Phys. Lett. **70**, 2568 (1997)
704. S.H. Ahn, S. Zhao, A.L. Smith, L.L. Chalfoun, M. Platero, H. Nakashima, L.C. Kimerling: In *Defects in Electronic Materials II*, ed. by J. Michel, T. Kennedy, K. Wada, K. Thonke (Mater. Res. Soc., Pittsburgh 1997) p. 169
705. H. Baker: *Alloy Phase Diagrams* (ASM International, Materials Park, Ohio 1992)
706. P. Villars, A. Prince, H. Okamoto: *Handbook of Ternary Alloy Phase Diagrams* (ASM International, Materials Park, OH 1995)
707. M.P. Godlewski, C.R. Baraona, H.W. Brandhorst: In Proceedings of 10th IEEE Photovoltaic Specialists Conference (Palo Alto, CA USA, 1973) p. 40
708. J. Mandelkorn, J.H. Lamneck, Jr.: J. Appl. Phys. **44**, 4785 (1973)
709. M. Apel, I. Hanke, R. Schindler, W. Schröter: J. Appl. Phys. **76**, 4432 (1994)
710. R.L. Meek, T.E. Seidel, A.G. Cullis: J. Electrochem. Soc. **122**, 786 (1975)
711. S.P. Murarka: J. Electrochem. Soc. **123**, 765 (1976)
712. A. Goetzberger, W. Shockley: J. Appl. Phys. **31**, 1821 (1960)
713. J.L. Lambert, M. Reese: Solid-State Electron. **11**, 1055 (1968)
714. A.G. Shaikh, W. Schröter, W. Bergholz: J. Appl. Phys. **58**, 2519 (1985)
715. W.R. Wilcox, T.J. LaChapelle: J. Appl. Phys. **35**, 240 (1964)
716. W.R. Wilcox, T.J. LaChapelle, D.H. Forbes: J. Electrochem. Soc. **111**, 1377 (1964)
717. G.J. Sprokel, J.M. Fairchild: J. Electrochem. Soc. **112**, 200 (1965)
718. M.L. Joshi, S. Dash: J. Appl. Phys. **37**, 2453 (1966)
719. S.F. Cagnina: J. Electrochem. Soc. **116**, 498 (1969)
720. T.A. O'Shaughnessy, H.D. Barber, D.A. Thompson, E.L. Heasell: J. Electrochem. Soc. **121**, 1350 (1974)
721. S.L. Chou, J.F. Gibbons: J. Appl. Phys. **46**, 1197 (1975)
722. T.E. Seidel, R.L. Meek, A.G. Cullis: J. Appl. Phys. **46**, 600 (1975)
723. A. Ourmazd, W. Schröter: In *Materials Research Society, Impurity Diffusion and Gettering in Silicon*, ed. by R.B. Fair, C.W. Pearce, J. Washburn (Mater. Res. Soc., Pittsburgh 1985) p. 25
724. D. Gilles, W. Schröter: Mater. Sci. Forum **10-12**, 169 (1986)
725. R. Kühnapfel, W. Schröter: In *Semiconductor Silicon-1990*, ed. by H.R. Huff, K.G. Barraclough, J. Chikawa (The Electrochem. Soc., Pennington 1990) p. 651
726. E.O. Sveinbjörnsson, O. Engström, U. Sodervall: J. Appl. Phys. **73**, 7311 (1993)
727. F. Gaiseanu, W. Schröter: J. Electrochem. Soc. **143**, 361 (1996)
728. S. Coffa, G. Franco, C.M. Camalleri, A. Giraffa: J. Appl. Phys. **80**, 161 (1996)
729. E. Spiecker, M. Seibt, W. Schröter: Phys. Rev. B **55**, 9577 (1997)
730. W. Schröter, R. Kühnapfel: Appl. Phys. Lett. **56**, 2207 (1990)
731. A. Bourret, W. Schröter: Ultramicroscopy **14**, 97 (1984)
732. H. Reiss: J. Chem. Phys. **21**, 1209 (1953)
733. H. Reiss, C.S. Fuller, F.J. Morin: Bell Syst. Techn. J. **35**, 535 (1956)
734. W. Shockley, J.L. Moll: Phys. Rev. **119**, 1480 (1960)
735. W. Shockley, J.T. Last: Phys. Rev. **107**, 392 (1957)
736. H.J. Queisser: J. Appl. Phys. **32**, 1776 (1961)
737. W.F. Tseng, T. Koji, J.W. Mayer, T.E. Seidel: Appl. Phys. Lett. **33**, 442 (1978)
738. H. Zimmermann, N.Q. Khanh, G. Battistig, J. Gyulai, H. Ryssel: Appl. Phys. Lett. **60**, 748 (1992)
739. A. Armigliato, M. Servidori, S. Solmi, I. Vecchi: J. Appl. Phys. **48**, 1806 (1977)
740. H. Strunk, U. Gösele, B.O. Kolbesen: Appl. Phys. Lett. **34**, 530 (1979)
741. H. Strunk, U. Gösele, B.O. Kolbesen: J. Microscopy **118**, 35 (1980)
742. E. Yakimov, I. Périchaud: Appl. Phys. Lett. **67**, 2054 (1995)
743. W.B. Knowlton, J.T. Walton, J.S. Lee, D. Lewak, Y.K. Wong, E.E. Haller: In *Process Physics and Modeling in Semiconductor Technology*, ed. by G.R. Srinivasan, C.S. Murthy, S.T. Dunham (The Electrochem. Soc., Pennington 1996) p. 324
744. U. Gösele, W. Frank, A. Seeger: Appl. Phys. **23**, 361 (1980)
745. M.L. Polignano, G.F. Cerofolini, H. Bender, C. Claeys: J. Appl. Phys. **64**, 869 (1988)
746. M. Loghmarti, R. Stuck, J.C. Muller, D. Sayah, P. Siffert: Appl. Phys. Lett. **62**, 979 (1993)
747. R. Gafiteanu, U. Gösele, T.Y. Tan: In *Defect and Impurity Engineered Semiconductors and Devices*, ed. by S. Ashok, J. Chevallier, I. Akasaki, N.M. Johnson, B.L. Sopori (Mater. Res. Soc., Pittsburgh 1995) p. 297
748. K. Mahfoud, M. Loghmarti, J.C. Muller, P. Siffert: Mater. Sci. Engin. B **36**, 63 (1996)
749. S. Narayanan, S.R. Wenham, M.A. Green: Appl. Phys. Lett. **48**, 873 (1986)
750. P. Sana, J. Salami, A. Rohatgi: IEEE Trans. Electron. Devices **40**, 1461 (1993)
751. S. Martinuzzi, I. Périchaud: Mater. Sci. Forum **143-7**, 1629 (1994)
752. I. Périchaud, F. Floret, M. Stemmer, S. Martinuzzi: Solid State Phenom. **32-33**, 77 (1993)
753. L. Jastrzebski, W. Henley, D. Schielein, J. Lagowski: J. Electrochem. Soc. **142**, 3869 (1995)
754. R.L. Meek, C.F. Gibbon: J. Electrochem. Soc. **121**, 444 (1974)
755. L. Baldi, G.F. Cerofolini, G. Ferla, G. Frigerio: Phys. Status Solidi A **48**, 523 (1978)
756. G.F. Cerofolini, M.L. Polignano: J. Appl. Phys. **55**, 579 (1984)
757. J.J. Simon, I. Périchaud, N. Burle, M. Pasquinelli, S. Martinuzzi: J. Appl. Phys. **80**, 4921 (1996)
758. P.W. Mertens, B. Vermeire, M. Depas, M.J. McGeary, J. Sees, S.C. O'Brien, M. Meuris, M.M. Heyns, D. Gräf: In 1995 Proceedings of the Institute of Enviromental Sciences: Contamination Control (ISBN 1-877862-42-8) (IES, Mount Prospect, IL, USA 1994) p. 474
759. P.W. Mertens, M.J. McGeary, M. Schaekers, H. Sprey, B. Vermeire, M. Depas, M. Meuris, M.M. Heyns: In *Science and Technology of Semiconductor Surface Preparation*, ed. by G.S. Higashi, M. Hirose, S. Raghavan, S. Verhaverbeke (Mater. Res. Soc., Pittsburgh 1997) p. 89
760. R.J. Kriegler: Thin Solid Films **13**, 11 (1972)
761. R.J. Kriegler: Appl. Phys. Lett. **20**, 449 (1972)
762. R.J. Kriegler, Y.C. Cheng, D.R. Colton: J. Electrochem. Soc. **119**, 388 (1972)
763. G.J. Declerck, T. Hattori, G.A. May, J. Beaudouin, J.D. Meindl: J. Electrochem. Soc. **122**, 436 (1975)
764. D.W. Hess: J. Electrochem. Soc. **124**, 740 (1977)
765. P.H. Robinson, F.P. Heiman: J. Electrochem. Soc. **118**, 141 (1971)
766. P.M. Engel, J.P. de Souza: J. Appl. Phys. **54**, 4211 (1983)
767. T.A. Baginski, J.R. Monkowski: J. Electrochem. Soc. **132**, 2031 (1985)
768. P.W. Mertens, S. De Gendt, M. Depas, K. Kenis, A. Opdebeeck, P. Snee, D. Gräf, G. Brown, M.M. Heyns: In *Ultra Clean Processing of Silicon Surfaces '96*, ed. by M. Heyns, M. Meuris, P. Mertens (Acco, Leuven 1996) p. 33
769. J.M. Green, C.M. Osburn, T.O. Sedgwick: J. Electron. Mat. **3**, 579 (1974)
770. T.M. Buck, K.A. Pickar, J.M. Poate, C.M. Hsieh: Appl. Phys. Lett. **21**, 485 (1972)
771. O. Kononchuk, R.A. Brown, S. Koveshnikov, K. Beaman, F. Gonzalez, G.A. Rozgonyi: Solid State Phenom. **57-58**, 69 (1997)
772. S.V. Koveshnikov, G.A. Rozgonyi: J. Appl. Phys. **84**, 3078 (1998)
773. M. Tamura, T. Ando, K. Ohyu: Nucl. Instrum. Methods Phys. Res. B **59-60**, 572 (1991)
774. R. Kögler, M. Posselt, R.A. Yankov, J.R. Kaschny, P. Werner, A.B. Danilin, W. Skorupa: In *Defects and Diffusion in Silicon Processing*, ed. by T. Diaz de la Rubia, S. Coffa, P.A. Stolk, C.S. Rafferty (Mater. Res. Soc., Pittsburgh 1997) p. 463
775. R. Kögler, R.A. Yankov, M. Posselt, A.B. Danilin, W. Skorupa: Nucl. Instrum. Methods Phys. Res. B **147**, 96 (1999)
776. R. Kögler, A. Peeva, W. Anwand, G. Brauer, W. Skorupa, P. Werner, U. Gösele: Appl. Phys. Lett. **75**, 1279 (1999)
777. R.A. Brown, O. Kononchuk, G.A. Rozgonyi, S. Koveshnikov, A.P. Knights, P.J. Simpson, F. Gonzalez: J. Appl. Phys. **84**, 2459 (1998)
778. Y.M. Gueorguiev, R. Kögler, A. Peeva, D. Panknin, A. Mücklich, R.A. Yankov, W. Skorupa: Appl. Phys. Lett. **75**, 3467 (1999)
779. K.D. Beyer, T.H. Yeh: J. Electrochem. Soc. **129**, 2527 (1982)

780. J. Wong-Leung, J.S. Williams, R.G. Elliman, E. Nygren, D.J. Eaglesham, D.C. Jacobson, J.M. Poate: Nucl. Instrum. Methods Phys. Res. B **96**, 253 (1995)
781. J. Wong-Leung, E. Nygren, J.S. Williams: Appl. Phys. Lett. **67**, 416 (1995)
782. O. Kononchuk, R.A. Brown, Z. Radzimski, G.A. Rozgonyi, F. Gonzalez: Appl. Phys. Lett. **69**, 4203 (1996)
783. R.A. Brown, O. Kononchuk, I. Bondarenko, A. Romanowski, Z. Radzimski, G.A. Rozgonyi, F. Gonzalez: J. Electrochem. Soc. **144**, 2872 (1997)
784. H. Wong, N.W. Cheung, P.K. Chu: Appl. Phys. Lett. **52**, 889 (1988)
785. H. Wong, N.W. Cheung, P.K. Chu, J. Liu, J.W. Mayer: Appl. Phys. Lett. **52**, 1023 (1988)
786. H. Wong, N.W. Cheung, K.M. Yu, P.K. Chu, J. Liu: In *Ion Beam Processing of Advanced Electronic Materials*, ed. by N.W. Cheung, A.D. Marwick, J.B. Roberto (Mater. Res. Soc. 1989) p. 97
787. W. Skorupa, R. Kögler, K. Schmalz: Electron. Lett. **26**, 1898 (1990)
788. W. Skorupa, R. Kögler, K. Schmalz, P. Gaworzewski, G. Morgenstern, H. Syhre: Nucl. Instrum. Methods Phys. Res. B **74**, 70 (1993)
789. M.H.F. Overwijk, J. Politiek, R.C.M. de Kruif, P.C. Zalm: Nucl. Instrum. Methods Phys. Res. B **96**, 257 (1995)
790. T.I. Kamins, S.Y. Chiang: J. Appl. Phys. **58**, 2559 (1985)
791. M. Delfino, M. Jaczynski, A.E. Morgan, C. Vorst, M.E. Lunnon, P. Maillot: J. Electrochem. Soc. **134**, 2027 (1987)
792. J. Jablonski, Y. Miyamura, M. Imai, H. Tsuya: J. Electrochem. Soc. **142**, 2059 (1995)
793. W. Skorupa, N. Hatzopoulos, R.A. Yankov, A.B. Danilin: Appl. Phys. Lett. **67**, 2992 (1995)
794. K.L. Beaman, A. Agarwall, O. Kononchuk, S. Koveshnikov, I. Bondarenko, G.A. Rozgonyi: Appl. Phys. Lett. **71**, 1107 (1997)
795. R. Kögler, J.R. Kaschny, R.A. Yankov, P. Werner, A.B. Danilin, W. Skorupa: Solid State Phenom. **57-58**, 63 (1997)
796. W. Deweerd, T. Barancira, G. Langouche, K. Milants, R. Moons, J. Verheyden, H. Patryn: Nucl. Instrum. Methods Phys. Res. B **120**, 51 (1996)
797. M. Zhang, L. Wang, J. Gao, C. Lin, P.L.F. Hemment, K. Gutjahr, U. Gösele: Nucl. Instrum. Methods Phys. Res. B **134**, 360 (1998)
798. S.M. Myers, D.M. Follstaedt, D.M. Bishop, J.W. Medernach: In *Semiconductor Silicon-1994*, ed. by H.R. Huff, W. Bergholz, K. Sumino (The Electrochem. Soc., Pennington 1994) p. 808
799. V. Raineri, A. Battaglia, E. Rimini: Nucl. Instrum. Methods Phys. Res. B **96**, 249 (1995)
800. S.M. Myers, D.M. Follstaedt: J. Appl. Phys. **79**, 1337 (1996)
801. S.M. Myers, G.A. Petersen, C.H. Seager: J. Appl. Phys. **80**, 3717 (1996)
802. S.A. McHugo, E.R. Weber, S.M. Myers, G.A. Petersen: Appl. Phys. Lett. **69**, 3060 (1996)
803. J. Min, P.K. Chu, X. Lu, S.S.K. Iyer, N.W. Cheung: Thin Solid Films **300**, 64 (1997)
804. S.A. McHugo, E.R. Weber, S.M. Myers, G.A. Petersen: J. Electrochem. Soc. **145**, 1400 (1998)
805. S.M. Myers, G.A. Petersen: Phys. Rev. B **57**, 7015 (1998)
806. S.M. Myers, G.A. Petersen, D.M. Follstaedt, T.J. Headley, J.R. Michael, C.H. Seager: Nucl. Instrum. Methods Phys. Res. B **120**, 43 (1996)
807. V. Raineri: Solid State Phenom. **57-58**, 43 (1997)
808. H.J. Geipel, W.K. Tice: IBM J. Res. Dev. **24**, 310 (1980)
809. D. Lecrosnier, J. Paugam, G. Pelous, F. Richou, M. Salvi: J. Appl. Phys. **52**, 5090 (1981)
810. A.G. Nassibian, B. Golja: J. Appl. Phys. **53**, 6168 (1982)
811. D. Jaworska, J. Sielanko, E. Tarnowska: Appl. Phys. A **A35**, 119 (1984)
812. S.S. Gong, D.K. Schroder: Solid-State Electron. **30**, 209 (1987)
813. A. Grob, P. Rohr, G. Mariani, J. Sevely, J.J. Grob: Nucl. Instrum. Methods Phys. Res. B **112**, 169 (1996)
814. D. Jaworska, E. Tarnowska: J. Phys. D **26**, 2226 (1993)
815. S.M. Myers, D.M. Bishop, D.M. Follstaedt, H.J. Stein, W.R. Wampler: In *Microcrystalline Semiconductors: Materials Science and Devices*, ed. by P.M. Fauchet, C.C. Tsai, L.T. Canham, I. Shimizu (Mater. Res. Soc., Pittsburgh 1993) p. 549
816. J. Wong-Leung, J.S. Williams, E. Nygren: In *Defect and Impurity Engineered Semiconductors and Devices*, ed. by S. Ashok, J. Chevallier, I. Akasaki, N.M. Johnson, B.L. Sopori (Mater. Res. Soc., Pittsburgh 1995) p. 273
817. T.A. Baginski: J. Electrochem. Soc. **135**, 1842 (1988)
818. C.J. Barbero, J.W. Corbett, C. Deng, Z. Atzmon: J. Appl. Phys. **78**, 3012 (1995)
819. F. Namavar, J.I. Budnick, F.A. Otter: In *Impurity Diffusion and Gettering in Silicon*, ed. by R.B. Fair, C.W. Pearce, J. Washburn (Mater. Res. Soc., Pittsburgh 1985) p. 55
820. S.A. McHugo, E.R. Weber, S.M. Myers, G.A. Petersen: In *Microstructure Evolution During Irradiation. Symposium Microstructure Evolution During Irradiation*, ed. by I.M. Robertson, G.S. Was, L.W. Hobbs, T.D. de la Rubia (Mater. Res. Soc., Pitsburgh 1997) p. 149
821. P.A. Stolk, H.J. Gossmann, D.J. Eaglesham, J.M. Poate: Nucl. Instrum. Methods Phys. Res. B **96**, 187 (1995)
822. W.F. Ames: *Numerical Methods for Partial Differential Equations* (Academic Press, New York 1977)
823. G.J. Reece: *Microcomputer Modelling by Finite Differences* (Macmillan, Basingstoke 1986)
824. W.J. Minkowycz: *Handbook of numerical heat transfer* (Wiley, New York 1988)
825. D. Greenspan, V. Casulli: *Numerical Analysis for Applied Mathematics, Science, and Engineering* (Addison-Wesley, Redwood City 1988)
826. T.Y. Tan, R. Grafiteanu, S.M. Joshi, U. Gösele: In *Semiconductor Silicon-1998*, ed. by H. Huff, U. Gösele, H. Tsuya (The Electrochem. Soc., Pennington 1998) p. 1050
827. A.L. Smith, S.H. Ahn, L.C. Kimmerling: In *Semiconductor Silicon 1998*, ed. by H. Huff, U. Gösele, H. Tsuya (The Electrochem. Soc., Pennington 1998) p. 1138
828. T.Y. Tan, R. Gafiteanu, U.M. Gösele: In *Semiconductor Silicon 1994*, ed. by H.R. Huff, W. Bergholz, K. Sumino (The Elecrochem. Soc., Pennington 1994) p. 920
829. D.A. Antoniadis, R.W. Dutton: IEEE J. Solid-State Circuits **SC-14**, 412 (1979)
830. T.Y. Tan: Appl. Phys. Lett. **73**, 2678 (1998)
831. H. Hieslmair: Ph.D. thesis (Uiversity of California 1998)
832. P.S. Plekhanov, R. Gafiteanu, U.M. Gosele, T.Y. Tan: J. Appl. Phys. **86**, 2453 (1999)
833. C.S. Chen, D.K. Schroder: J. Appl. Phys. **71**, 5858 (1992)
834. F.C. Frank, D. Turnbull: Phys. Rev. **104**, 617 (1956)
835. H. Gdanitz, K. Schmalz: Phys. Status Solidi A **117**, 395 (1990)
836. G.B. Bronner, J.D. Plummer: J. Appl. Phys. **61**, 5286 (1987)
837. U. Gösele, T.Y. Tan: In *Impurity Diffusion and Gettering in Silicon Symposium*, ed. by R.B. Fair, C.W. Pearce, J. Washburn (Mater. Res. Soc., Pittsburgh 1985) p. 105
838. H. Zimmermann: Mater. Sci. Forum **143-147**, 1647 (1994)
839. L. Fabry: Accred Qual. Assur. **1**, 99 (1996)
840. K. Nauka, D.A. Gomez: J. Electrochem. Soc. **142**, L98 (1995)
841. K. Nauka: In *Semiconductor Characterization–Present Status and Future Needs*, ed. by W.M. Bullis, D.G. Seiler, A.C. Diebold (AIP Press 1996) p. 231
842. H. Schwenke, J. Knoth: Nucl. Instrum. Methods Phys. Res. **239**, 193 (1982)
843. K. Ketata, M. Masmoudi, M. Katata, R. Debrie: Mater. Sci. & Eng. B **33**, L1 (1995)
844. A. Cacciato, S. Vleeshouwers, S. Evseev: J. Electrochem. Soc. **145**, 701 (1998)
845. W. Bergholz, V. Penka, G. Zoth: In *Analytical Techniques for Semiconductor Materials and Process Characterization*, ed. by B.O. Kolbesen, D.V. McCaughan, W. Vandervorst (The Electrochem. Soc., Pennington 1990) p. 29
846. M. Miyazaki: In *Recombination Lifetime Measurements in Silicon*, ed. by D.C. Gupta, F.R. Bacher, W.M. Hughes (ASTM, West Conshohocken 1998) p. 294